LE

NASA Contractor Report 175040

Measurements of a Single Lateral Jet Injected into Swirling Crossflow

L.H. Ong and D.G. Lilley
Oklahoma State University
Stillwater, Oklahoma

January 1986

Prepared for
Lewis Research Center
Under Grant NAG 3-549

NASA
National Aeronautics and
Space Administration

TABLE OF CONTENTS

NOMENCLATURE

A_c	cross-sectional area of crossflow
A_J	cross-sectional area of jet
D	test section diameter
d	inlet nozzle diameter
d_J	lateral jet inlet diameter
R	jet-to-crossflow velocity ratio
Re	Reynolds number
$\bar{V} = (u,v,w)$	time-mean velocity in facility coordinates (x-, r-, θ-directions)
x,r,θ	axial, radial, azimuthal coordinates
δ	Arctan (u/w)
ϕ	swirl vane angle with respect to facility axis
θ	traverse azimuthal angle

Subscripts

o	value at inlet to flowfield
rms	root-mean-squared

Superscripts

$(\bar{})$	time-mean average
$( )'$	fluctuating component

CHAPTER I

INTRODUCTION

1.1 Lateral Jet Injection

Lateral injected jets are widely used in combustors of gas turbine engines to provide sufficient air for complete combustion as well as to evenly mix and cool the hot combustion products before their introduction to the turbine. As expected, the placement, size and injection velocities of lateral jets greatly affect the performance of the combustor in particular, and of the whole engine in general.

Clearly, the flowfields in such situations are turbulent, reacting, and fully three-dimensional. Design and development of these combustors usually require the building of expensive prototypes followed by painstaking experiments, requiring lengthy and costly research programs. Time and expense could be greatly reduced with the availability of reliable computer codes for direct prediction of these complicated flowfields. The development of these, a subject of intensive present-day research, requires the existence of an accurate data base with which to compare predictions and further develop mixing models, finite difference schemes, and iterative procedures for improved accuracy and efficiency. Several textbooks extensively review problems and progress in this area.[1-5]

The present study adds to the detailed data base being obtained in the on-going experimental combustor flow research program at Oklahoma

State University. A recent Ph. D. thesis[6] discusses hot-wire measurements of a single lateral jet being injected into nonswirling crossflow, and presents flow visualization results concerning injection into swirling crossflow, with crossflow swirl vane angle ϕ = 0 (swirler removed), 45 and 70 degrees. Three research papers have also evolved[7-9] from the recent study. All flowfields being investigated under this program at Oklahoma State University have no expansion of the crossflow (the test section to swirler diameter ratio D/d = 1), after its passage through an optional swirler, with swirl vane angle ϕ = 0 (swirler removed), 45 and 70 degrees. The lateral jet is located one test-section diameter downstream of the test section inlet (x/D = 1) and it emanates from a round nozzle whose area is 1/100th of the cross-sectional area of the crossflow (A_j/A_c = 1/100).

1.2 Objectives

The present study concentrates on a single lateral jet being injected normally into swirling crossflow. It complements previous studies which focused on corresponding situations with swirl but without lateral injection, and with lateral injection but without swirl.[6] It also complements a concurrent study investigating two opposed lateral jets being injected into swirling crossflow.[10] The present study investigates two particular flowfields having lateral jet-to-crossflow velocity ratio v_j/u_o = 4, with swirl vane angle ϕ = 45 and 70 degrees being used with the main crossflow. Specific objectives included, for the two flowfields:

1. The five-hole pitot probe was used to measure time-mean axial, radial and swirl velocities throughout the test section.

2. The six-orientation single-wire hot-wire technique was used to measure the three time-mean velocities, three normal and three shear turbulent stresses throughout the test section.

1.3 Outline of the Thesis

Chapter I of this manuscript described the phenomenon of lateral injection jets its application in engineering especially in the combustion of jet engines. The need for a reliable data base of a jet injected laterally into a swirling crossflow and the objectives of the present study was also discussed. Chapter II gives a brief insight into the history and previous studies of the injection jet. Included is also an overview of the recent work on combustor flowfields that led to the present undertaking.

The experimental set up used in the present study is described in Chapter III, with discussions on the wind tunnel, the vane swirler, the test section and the incorporation of the injection jet, as well as a brief discussion of the hot-wire instrumentation. Data acquisition techniques using the single normal hot-wire and the five-hole pitot-probe are described in Chapter IV.

Chapter V presents and analyses the extensive results that were obtained during this investigation. Finally, Chapter VI concludes the present study and makes some recommendations for further work.

CHAPTER II

BACKGROUND

2.1 Previous Studies of Deflected Jets

Ferrell[9] provides an extensive description and classification of significant earlier studies on deflected jets. These studies include experimental (pitot probe, hot-wire and laser anemometer methods) and theoretical (empirical relationships and direct solution of the appropriate governing equations) contributions. Most of them were concerned with a single lateral jet injected into 'infinite' uniform crossflow.

Chassaing et al[11] compared several zones of similarity in injected jets. Laser doppler investigations were conducted by Crabb et al[12] on the velocity and turbulence fields, especially the vortex pairs generated by the crossflow being obstructed by the injected round jet. Of more significance to combustion chamber applications was the work by Rathgeber and Becker.[13] They measured the trajectory and mixing of injected jets into cylindrical crossflows. However, the study lacks turbulence data. Recent NASA sponsored experimental work led to empirical evidence about the effects of multi-injected jets into rectangular crossflow. The most recent published article about these studies is by Holdeman et al.[14]

Significant is that these previous studies did not address the problem of injection into swirling crossflows which are typical of that

occurring in combustors. As a contribution to this a research program was initiated at Oklahoma State University which built upon earlier experience without lateral injection jets.[15] Ferrell[6] completed his Ph. D. thesis on the single lateral injected jet with velocity ratios R = v_j/u_o = 2, 4 and 6 entering into nonswirling crossflow. The six-orientation single hot-wire measurement technique was used. In addition to this, several flow visualization techniques (bubbles, smoke and sparks) were used with these same velocity ratios into swirling crossflow, with swirl vane angle ϕ = 0 (swirler removed), 45 and 70 degrees. Detailed measurements were not made for these swirling cases, leading to the objectives of the present research to emphasize the swirl effect, via the five-hole pitot probe and the hot-wire measurement methods, on the single lateral injection jet with R = 4 only. Ferrell and colleagues wrote conference papers dealing with preliminary results and computer simulation of the fully 3-D flowfield,[7] flow visualization studies,[8] and the detailed hot-wire measurements.[9] A concurrent research effort on two opposed lateral jets, each with R = 4 entering the 0, 45 and 70 degree swirling crossflow, is being undertaken by McMurry.[10]

2.2 Recent Work at Oklahoma State University

Lilley[15] summarizes recent extensive experimental and theoretical research which has been completed at Oklahoma State University on 2-D axisymmetric geometries under low speed, nonreacting, turbulent swirling flow conditions, in the absence of any lateral jets. The flow enters the test section and proceeds into a larger chamber (the expansion D/d = 2) via a sudden or gradual expansion (side-wall angle α = 90 and 45

degrees). A weak or strong nozzle may be positioned downstream to form a contraction exit to the test section. Inlet swirl vanes are adjustable to a variety of vane angles with values of ϕ = 0, 38, 45, 60 and 70 degrees being emphasized. The objective was to determine the effect of these parameters on isothermal flowfield patterns, time-mean velocities and turbulence quantities, and to establish an improved simulation in the form of a computer prediction code equipped with a suitable turbulence model. Experimental developments included:

1. Flow visualization was accomplished via still and movie photography of neutrally-buoyant helium-filled soap bubbles, smoke produced by an injector and multisparks across the flowfield.
2. Time-mean velocities have been measured with a five-hole pitot probe for a complete range of swirl strengths.
3. Turbulence measurements have been completed on swirling (up to ϕ = 70 degrees) as well as nonswirling flows using a six-orientation single-wire hot-wire technique enabling all Reynolds stress components to be deduced.

Theoretical developments included:

1. An advanced computer code has been developed and improved to predict corresponding confined swirling flows to those studied experimentally.
2. Tentative predictions have now been supplemented by predictions made from realistic inlet conditions for a complete range of swirl strengths with downstream nozzle effects.

CHAPTER III

EXPERIMENTATION

3.1 Wind Tunnel And Vane Swirler

Figure 1 of Appendix B shows a schematic of the test facility which is described at length elsewhere.[6] It consists of a wind tunnel, a variable-angle vane swirler, and a plexiglass test section of diameter 15 cm. The wind tunnel has an axial-flow fan whose speed can be changed by altering a varidrive mechanism. Numerous fine screens and straws produce flow in the settling chamber of relatively low turbulence intensity. The contraction section leading to the test section has been designed by the method of Morel[16] to produce a minimum adverse pressure gradient on the boundary layer and thus avoid unsteady problems associated with local separation regions. The air-flow passes through a 15 cm diameter circular jet nozzle, exiting into a 15 cm diameter test section of length 90 cm, which is constructed of plexiglass to facilitate flow visualization.

A variable-angle vane swirler may be positioned immediately before the test section. Its flow area has an outer diameter of 15 cm. The swirler has ten vanes which are individually adjustable to any angle ϕ and a hub with a streamlined upstream nose and a flat downstream face. The nose has a hyperbolic shape with a very smooth surface so as to offer minimal flow interference. The flat blades are wedge-shaped to give a constant pitch-to-chord ratio of 0.68 which gives good turning

efficiency.[3] Its performance is documented elsewhere.[15] The test section normally begins at a location x/D = 0, which is 3.2 cm downstream of the swirler exit.

Figure 1 shows the configuration of the 15 cm diameter test section mounted on the wind tunnel with the swirler omitted. Air to the lateral jet is supplied from a compressed air line via piping and a carefully-designed nozzle. Upstream of each nozzle, a stagnation chamber, turbulence management screens, flow straightening straws, and flow metering equipment are used for flow conditioning. Experiments are being performed with the lateral jet located one test-section diameter downstream of the inlet.

3.2 Test Section and Dilution Jet

Clear acrylic tubing is used for the test section. Of length 90 cm, it is attached to the wind tunnel throat or immediately after the optional swirler. Standard commercial acrylic tube is used with 15.24 cm (6.0 in.) outside diameter, 0.318 cm (0.125 in.) wall thickness. The inside diameter is 14.61 cm with a measured variation of $\pm$ 0.05 cm. To adapt the test section to the wind tunnel throat (inside diameter 15 cm), an adaptor section was machined to provide a smooth transition from wind tunnel throat to test section. Two test-section tubes were constructed. Both test sections have the dilution jet inlet located at x/D = 1.00 where x is measured from the tube inlet. The first tube has a series of probe access holes located at x/D = 1.00, 1.25, and 1.50 and at all six azimuthal locations 270, 300, 330, 0, 30 and 60 degrees as shown in Figure 2. The second tube allows probe access to locations downstream of x/D = 1.50 (for example x/D = 1.75, 2.00, 2.50, 3.00) and

at any azimuthal angle. This is accomplished via a tube rotation section, shown in Figure 3, and constructed from machined aluminum rings, acrylic, and ball bearings.

The lateral jet is fed from laboratory compressed air at 6 to 7 atmospheres gauge pressure. For stability, the supply air lines are large and are routed through two line regulators with an intermediate tank (volume approximately 0.006 m^3) to dampen line oscillations. The second regulator is used to meter the flow rate. After the second regulator, the air is routed through a Fisher and Porter model 10A1735A rotometer for monitoring of the volume flow before introduction to the dilution jet. The dilution jet assembly consists of a stagnation chamber, flow straightening section, and the jet nozzle. The stagnation chamber was constructed from 15 cm inside diameter aluminum pipe and filled with plastic household scrub pads to evenly distribute the internal flow. A hemispherically-shaped screen and convergent transition smooth the flow into the flow straightening section. Here the air flows through four brass screens for turbulence reduction. The nozzle is constructed of fiberglass with its precise contour being determined according to Morel[16] in a manner similar to that used for the main wind tunnel facility. The nozzle diameter is one-tenth of the test-section diameter, giving a crossflow to jet area ratio A_c/A_j = 100. Once assembled, the dilution jet was attached to the air line coming from the rotometer, and the nozzle was pressed into a special acrylic adaptor which is permanently attached to the test section.

3.3 Hot-Wire Instrumentation

A normal hot-wire probe, DISA type 55P01, is used as the sensing

transducer. It has two prongs set 3 mm apart with a 5 μm diameter tungsten wire between them. The exposed, effective length of the wire is approximately 1 mm, since the ends have been gold plated to strengthen the wire and reduce end effects. The probe support is a standard DISA 55H21 straight mounting tube. The anemometer used is a DISA type 55MØ1, constant-temperature standard bridge.

Calibration of the hot-wire in three mutually perpendicular directions is done using the laboratory calibration jet -- a small axisymmetric free jet. An extended King's law calibration expression is used. An automated computer controlled probe drive is used for data acquisition. Hot-wire voltages are processed through a Burr-Brown SDM853 12-bit A/D converter and the average and standard deviation of 5000 readings (taken over 5 seconds for each orientation of the wire at each measurement location) are stored on diskette using an Apple II computer. Ferrell[6] provides greater detail about the instrumentation, calibration, probe drive and data acquisition systems.

CHAPTER IV

DATA ACQUISITION TECHNIQUES

4.1 Five-Hole Pitot Probe

Time-mean velocity measurements in a flow of unknown prominent direction may be obtained using a five-hole pitot probe. It is one of the simplest instruments capable of simultaneously sensing both magnitude and direction of the local velocity vector. The particular probe employed is model DC-125-12-DC from United Sensor and Control Corp. It has a 3.2 mm diameter sensing tip and shaft containing five tubes. The sensing head is hook-shaped to allow probe shaft rotation without altering the probe tip location.

The instrumentation system, in addition to the five-hole pitot probe, consists of a manual traverse mechanism, two five-way ball valves, a very sensitive pressure transducer, a power supply, and an integrating voltmeter. The differential pressure transducer is model 590D from Datametrics, Inc. It has a differential pressure range of from 0 to 1.3×10^3 N/m^2 (equivalently, 0 to 10 torr). The integrating voltmeter is the TSI model 1076. A pitot-static probe is used to measure the dynamic pressure in the nozzle throat just upstream of the swirler, and therefrom deduce the swirler inlet uniform axial velocity u_o which is used later for velocity normalizations. Also, a barometer/thermometer unit from Cenco Corp. is used for local pressure and temperature readings.

As on previous studies at Oklahoma State University without the lateral jet operating,[15] at a location in the flowfield the east and west pressures are equalized to yaw out in the rθ-plane and then the north and south pressures are used with a correlation to determine the radial velocity v. Knowledge of the central pressure is also required during this data reduction. Further details appear in the studies of Rhode, Yoon, Sander, and Scharrer which are documented in Reference 15.

4.2 Normal Hot-Wire

When turbulence data are needed in addition to time-mean values, pitot probes are inadequate -- their response time is too slow. A more involved technique is then required, using hot-wire or laser doppler anemometry. A novel technique developed at Oklahoma State University for swirl flows without lateral injection is the six-orientation single-wire hot-wire method.[15] It is very cost effective for flows of unknown dominant direction and has already been used on the nonswirling flow with lateral injection.[6-9] It is used in the present work without further refinement. Instrumentation used with this measurement technique has been described in Section 3.3. The six-orientation technique permits measurements of time-mean velocity components and turbulence quantities in complex three-dimensional flowfields. Applied in this study to nonreacting flowfields, measurements of time-mean and root-mean-square voltages at six different orientations (each separated by a 30 degree probe support rotations) contain enough information to obtain the three time-mean velocities, the three normal and the three shear Reynolds stresses. At each location in the flow, there are six different values of each of the above quantities that can be deduced

using six sets of measurements of three adjacent orientations. Ensemble averages of the output quantities from the six combinations of data appear to produce estimates with the best agreement with independent measurements. The accuracy of the hot-wire method discussed in Section 5, where it is pointed out that severe inaccuracies may be present especially in the deduced shear stress values. Further information about the technique appears in the studies of Janjua, Jackson and Ferrell which are described in Refs. 6 and 15.

CHAPTER V

RESULTS AND DISCUSSION

Hot-wire time-mean and turbulence data, and time-mean velocity measurements using the five-hole pitot probe were obtained for swirling flow without expansion, and with a lateral injection jet to crossflow velocity ratio of $R = v_j/u_o = 4$. The lateral jet is situated at $x/D = 1$, which is one test-section diameter downstream of the test-section inlet plane.

The swirl cases investigated were that of swirler vane angle of 45 degrees and 70 degrees, represented moderate and strong swirl respectively. An earlier study presents corresponding results with no swirl in the crossflow.[6] Another previous study gives measurements with swirl in the crossflow, but without any lateral jet.[17] Lateral transverses, at traverse angles of 270, 300, 330, 0, 30 and 60 degrees, with the hot-wire were conducted at $x/D = 1.00$, 1.25, 1.50, 1.75, 2.00, 2.50, and 3.00. The test-section geometry is shown in Figure 3.

Hot-wire results of the experiment with moderately swirling crossflow are shown in and Figures 4 through 9. Similarly, Figures 10 through 15 show the data obtained for the strongly swirling crossflow. The figures just mentioned are subdivided into 12 parts (a through l) to present efficiently the normalized time mean velocity components (a, b, c) the normalized fluctuating velocity components or normal stresses (d, e, f), the normalized shear stresses (g, h, i), the normalized total

velocity (j), the normalized axial turbulence intensity (k), and the normalized turbulent kinetic energy (l). The accuracy of results for turbulence quantities - normal stresses and, especially, shear stresses - is in doubt. Jackson[17] discusses the quality of the hot-wire technique in a weakly swirling axisymmetric expanded flowfield with D/d = 2. The conclusion is that in turbulent shear regions, the maximum errors are 18, 24, 29, and 98 percent for time-mean values, normal stresses, shear stresses and $\overline{u'w'}$, respectively. The present study emphasizes the stronger swirl without expansion into the test section and may have potentially further accuracy problems. One major limitation with the present data acquisition system is the limited sampling rate of 1000 Hz. Thus, the higher frequency signals of the hot-wire would not be properly digitized. Normally, an appropriate filter would be used in the data acquisition system to reduce this aliasing effect. The present study does not use such a filter. However, in this case, where the turbulence energies might be in excess of 1000 Hz, the lack of a filter might actually improve the data by inclusion of the aliased high frequency signals. The amalgamated effect of these uncertainties leads to an unknown degree of error in the calculated values of turbulence quantities, especially the shear stresses. There are no alternative sources of data with which to compare the deduced values.

Pitot probe time-mean velocity measurements were also obtained for the same swirling cases mentioned above. Lateral traverses using the pitot probes were completed at x/D = 1.00, 1.50, 2.00 and 2.50. Results for the moderate swirling crossflow case are given in and Figures 16 to 21. Measurements of the strongly swirling crossflow situation are

presented in Figures 22 to 27, with subparts a, b and c containing plots of normalized time-mean u, v and w velocity components.

5.1 Moderate Swirl, ϕ = 45 Degrees

The entry of the injection jet can be clearly observed in parts a, b, c and j of Figures 4 through 9, which show axial, radial, swirl and total velocity plots, respectively. Even with this moderate swirl strength, the lateral jet is immediately swept along with the main flow in its swirling path after penetrating only up to r/D = -0.4 as shown in Figure 7 at x/D = 1.00 (the inlet plane of the jet). This may be seen by inspection of the radial component of velocity v at the location x/D = 1.00 as shown in Figure 7b, which gives vertical traverses. The axial u and swirl w velocity components are increased in value close to the injection location along the path of the injected jet. For example, parts a and c of the vertical traverse of Figure 7 show this at the x/D = 1.00 and 1.25 axial locations.

The traverses presented in Figure 6 are aligned at 30 degrees to the vertical plane and give an indication of the path of the injected jet after injection, when the effects are no longer observable in the vertical plane. This rapid turning of the injected jet is expected as the swirl velocity component of the crossflow effectively increases the local velocity normal to the injected jet. This results in a reduced true jet-to-crossflow velocity ratio and subsequently reduces the lateral jet penetration into the main flowfield. For the 45 degree case, the R value is reduced to approximately 2.8. Part a of Figure 6 shows enlarged axial velocity u at r/D = -0.25 on the x/D = 1.25 axial location; part b of the same figure shows increased upward velocity v

near the same position; on the other hand, part c shows reduced swirl velocity w in the wake of the injected jet near this same location. Notice that the swirl velocity nearer to the confining wall has not been affected since it is away from the path of the injected jet.

The angle between the local crossflow direction and the plane normal to the facility centerline is provided by calculating δ = arctan (u/w) locally. Near the lateral jet injection location this angle is approximately δ = 45 degrees for the moderate swirl ϕ = 45 degree case; it is approximately δ = 27 degrees for the strong swirl ϕ = 70 degrees case as discussed in Section 5.2. A spiralling path on the tube wall would require a normalized downstream distance of L/D = π(tan δ) to complete one revolution of the tube, if the angle θ remains constant. The trajectory of the lateral jet follows roughly this path, but the angle δ changes as the jet penetrates into the field. Hence, approximately, for the moderate swirl case of ϕ = 45 degrees, the required normalized downstream distance is L/D = 3.14; for the ϕ = 70 degree case, it is L/D = 1.5. Hence, evidence of the lateral jet is expected to be seen at x/D = 1.25 in the θ = 330 degree traverse, at x/D = 1.5 in the θ = 300 degree traverse, etc. for the moderate swirl case. For the strong swirl case, it is expected to be seen at x/D = 1.25 in the θ = 300 degree traverse, at x/D = 1.5 in the θ = 60 degree traverse, etc.

The progress of the jet can be traced further downstream at x/D = 1.50 by careful inspection of Figure 5 (a, b, c and j), which are plots of the mean velocity data at a plane inclined at 60 degrees to the vertical. Similarly, the increase in axial velocity component shown in Figure 4a at x/D = 2.00 shows further progression of the jet. In this

figure, the spread of the injected jet can be deduced as one also notices larger u and v velocity components at x/D = 1.5. It would seem that the traverse shown in Figure 5, at x/D = 1.50 obtained a velocity profile near the center-line of the injected jet, while the traverse of Figure 4, at the same axial location would slice through the outer boundaries of the path of the injected jet. This evidence of the path and spread of the injection jet can be correlated to the bubble flow visualization photographs of the same flow conditions obtained by Ferrell.[6] After x/D = 2.00, the spiral path of the jet, though not as pronounced, can still be traced by picking out the locations where higher axial and total velocities are observed. For instance at x/D = 3.00, the jet would appear to be near the top right quadrant of the test section, viewed towards the upstream direction. We can also deduce that the center-line is located near the bottom of the traverse of θ = 270 degrees as indicated by the higher mean axial and total velocity, shown in Figure 4 at x/D = 3.00, when compared with the other traverse angle planes at the same axial location. Pitot-probe time-mean measurements, displayed later in Figures 16 through 21, are comparable to the corresponding hot-wire measurements.

As expected, the introduction of the lateral jet into the crossflow destroyed the symmetry of the swirling crossflow. Jackson[17] and Scharrer[18] used the same hot-wire and pitot-probe measurement techniques, respectively, to measure the axisymmetric, swirling non-expanding flowfield. Their data were used as a basis of comparison for the current experiments. The injected jet contributes less than 4 percent of the total mass flow, so that the flowfield is not drastically changed from the axisymmetric case at locations away from the injected

jet path, and after it has spread and mixed with the crossflow.

The disturbance of the precessing vortex core noticed by Ferrell[6] is also obvious in the mean axial and swirl velocity plots. The centerline of the vortex core is characterized by low axial and swirl velocities and hence its deflection can be observed, for example, in Figure 4 (a and c) at x/D = 2.0, 2.5 and 3.0, because the low velocity regions is not only away from the centerline of the test section but is also at different positions in each of the axial locations.

Higher turbulence intensities, as shown in parts d through f of the above mention figures, were measured at locations where the intruding jet interacts with the main crossflow. However, the shear stress does not appear to be affected by the injection jet. This shear stress data shows the same trends as previous swirl flow data without lateral injection, obtained by Jackson.[17]

5.2 Strong Swirl, ϕ = 70 Degrees

As discussed in Section 5.1, the angle between the local crossflow direction and the plane normal to the facility centerline δ = arctan (u/w) = 27 degrees for this strong swirl case near the lateral jet injection location. This requires approximately a downstream distance of L/D = 1.5 for the path of the jet to ideally make one revolution, with evidence of the lateral jet expected to be seen at x/D = 1.25 in the θ = 300 degree traverse, at x/D = 1.5 in the θ = 60 degree traverse, etc.

The high swirl velocity of the crossflow in this case forces the injection jet to turn almost immediately into the local main flow direction. This is evidenced by the higher radial velocity component at

r/D = -0.4 and x/D = 1.00 of the vertical traverse of Figure 13. More significantly, the path at the next axial location, x/D = 1.25 appeared to be near θ = 300 degrees and r/D = 0.35 as compared to that of θ = 330 degrees and r/D = 0.25 of the moderate swirl case. This not only exhibits the rapid deflection of the injection jet but also indicated that the jet is sticking closer to the wall of test section due to higher centrifugal forces and also intensified jet-to-local crossflow velocity ratio as discussed previously in the moderate swirl case. The local strong swirl velocity now reduces the R value to approximately 1.2 which from previous work[6] would lead to very little penetration of the lateral jet into the main stream. Because of rapid mixing in this high swirl strength, the path of the jet is not clearly identified after x/D = 1.50. This fact is supported by the flow visualization photographs obtained by Ferrell.[6] The axisymmetric measurements for this swirl strength were also conducted by Jackson[17] and Scharrer[18] as described previously. The effect of the injection jet is even less pronounced than in the moderate swirl case because of higher swirl strength and increased mixing.

High turbulence intensities were again observed along the path of the injected jet. The shear stresses are again of very low magnitude and do not appear to have been affected by the injected jet. The normal and shear stress calculation using this hot-wire technique is unfortunately very sensitive to errors during data acquisition as can be observed in the corresponding plots. This idiosyncrasy was discussed by Ferrell[6] and especially by Jackson.[17]

CHAPTER VI

CLOSURE

6.1 Conclusions

Time-mean and turbulence measurements using a six-position single hot-wire technique have been completed for non-expanding swirling flowfields that were disturbed by a single lateral injection jet of jet-to-crossflow velocity ratio $R = v_j/u_o = 4$. The cases investigated consist of flowfields with the upstream swirler vane angle set at 45 and 70 degrees, representing moderate and strong swirl respectively. Time-mean velocity measurements using a five-hole pitot probe technique were also conducted for the same conditions. The results were presented in the form of r-x plots to help visualize the fully three-dimensional flowfield.

Data from the moderate swirl case showed that the trajectory of the injected jet can be easily traced. The spreading of the injected jet can also be observed. The swirl in the crossflow intensified the local velocity at the location of the injected jet, which effectively reduced the jet-to-crossflow velocity ratio. This caused the trajectory of the injected jet to follow the path of the local flow direction of the crossflow, and reduced its penetration into the crossflow. The lateral jet was also found to deflect the axis of the precessing vortex core.

At the higher swirl strength, the turning of the jet into the local crossflow direction is more pronounced for reasons described above and

higher centrifugal forces. The injection jet appears to disperse more rapidly in this case because of the high intensity of the mixing. The time-mean velocity measurements using the hot-wire corresponded to pitot-probe data obtained under identical flow conditions.

Turbulence stress-data show the same trends as previous swirl flow data without lateral injection. Discontinuities observed in the turbulence stress plots, especially that of the higher swirl strength, are unfortunately due to the sensitivity of the hot-wire data reduction technique to dwell time errors. These errors could be reduced by using a computer and data acquisition system with higher clock speed which would reduce the time between measurements.

6.2 Recommendations for Further Work

A useful addition to the data base generated by the present and concurrent study of two opposed injection jets by McMurry[10] would be to investigate cases with different injection jet-to-crossflow velocity ratios of, for example, $R = v_j/u_o = 2$, 6, and 8. The effects of additional jets could also be studied, as found, for example, in a practical case of a combustor with six inlets.

Use of a more advanced and complex hot-wire technique might improve the accuracy of measurements. For instance, a cross-wire or triple-wire probe could be used, but some of these data reduction techniques require a priori knowledge of local time-mean velocity, and more complicated probe handling systems. These methods might reduce the current dwell time measurement errors as multi-wire probes record correlation measurements almost simultaneously. However, there are problems with probe effects, interference and directional sensitivity of these multi-

wire probes. Instrumentation of these probes is also far more complex. A useful improvement of the present technique would be to conduct an energy spectrum analysis of hot-wire signals. This would enable the determination of the range of turbulence frequencies. Then a more accurate measurement would be obtained by increasing the sampling rate of the data acquisition system and appropriate filtering to reduce the effects of aliasing.

REFERENCES

1. Schetz, J. A., "Injection and Mixing in Turbulent Flow", Prog. in Astro. and Aero., AIAA, Vol. 68, 1980.

2. Lefebvre, A. H. "Gas Turbine Combustion." McGraw-Hill, New York, 1983.

3. Gupta, A. K., Lilley, D. G., and Syred, N., "Swirl Flows." Abacus Press, Tunbridge Wells, England, 1985.

4. Gupta, A. K. and Lilley, D. G., "Flowfield Modeling and Diagnostics." Abacus Press, Tunbridge Wells, England, 1985.

5. Cheremisinoff, N. P. and Gupta, R. (eds.) "Handbook of Fluids in Motion." Ann Arbor Science, Ann Arbor, Michigan, 1983.

6. Ferrell, G. B., "Deflected Jet Experiments in a Turbulent Combustor Flowfield." Ph.D. Thesis, Oklahoma State University, Stillwater, Okla., Dec. 1984. See also: Ferrell, G. B. and Lilley, D. G., "Deflected Jet Experiments in a Turbulent Combustor Flowfield." NASA CR-174863, Feb. 1985.

7. Ferrell, G. B., Abujelala, M. T., Busnaina, A A., and Lilley, D. G., "Lateral Jet Injection into Typical Combustor Flowfields." Paper AIAA-84-0374, Reno, Nevada, January 9-12, 1984.

8. Ferrell, G. B., Aoki, K. and Lilley, D. G., "Flow Visualization of Lateral Jet Injection into Swirling Crossflow." AIAA Paper 85-0059, Reno, Nevada, Jan. 14-17, 1985.

9. Ferrell, G. B. and Lilley, D. G., "Turbulence Measurements of Lateral Jet Injection into Confined Tubular Crossflow." Paper AIAA-85-1102, Monterey, Calif., July 8-10, 1985.

10. McMurry, C. B., "Experiments on Two Opposed Lateral Jets Injected into Swirling Crossflow." M.S. Thesis, Oklahoma State University, Stillwater, Okla., Dec. 1985.

11. Chassaing, P., George, J., Claria, A., and Sananes, F., "Physical Characteristics of Subsonic Jets in a Cross-Stream." Journal of Fluid Mechanics, Vol. 62, 1974, p. 41-64..

12. Crabb, D., Durao, D. F. G., and Whitelaw, J. W., "A Round Jet Normal to a Cross-Flow." ASME Trans., Vol. 103, 1981, pp. 142-153.

13. Rathgeber, D. E., and Becker, H. A., "Mixing Between a Round Jet and a Transverse Pipe Flow." Proceedings of 1st Symposium on Turbulent Flows, Penn. State University, 1977.

14. Holdeman, J. D., Srinivasan, R., and Berenfeld, A., "Experiments in Dilution Jet Mixing." AIAA Journal, Vol. 22, No. 10, Oct. 1984, pp. 1436-1443.

15. Lilley, D. G., "Investigation of Flowfields Found in Typical Combustor Geometries." NASA CR-3869, Feb. 1985. See also: Lilley, D. G. "Swirling Flows in Typical Combustor Geometries." AIAA-85-0184, Reno, Nevada, Jan. 14-17, 1985.

16. Morel, T., "Comprehensive Design of Axisymmetric Wind Tunnel Contractions." ASME Paper 75-FE-17, Minneapolis, MN, May 5-7, 1975.

17. Jackson, T. W., "Turbulence Characteristics of Swirling Flowfields." Ph. D. Thesis, Oklahoma State University, Stillwater, Okla., Dec. 1983. See also: Jackson, T. W. and Lilley, D. G., "Turbulence Characteristics of Swirling Flowfields." NASA CR-174918, May 1985.

18. Scharrer, G. L., "Swirl, Expansion Ratio and Blockage Effects on Confined Turbulent Flow." M. S. Thesis, Oklahoma State University, Stillwater, Okla. May 1984.

APPENDIX A

FIGURES

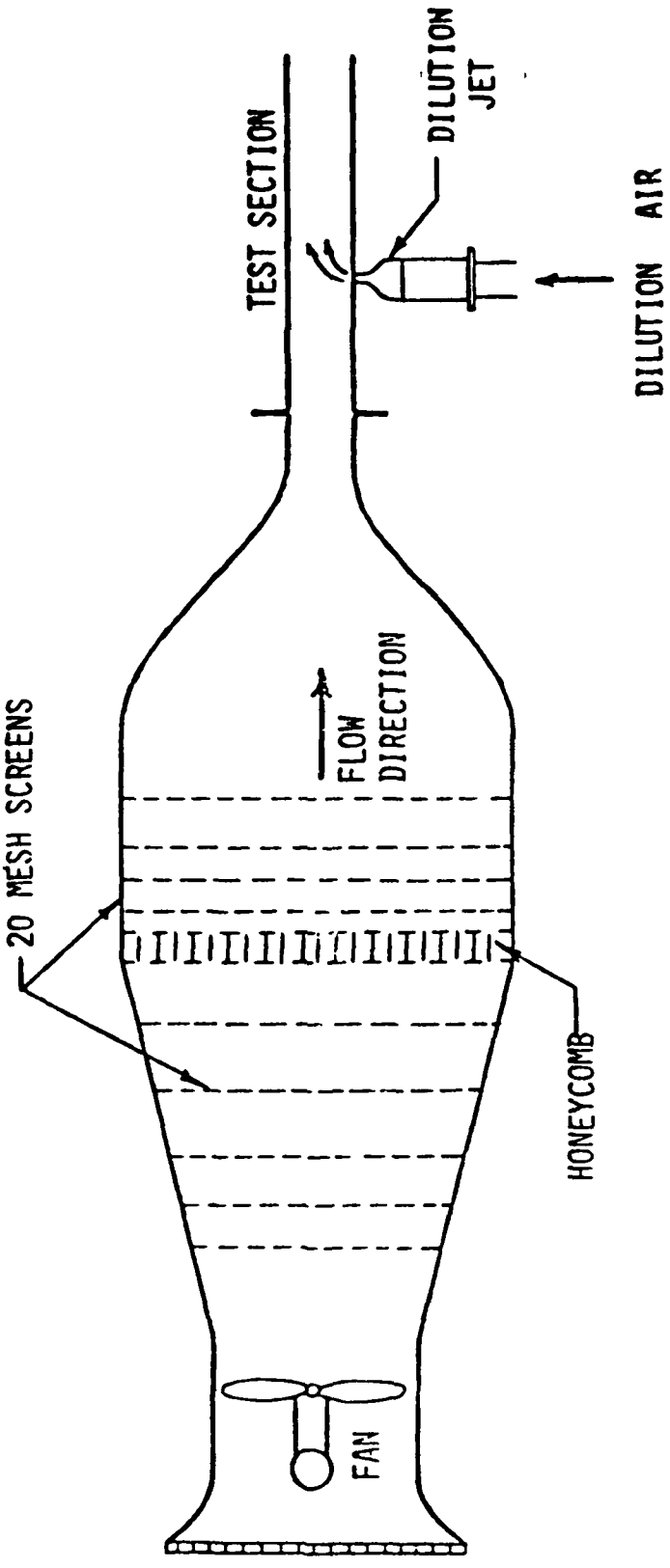

Figure 1. Schematic of Experimental Facility

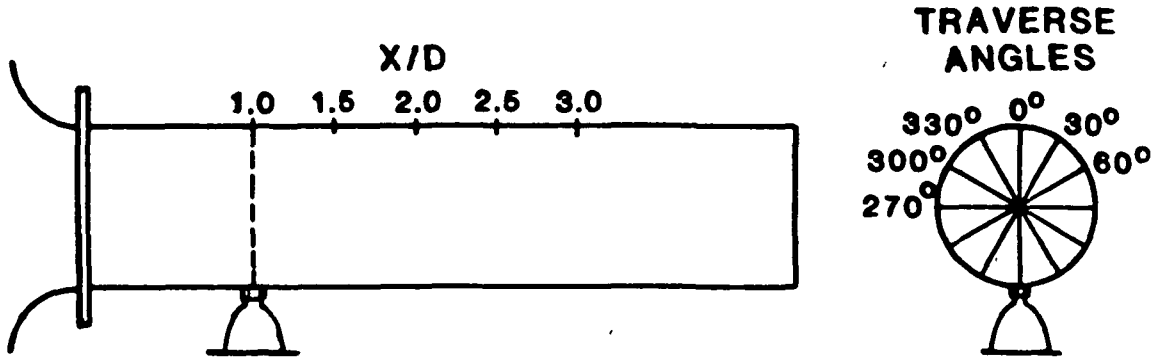

Figure 2. Test Section Geometry

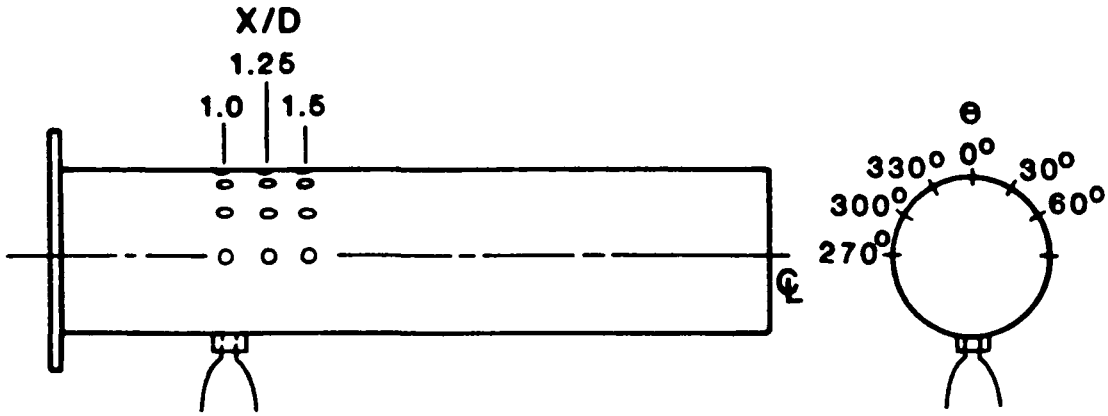

A. FIXED TUBE

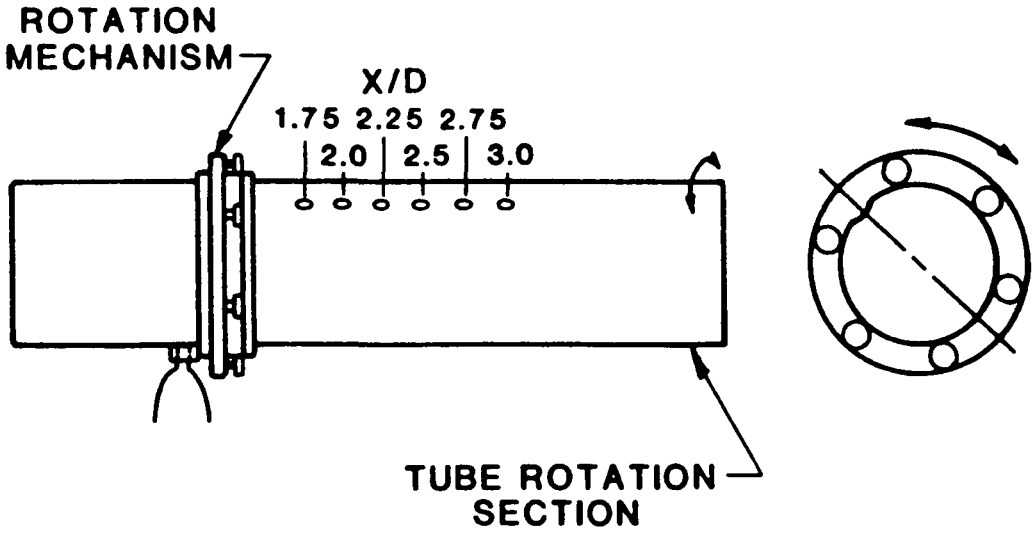

B. ROTATION TUBE

Figure 3. Test Sections

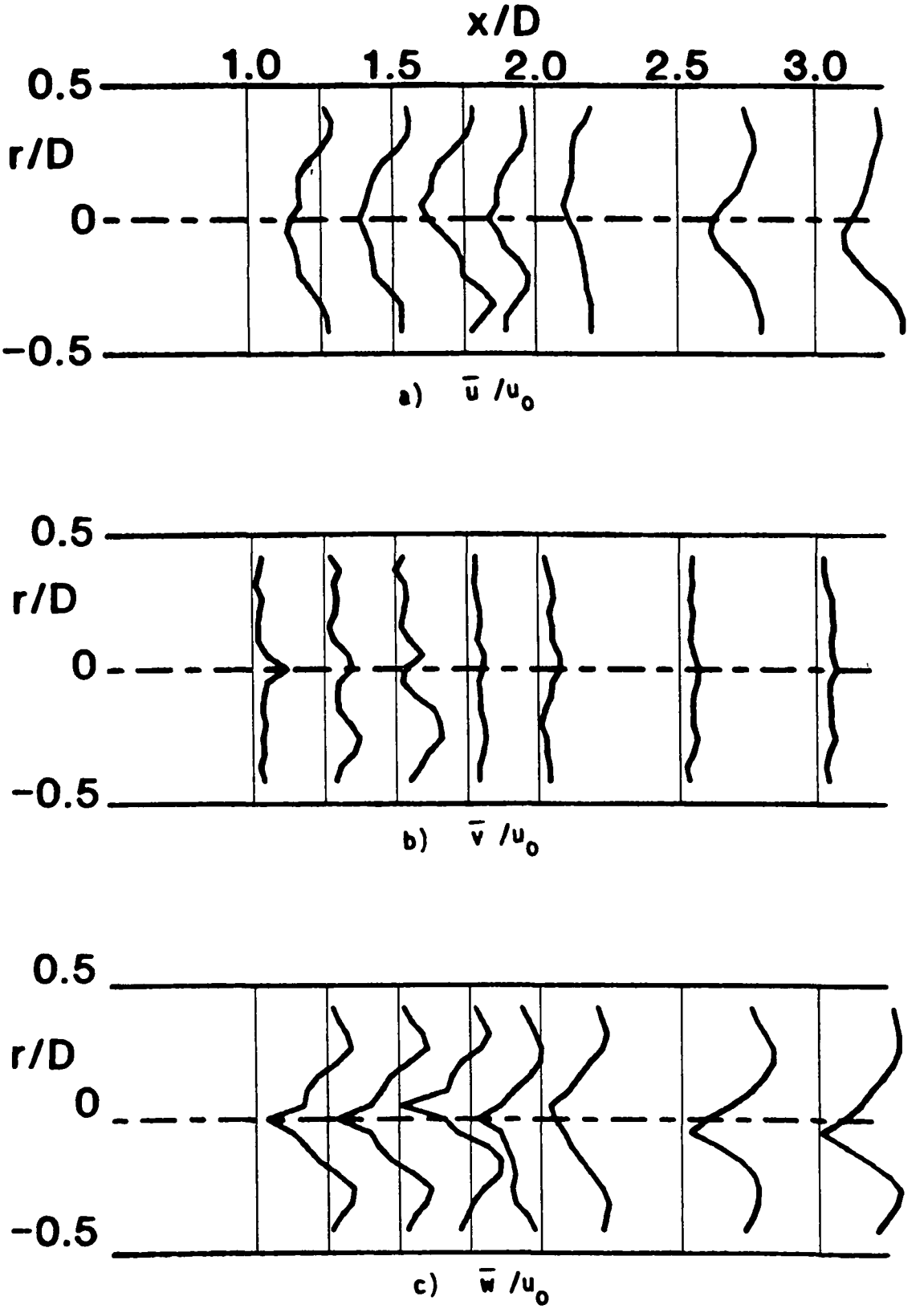

Figure 4. Time-Mean and Turbulent Flowfield (Hot-Wire Data) R = 4, ϕ = 45 Degrees, Traverse Angle θ = 270 Degrees

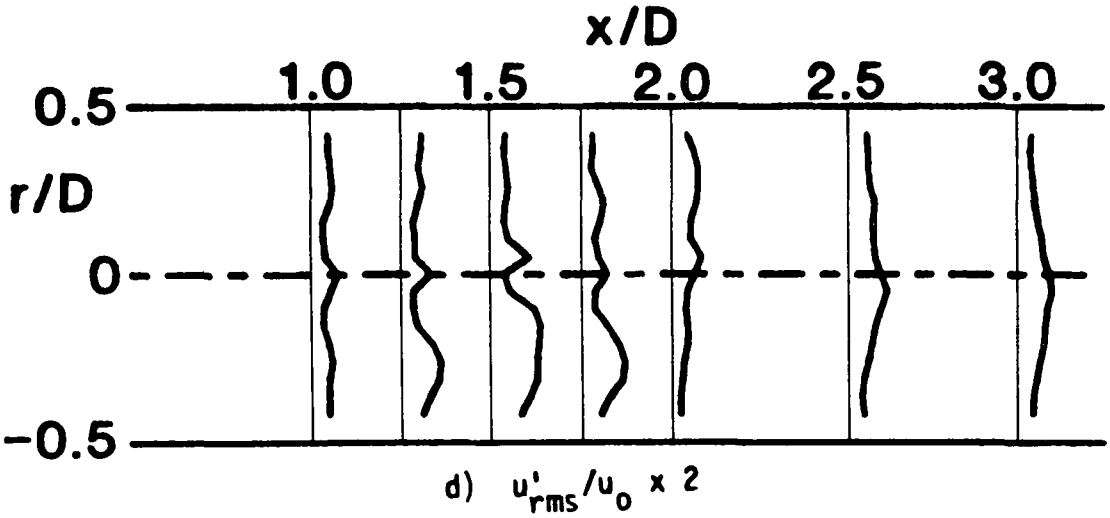

d) $u'_{rms}/u_o \times 2$

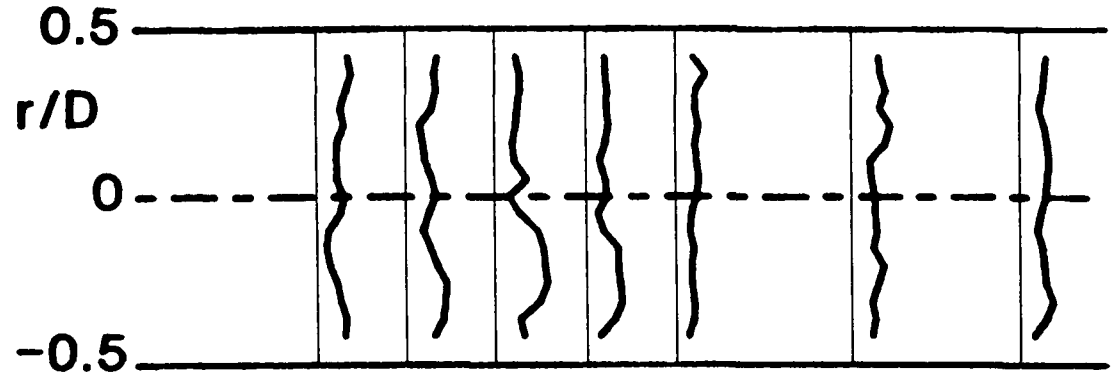

e) $v'_{rms}/u_o \times 2$

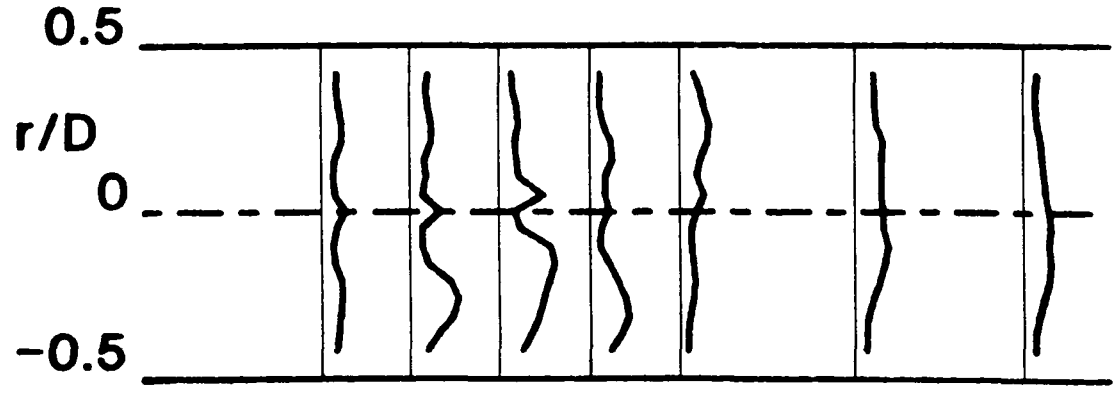

f) $w'_{rms}/u_o \times 2$

Figure 4. (Continued)

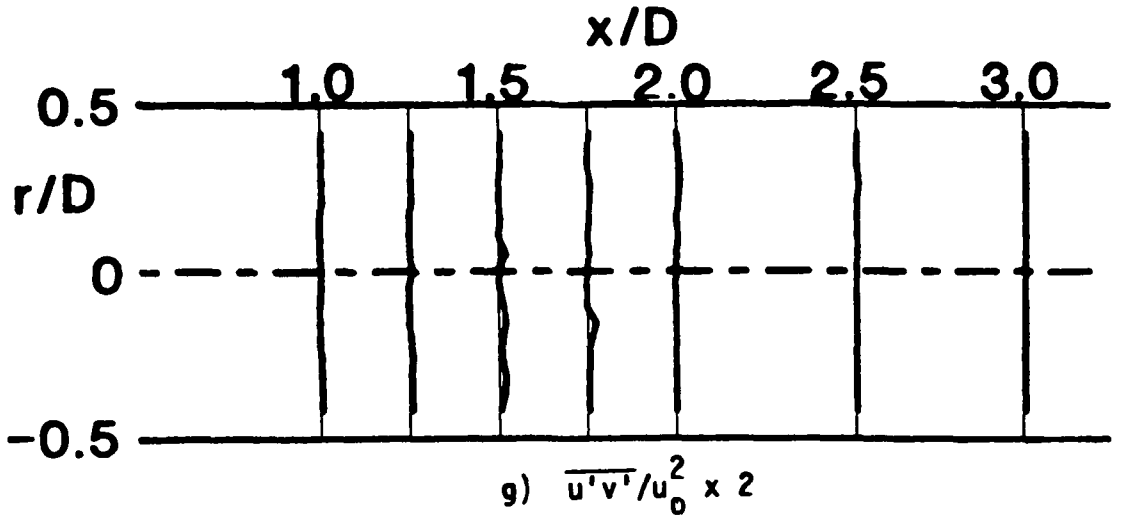

g) $\overline{u'v'}/u_o^2 \times 2$

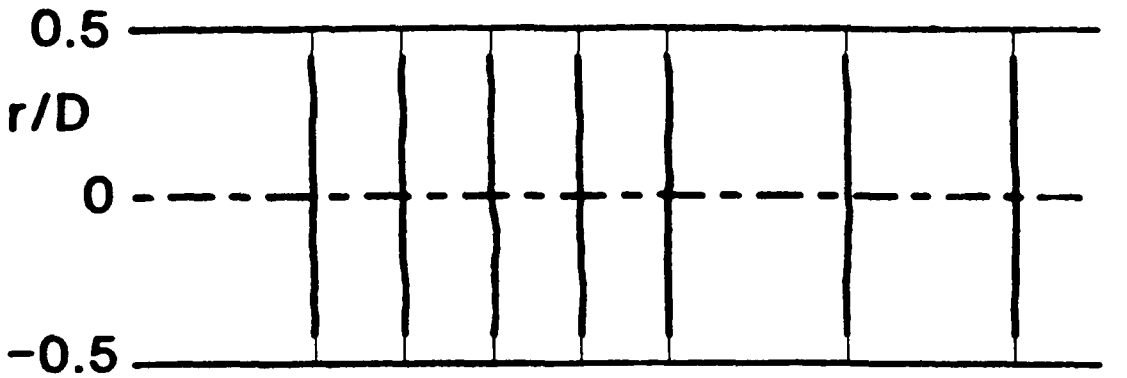

h) $\overline{u'w'}/u_o^2 \times 2$

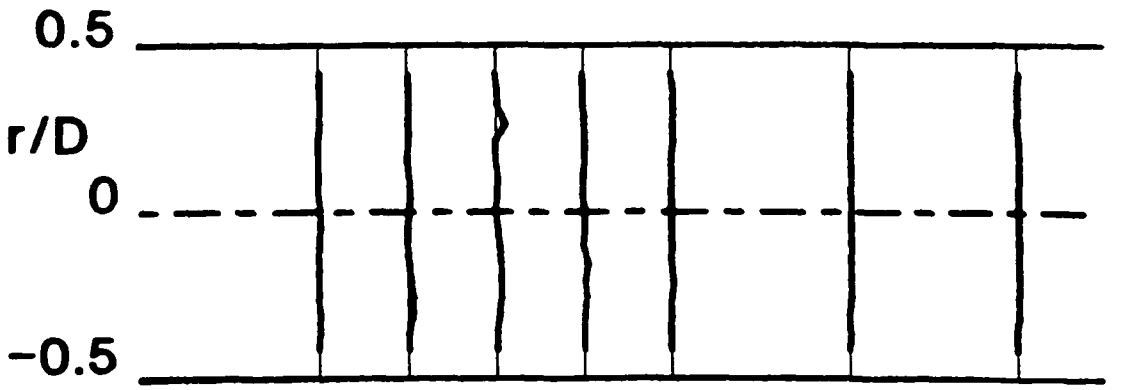

i) $\overline{v'w'}/u_o^2 \times 2$

Figure 4. (Continued)

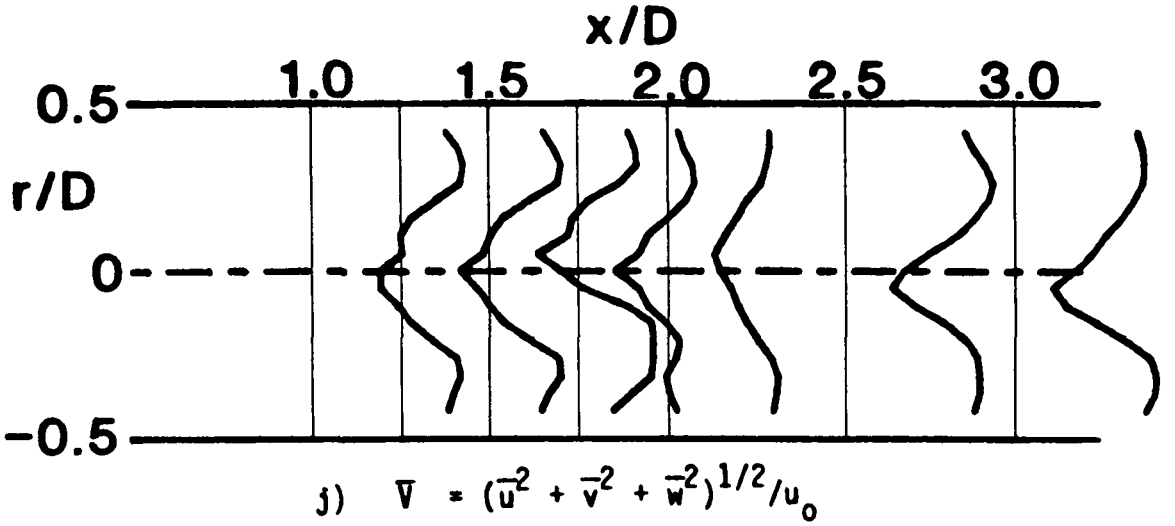

j) $\bar{V} = (\bar{u}^2 + \bar{v}^2 + \bar{w}^2)^{1/2}/u_o$

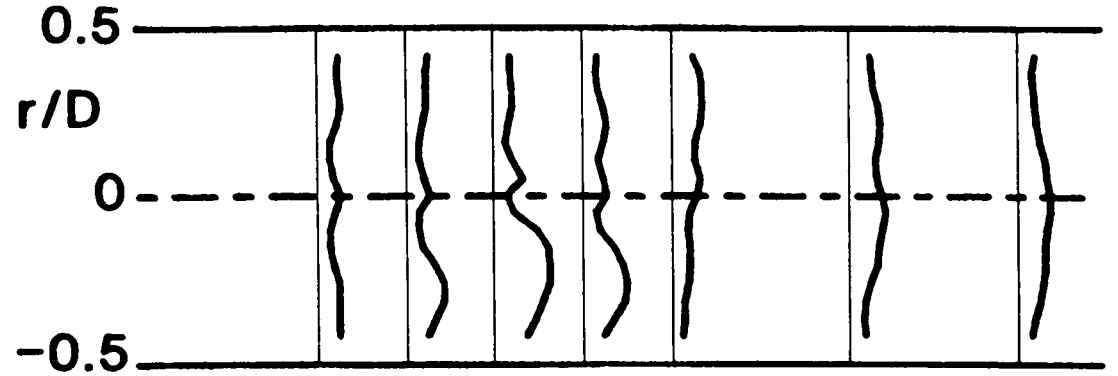

k) $u'_{rms}/\bar{u} \times 2$

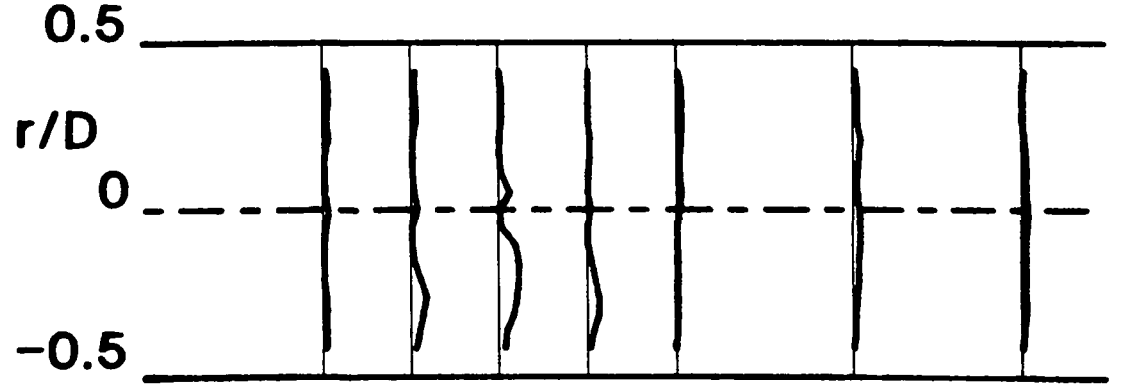

l) $\frac{1}{2}(u'^2_{rms} + v'^2_{rms} + w'^2_{rms})/u_o^2 \times 2$

Figure 4. (Continued)

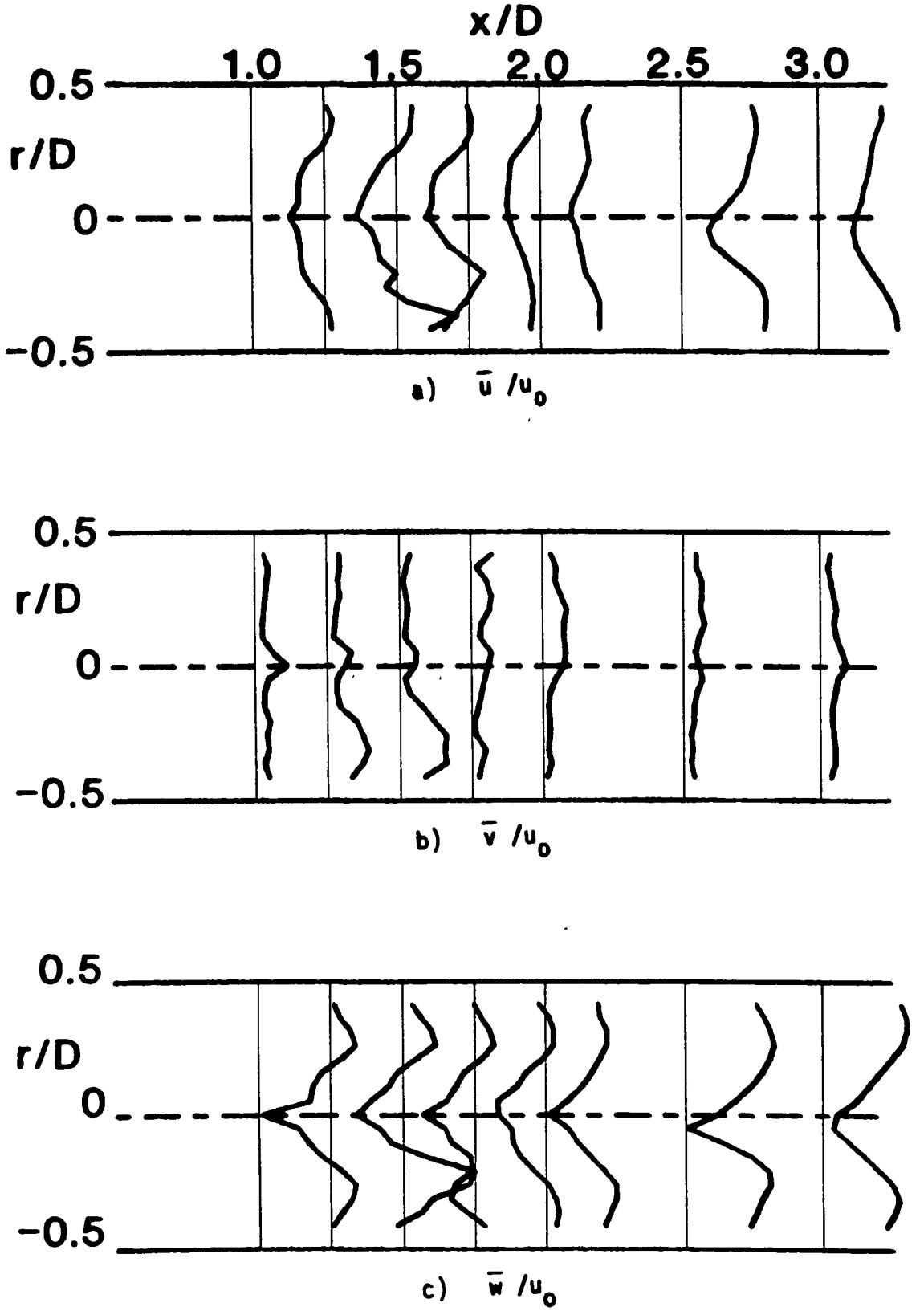

Figure 5. Time-Mean and Turbulent Flowfield (Hot-Wire Data) R = 4, ϕ = 45 Degrees, Traverse Angle θ = 300 Degrees

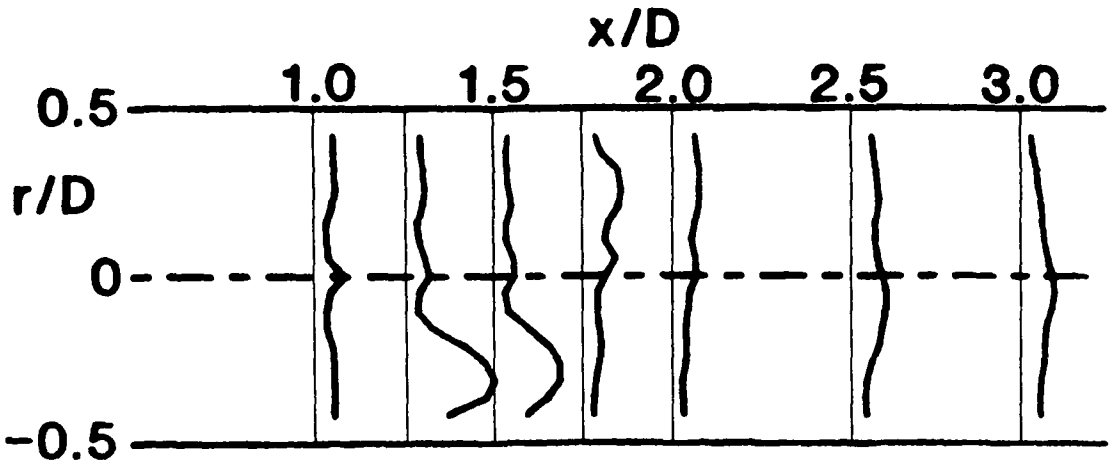

d) u'_{rms}/u_o x 2

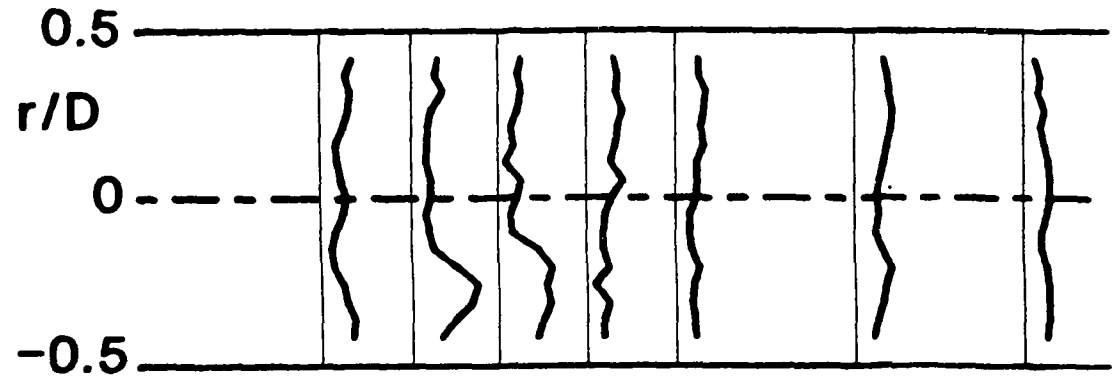

e) v'_{rms}/u_o x 2

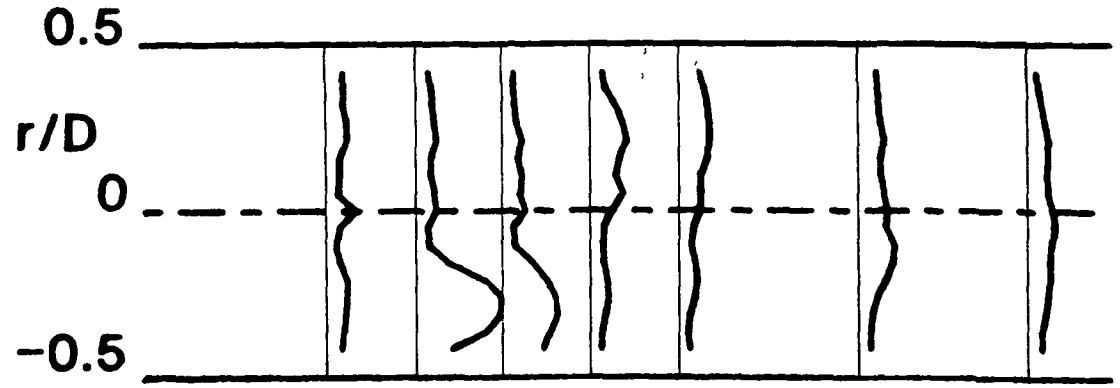

f) w'_{rms}/u_o x 2

Figure 5. (Continued)

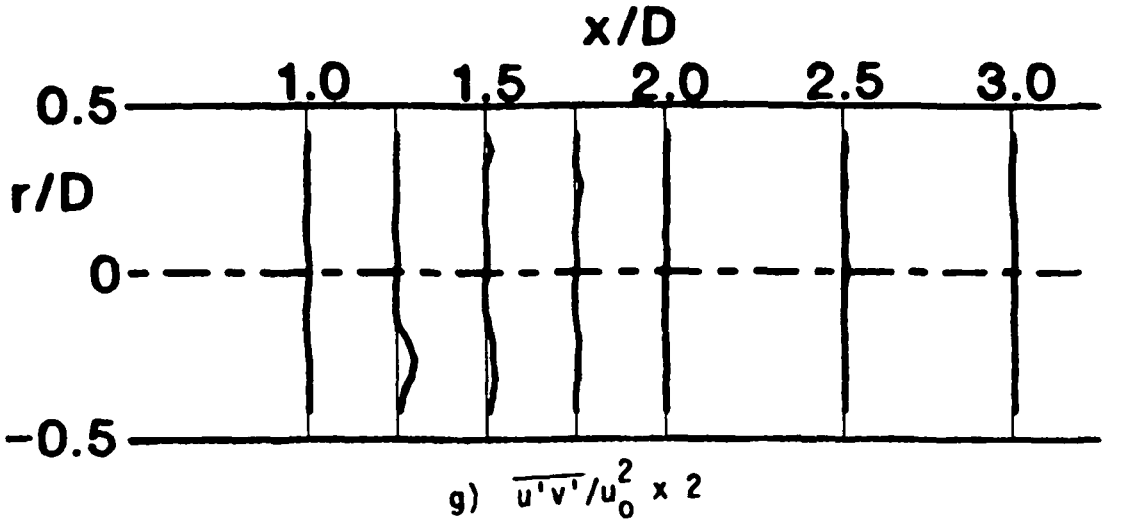

g) $\overline{u'v'}/u_o^2 \times 2$

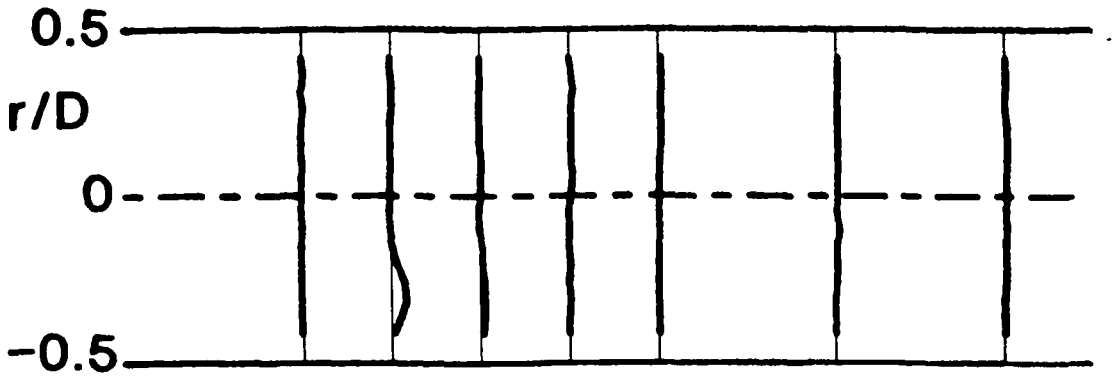

h) $\overline{u'w'}/u_o^2 \times 2$

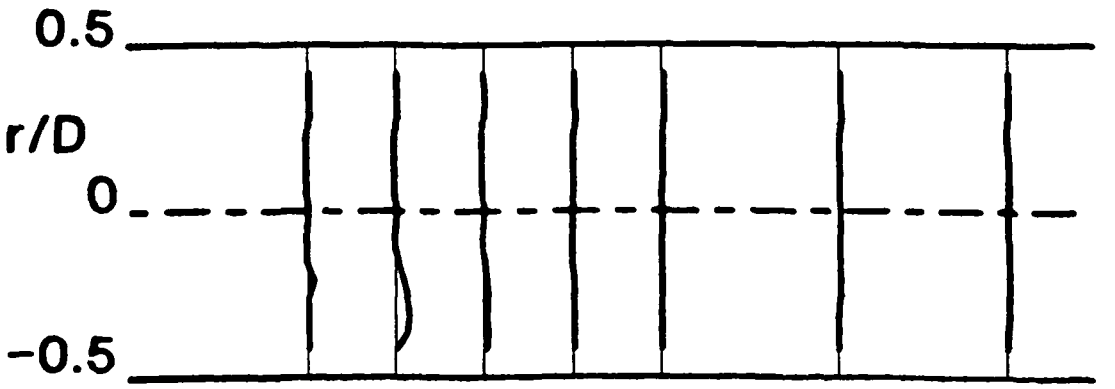

i) $\overline{v'w'}/u_o^2 \times 2$

Figure 5. (Continued)

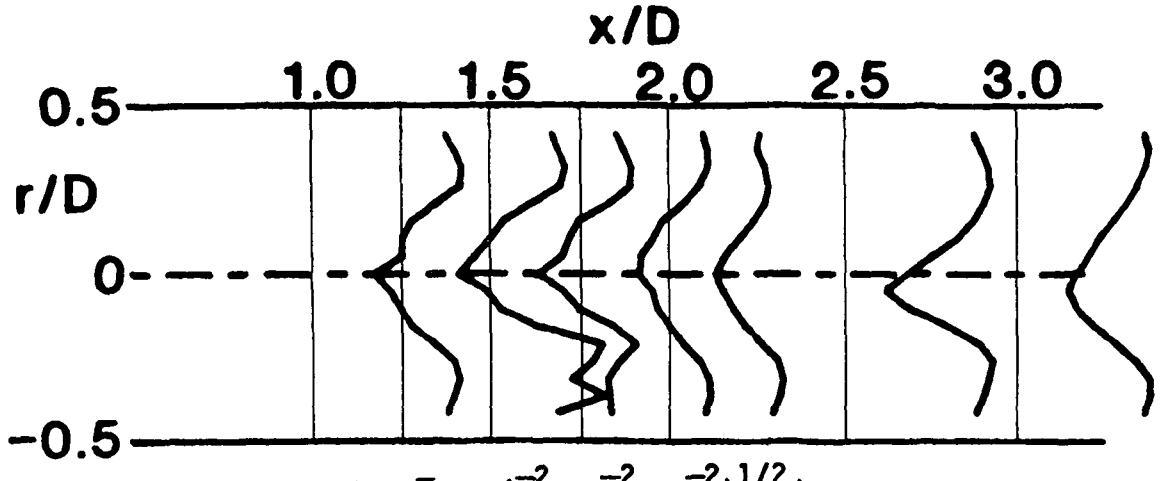

j) $\bar{V} = (\bar{u}^2 + \bar{v}^2 + \bar{w}^2)^{1/2}/u_o$

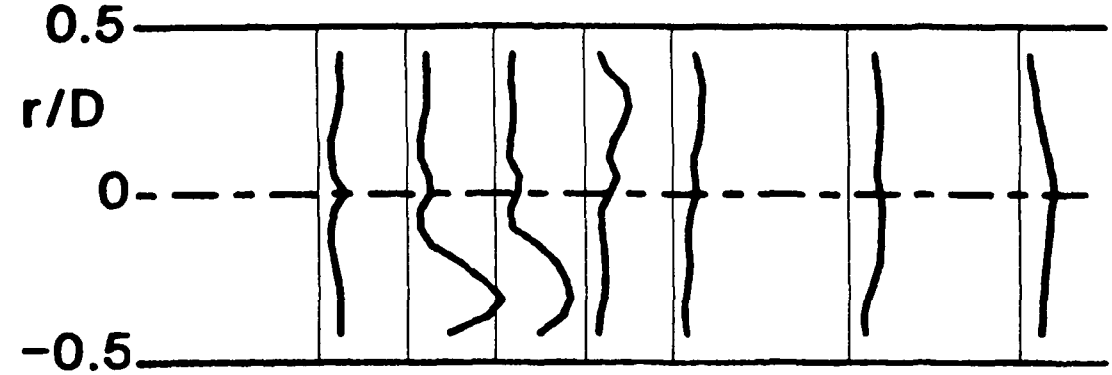

k) $u'_{rms}/\bar{u} \times 2$

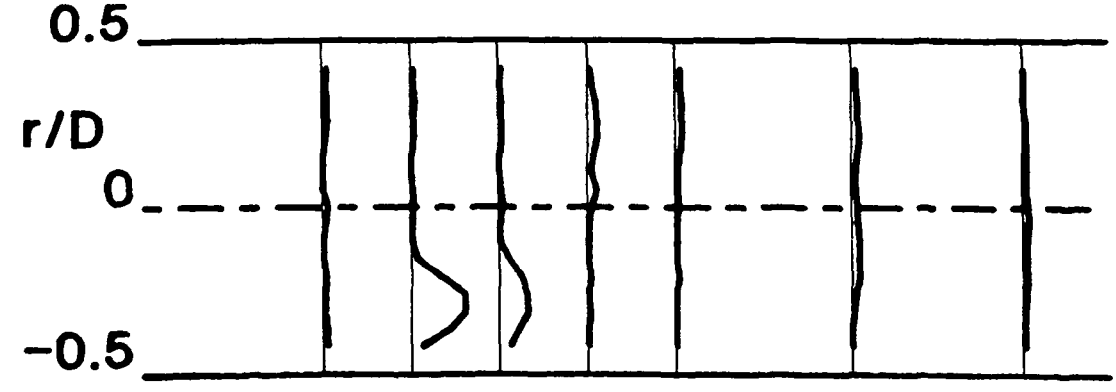

l) $\frac{1}{2}(u'^2_{rms} + v'^2_{rms} + w'^2_{rms})/u_o^2 \times 2$

Figure 5. (Continued)

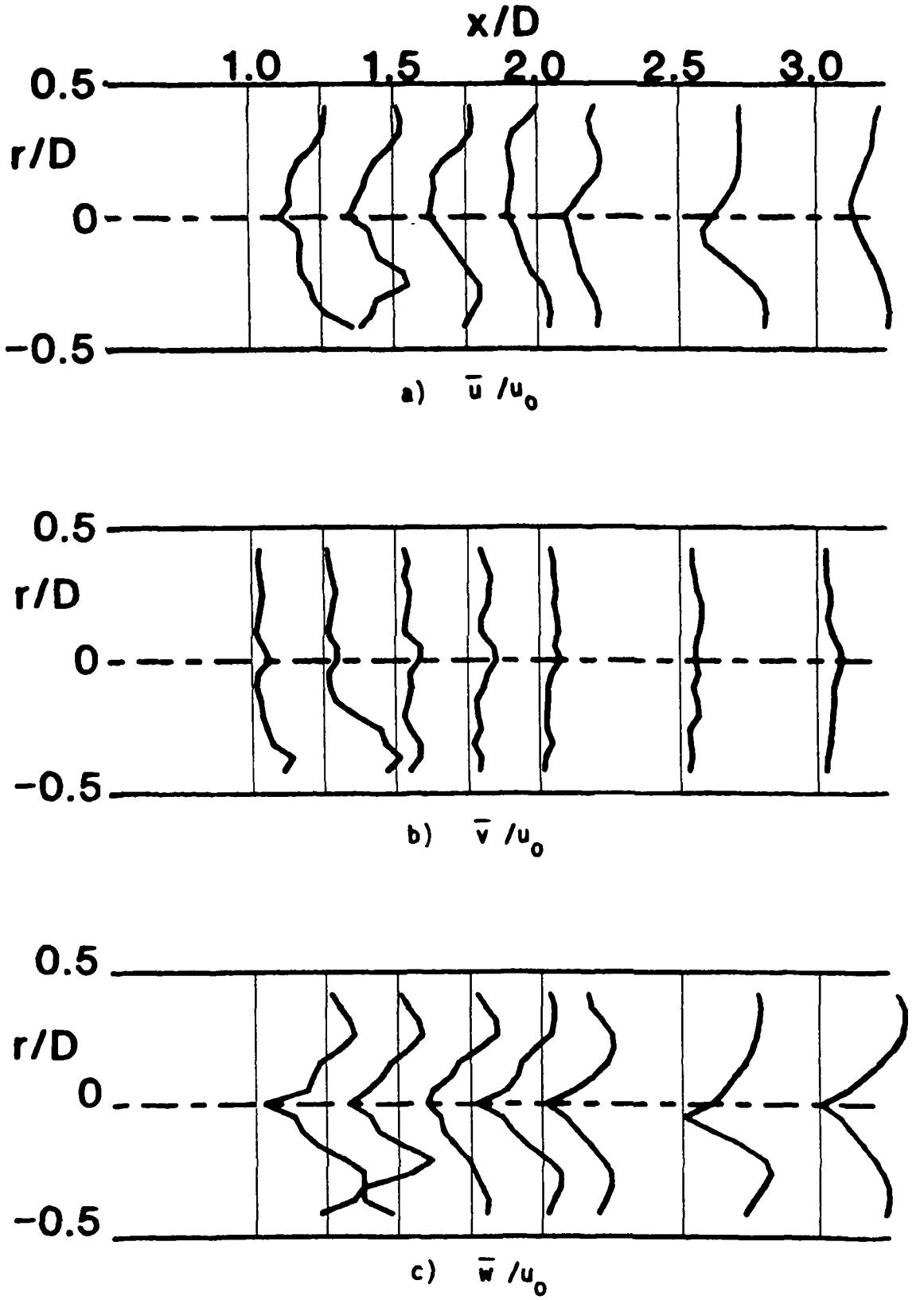

Figure 6. Time-Mean and Turbulent Flowfield (Hot-Wire Data) R = 4, ϕ = 45 Degrees, Traverse Angle θ = 330 Degrees

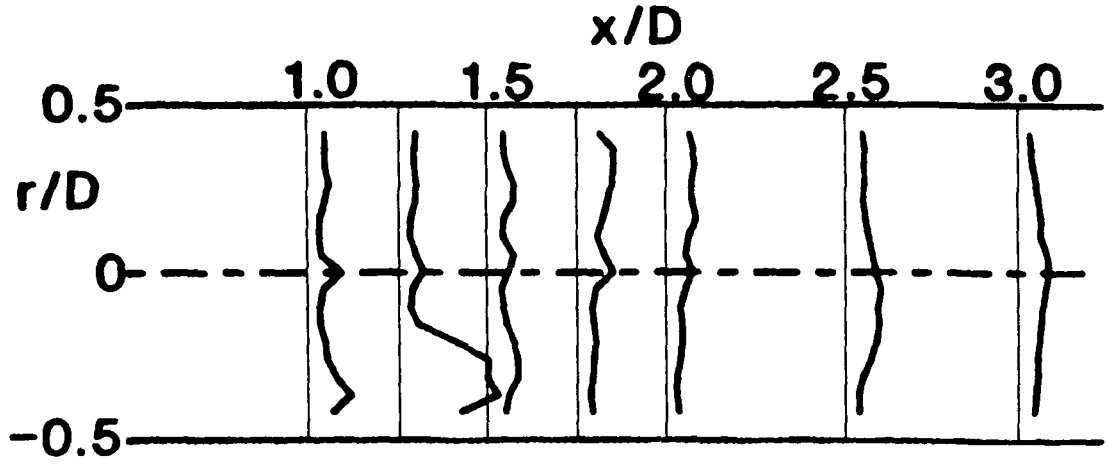

d) u'_{rms}/u_o x 2

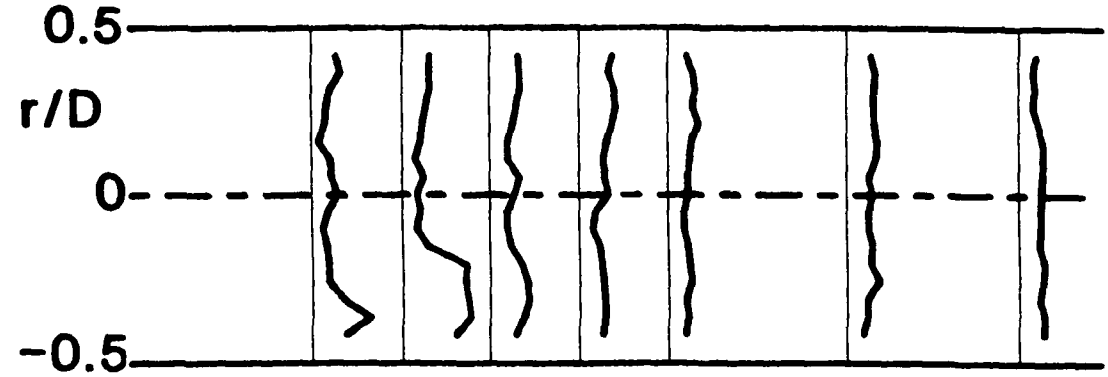

e) v'_{rms}/u_o x 2

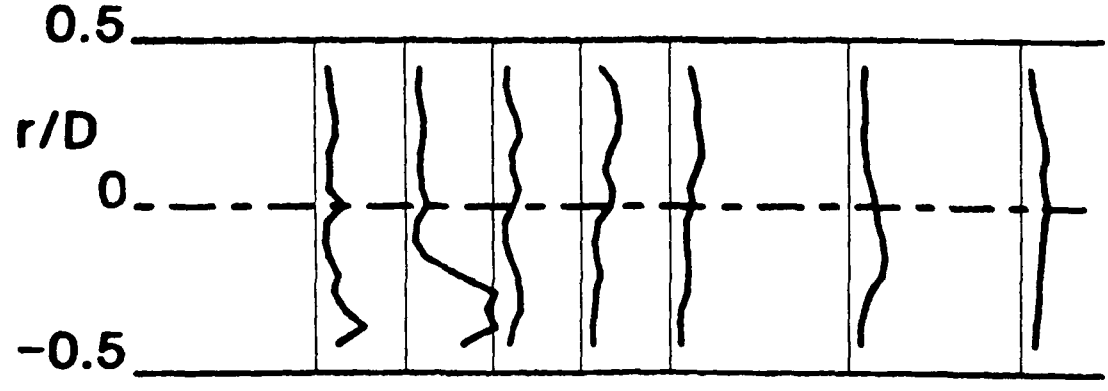

f) w'_{rms}/u_o x 2

Figure 6. (Continued)

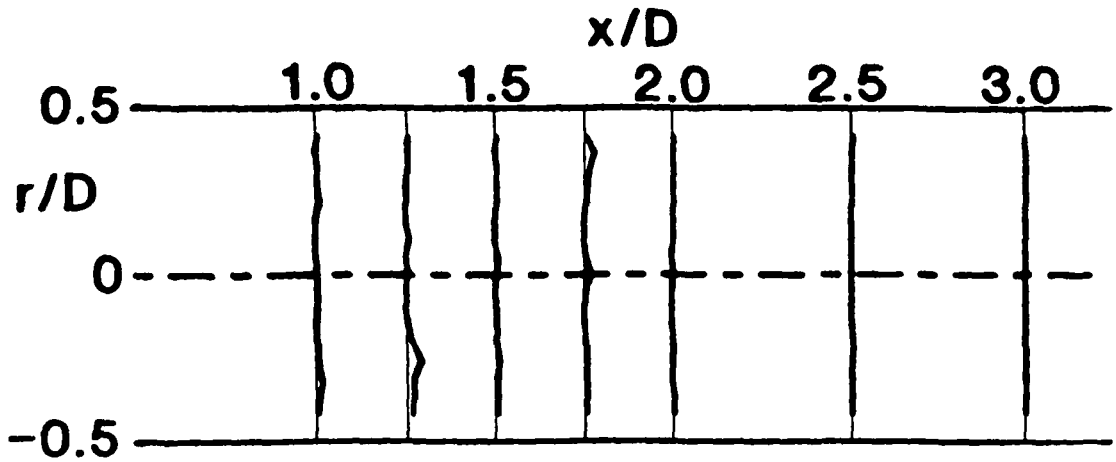

g) $\overline{u'v'}/u_o^2 \times 2$

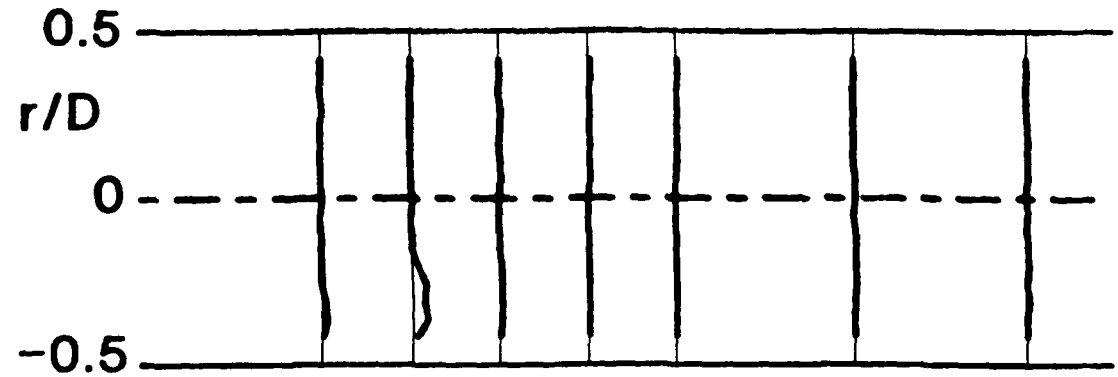

h) $\overline{u'w'}/u_o^2 \times 2$

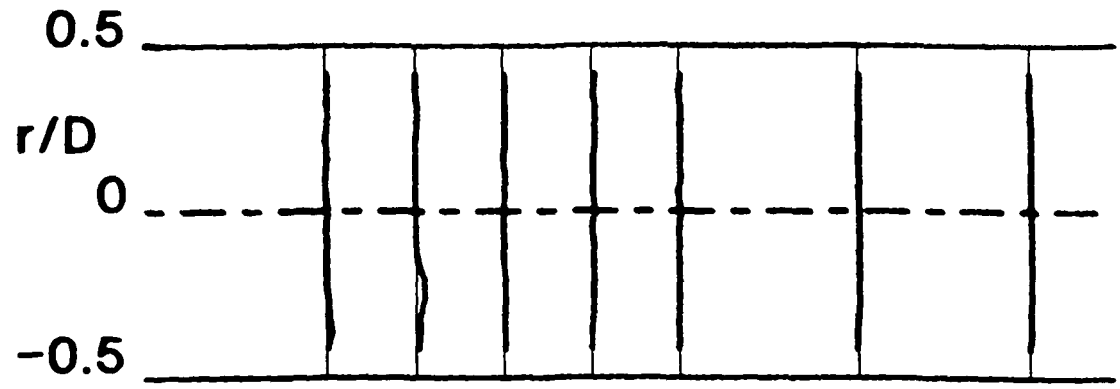

i) $\overline{v'w'}/u_o^2 \times 2$

Figure 6. (Continued)

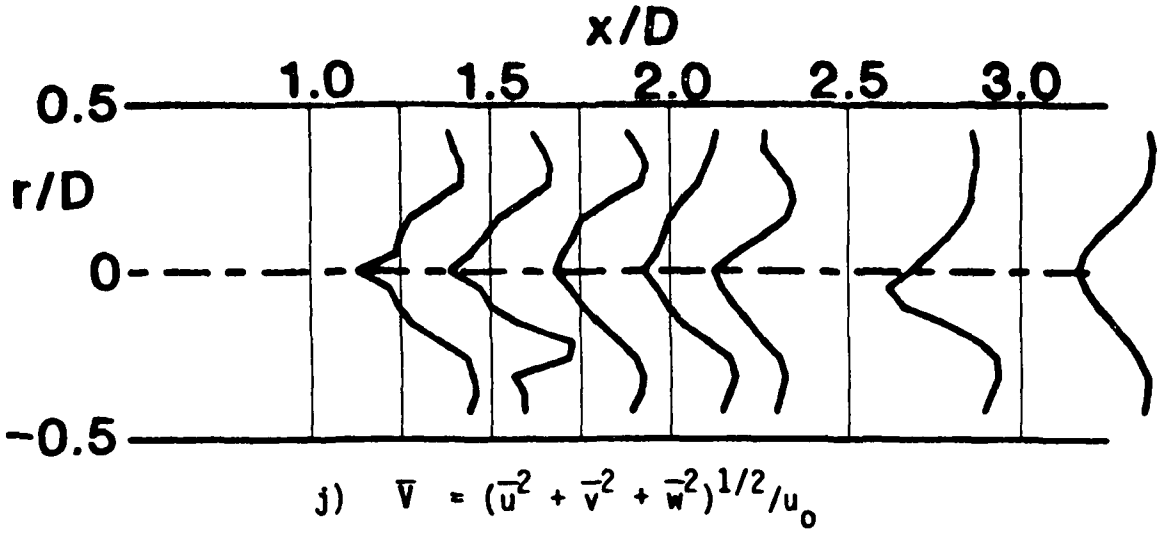

j) $\bar{V} = (\bar{u}^2 + \bar{v}^2 + \bar{w}^2)^{1/2}/u_o$

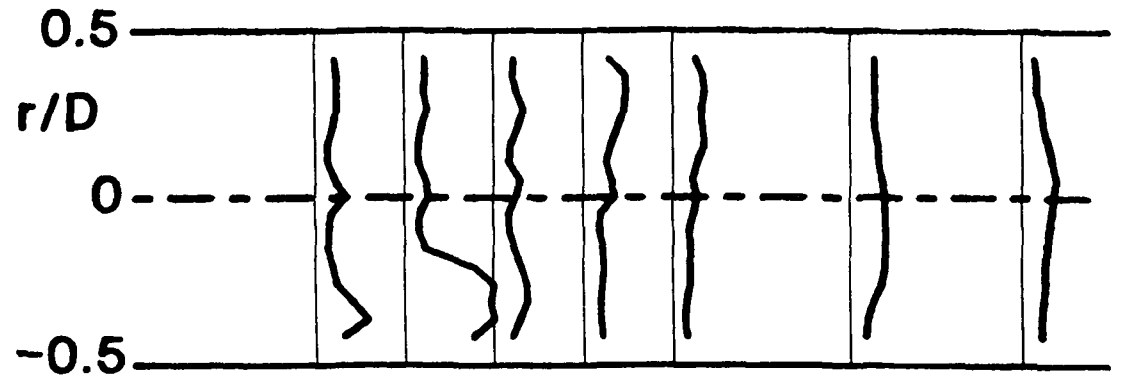

k) $u'_{rms}/\bar{u} \times 2$

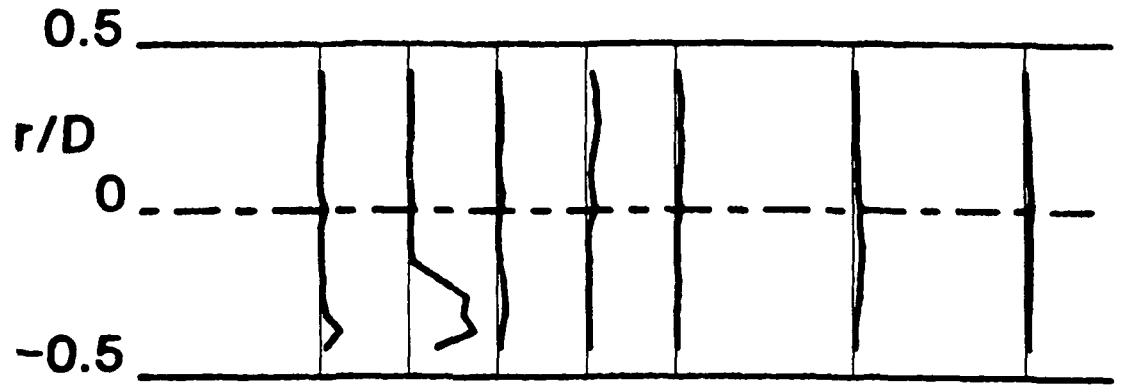

l) $\frac{1}{2}(u'_{rms}{}^2 + v'_{rms}{}^2 + w'_{rms}{}^2)/u_o^2 \times 2$

Figure 6. (Continued)

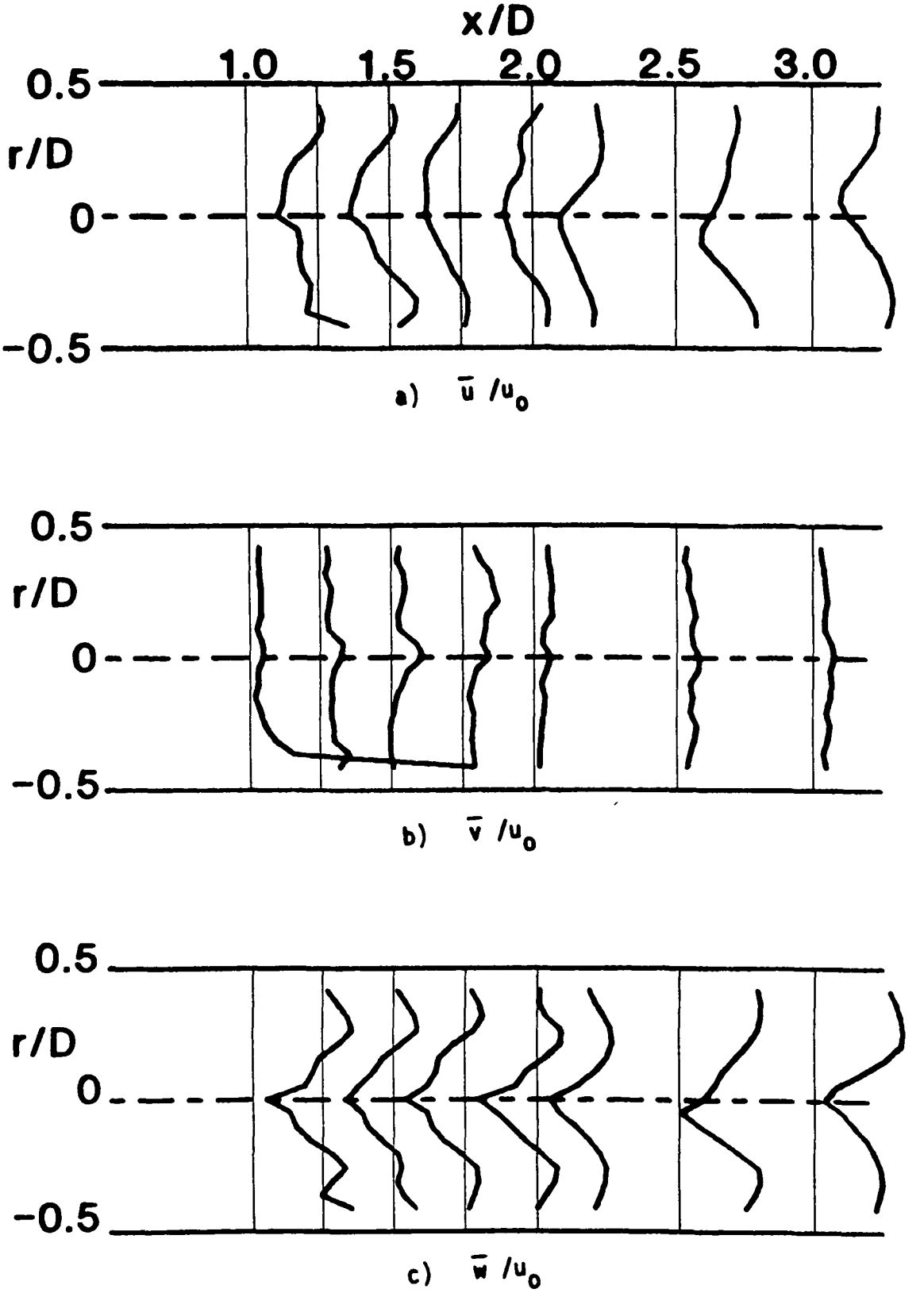

Figure 7. Time-Mean and Turbulent Flowfield (Hot-Wire Data) R = 4, ϕ = 45 Degrees, Traverse Angle θ = 0 Degrees

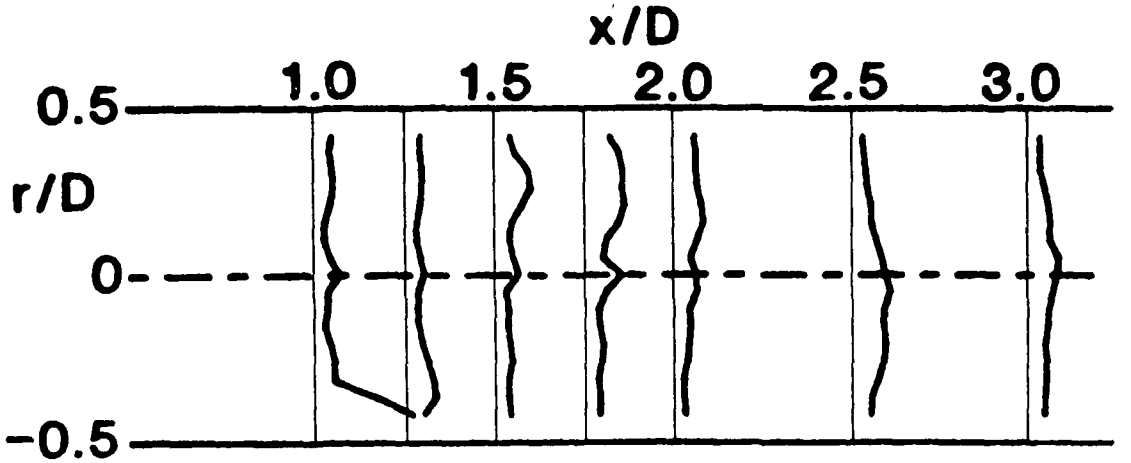

d) u'_{rms}/u_o x 2

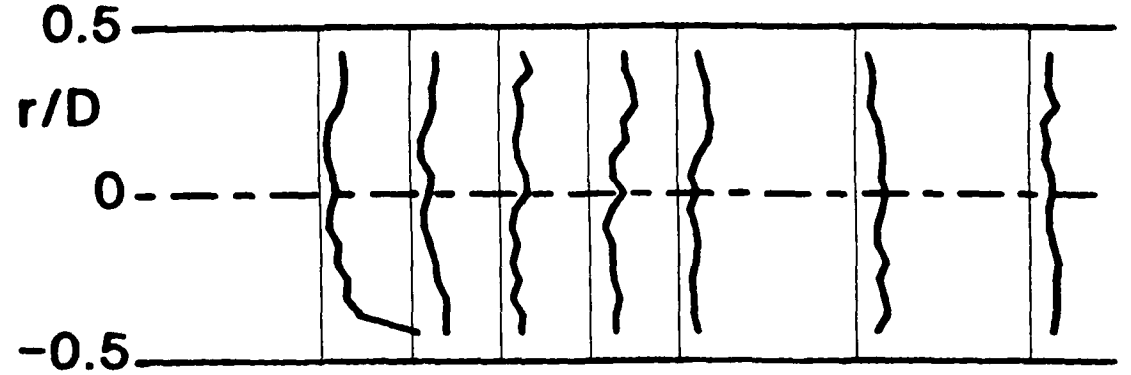

e) v'_{rms}/u_o x 2

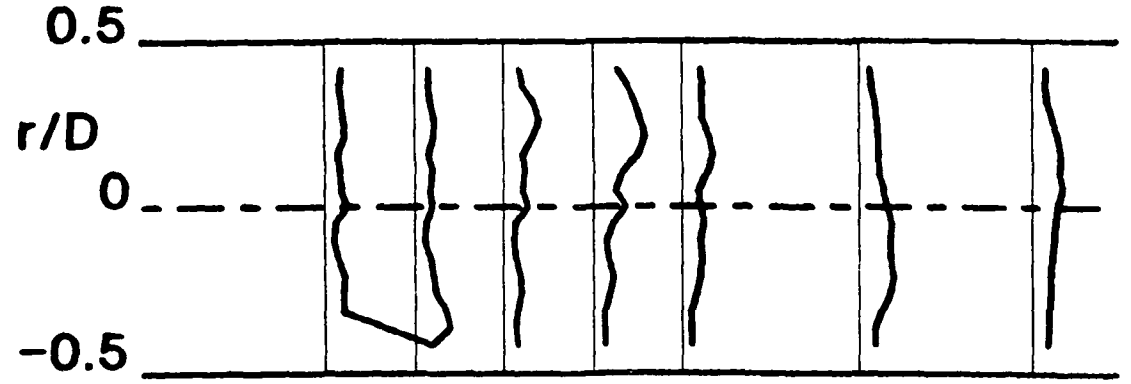

f) w'_{rms}/u_o x 2

Figure 7. (Continued)

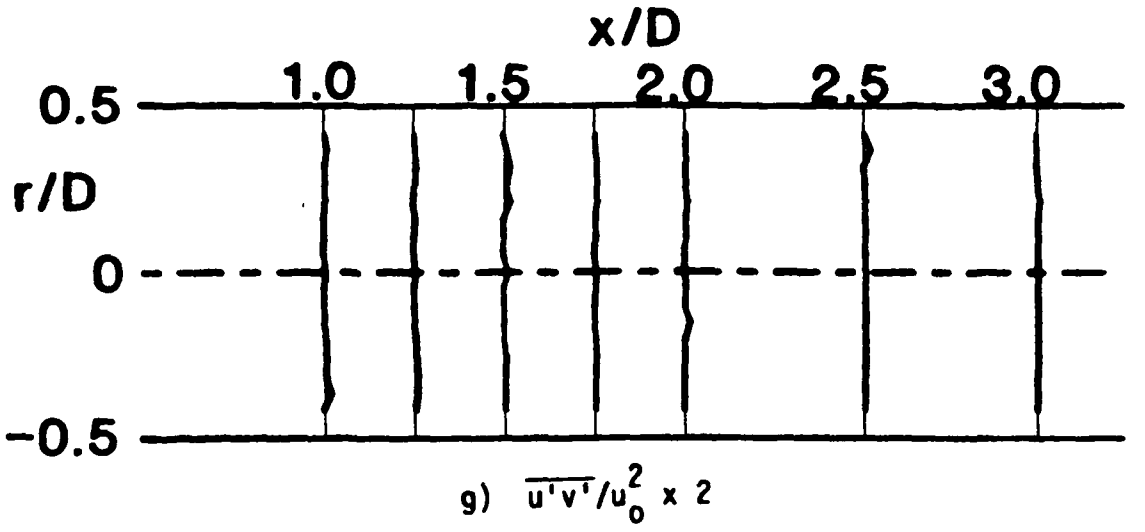

g) $\overline{u'v'}/u_o^2 \times 2$

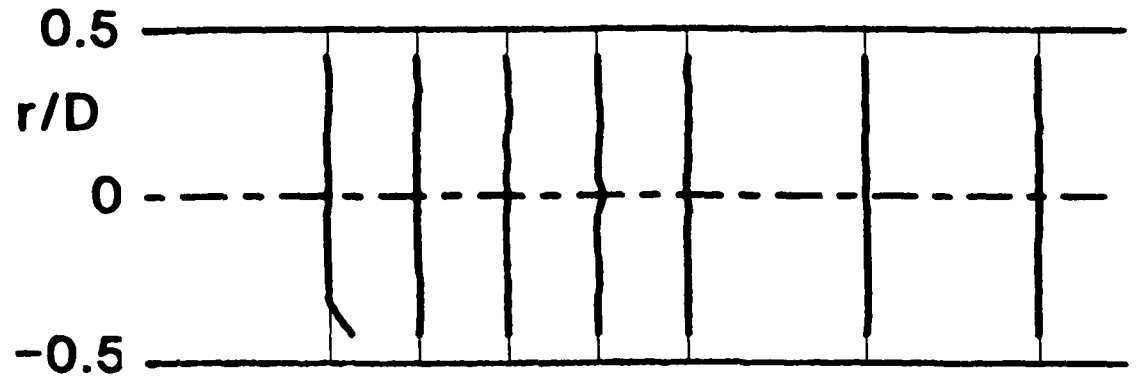

h) $\overline{u'w'}/u_o^2 \times 2$

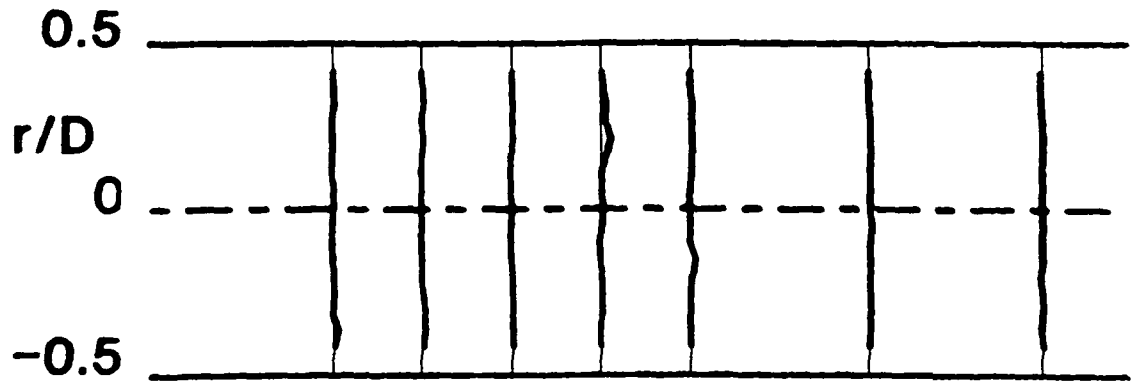

i) $\overline{v'w'}/u_o^2 \times 2$

Figure 7. (Continued)

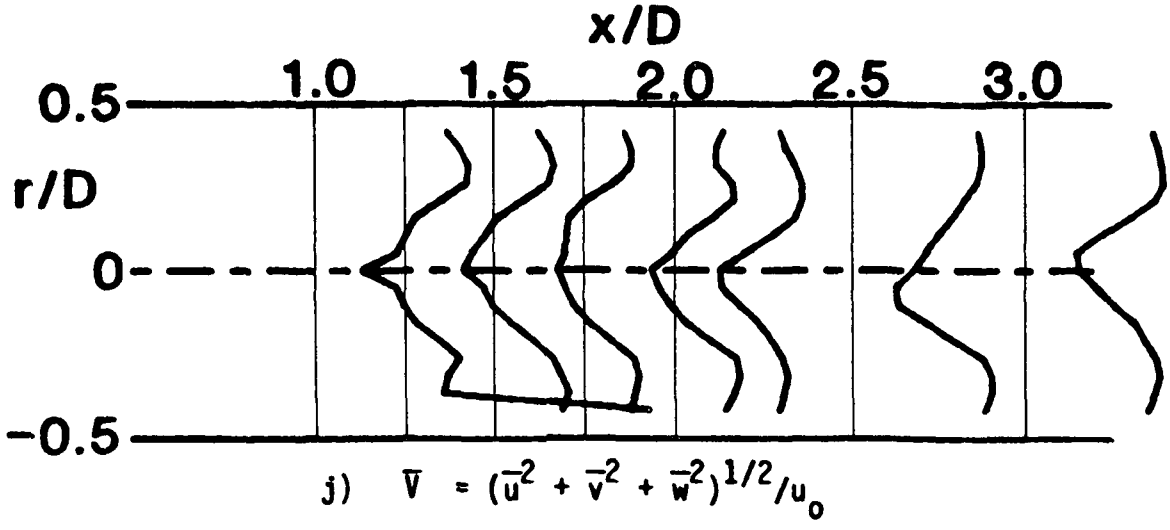

j) $\bar{V} = (\bar{u}^2 + \bar{v}^2 + \bar{w}^2)^{1/2}/u_o$

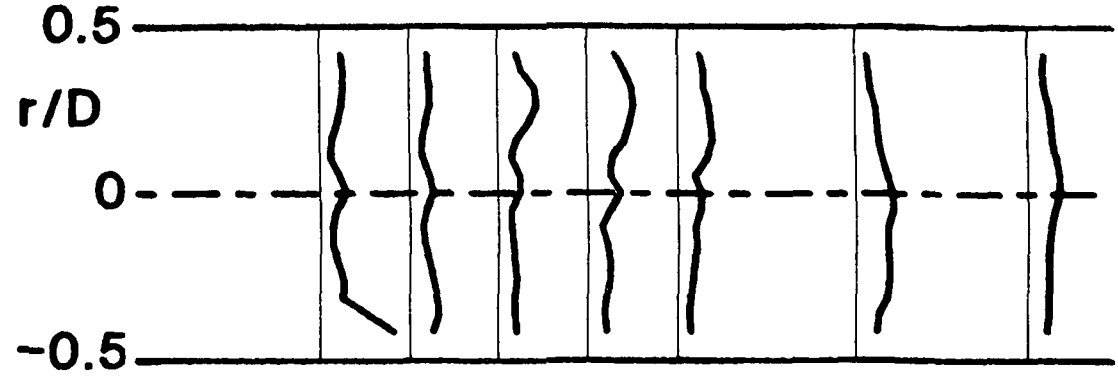

k) $u'_{rms}/\bar{u} \times 2$

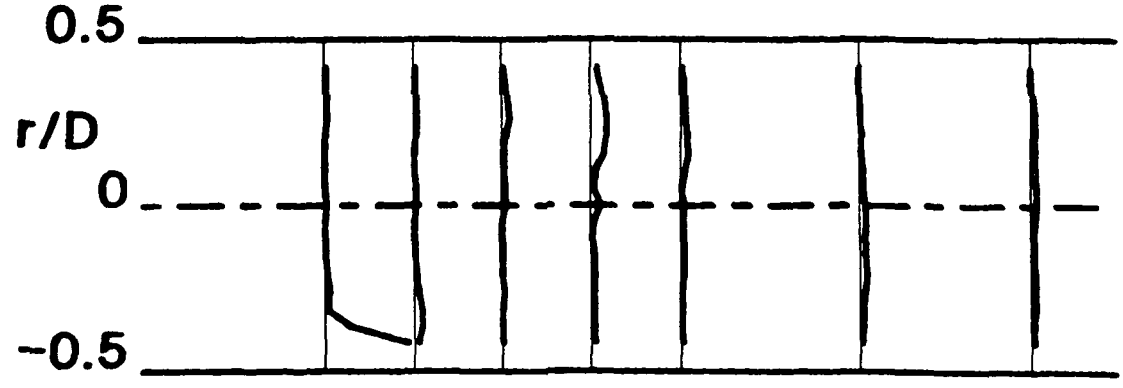

l) $\frac{1}{2}(u'^2_{rms} + v'^2_{rms} + w'^2_{rms})/u_o^2 \times 2$

Figure 7. (Continued)

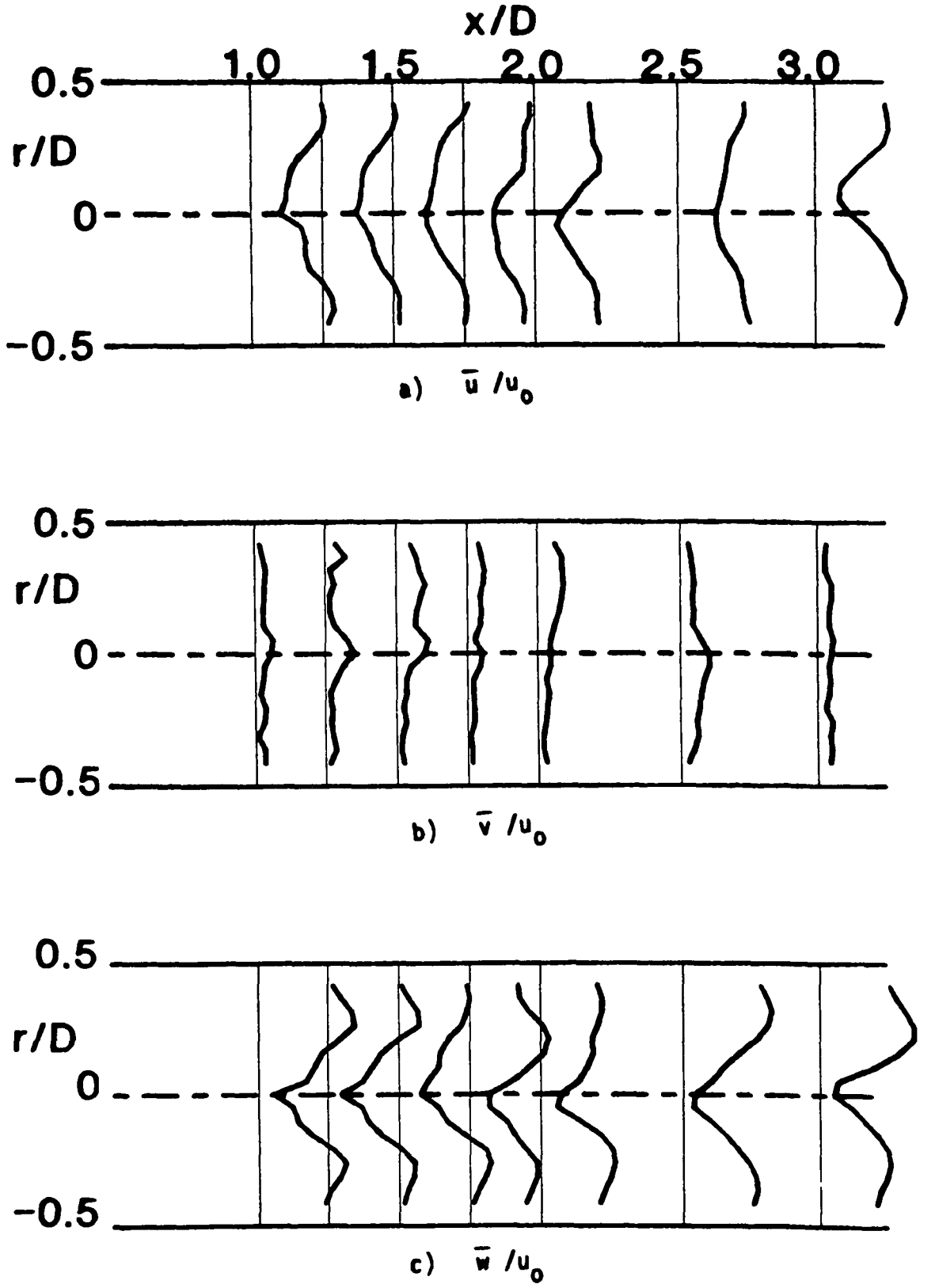

Figure 8. Time-Mean and Turbulent Flowfield (Hot-Wire Data) R = 4, ϕ = 45 Degrees, Traverse Angle θ = 30 Degrees

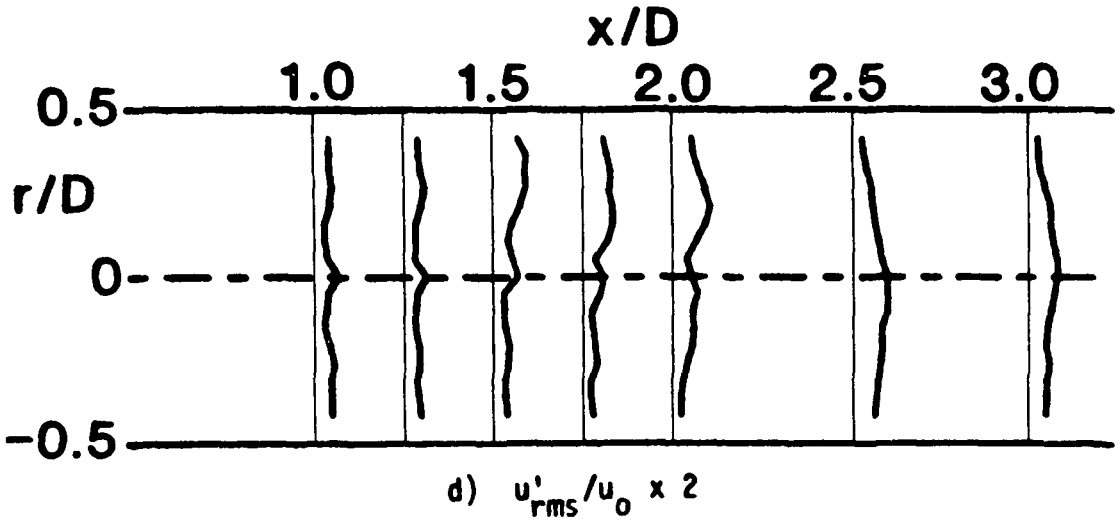

d) u'_{rms}/u_o x 2

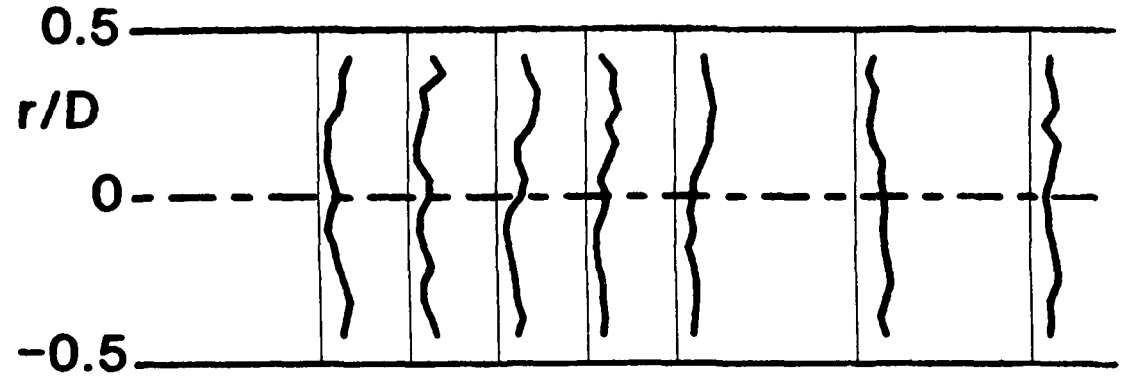

e) v'_{rms}/u_o x 2

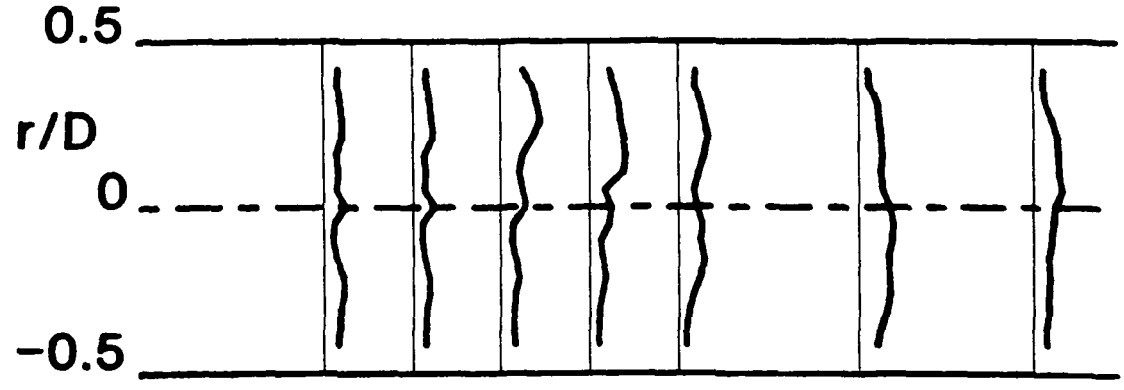

f) w'_{rms}/u_o x 2

Figure 8. (Continued)

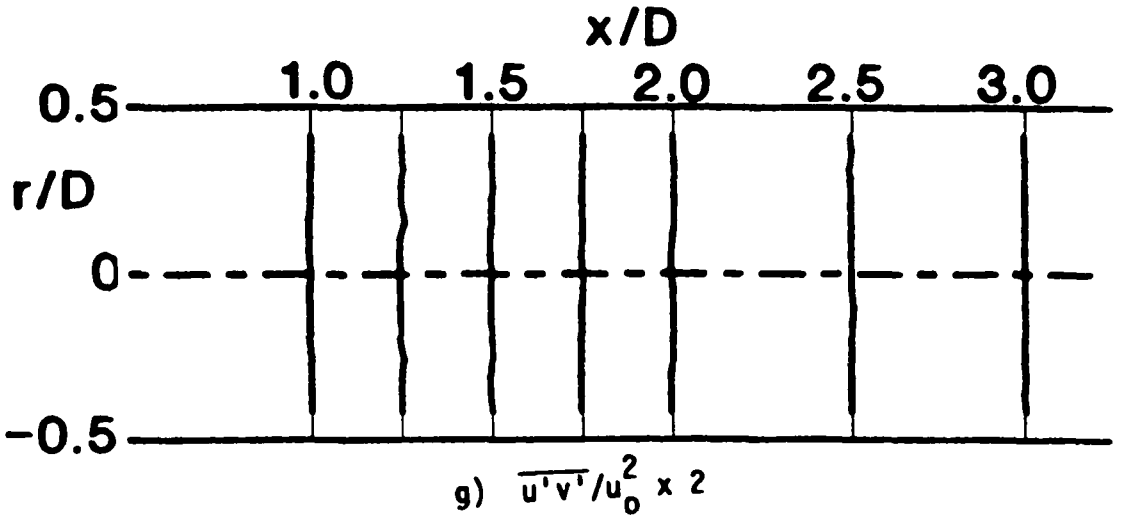

g) $\overline{u'v'}/u_o^2 \times 2$

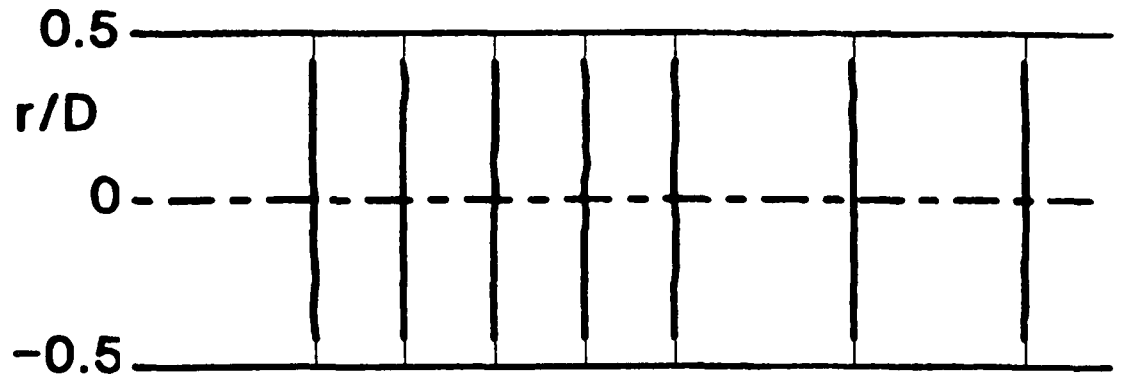

h) $\overline{u'w'}/u_o^2 \times 2$

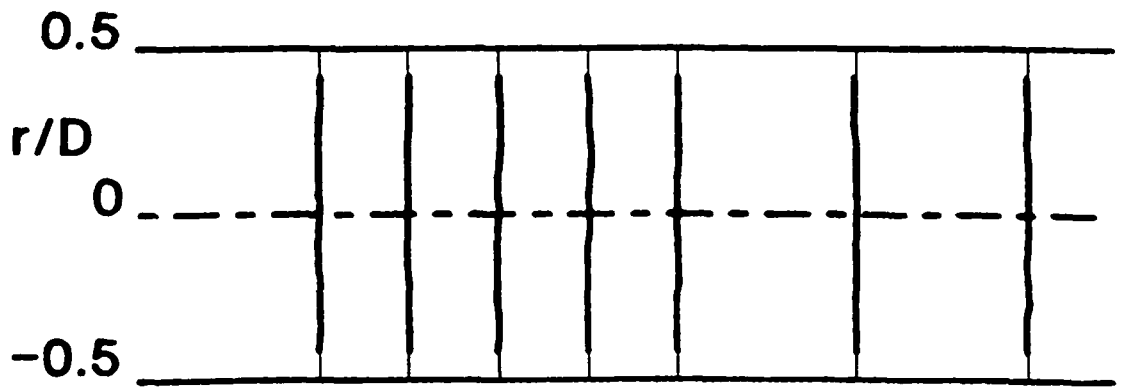

i) $\overline{v'w'}/u_o^2 \times 2$

Figure 8. (Continued)

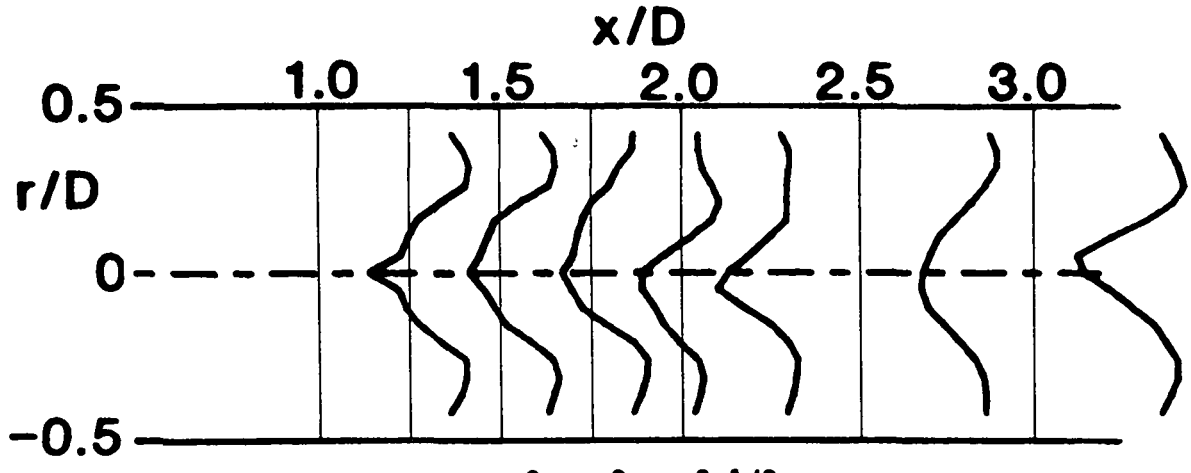

j) $\bar{V} = (\bar{u}^2 + \bar{v}^2 + \bar{w}^2)^{1/2}/u_o$

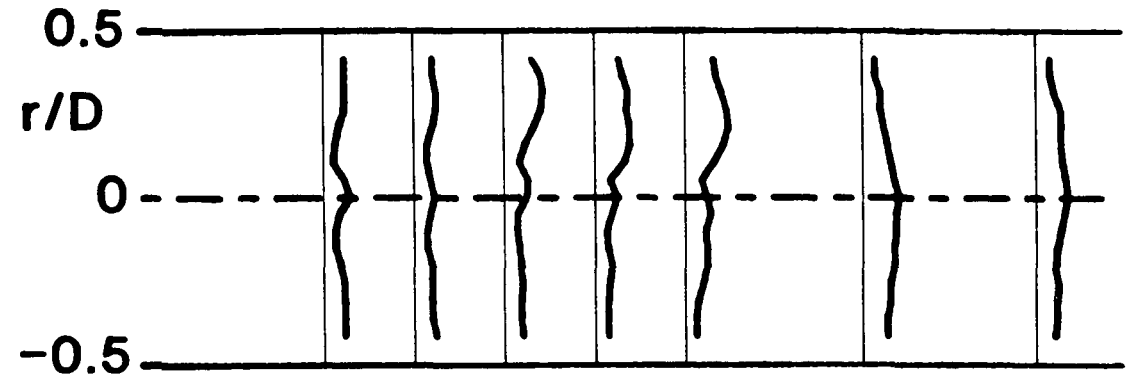

k) $u'_{rms}/\bar{u} \times 2$

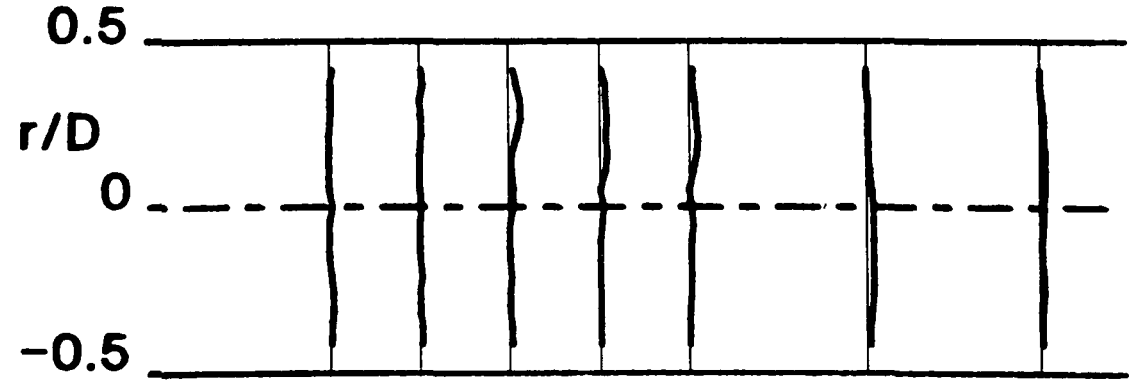

l) $\frac{1}{2}(u'^2_{rms} + v'^2_{rms} + w'^2_{rms})/u_o^2 \times 2$

Figure 8. (Continued)

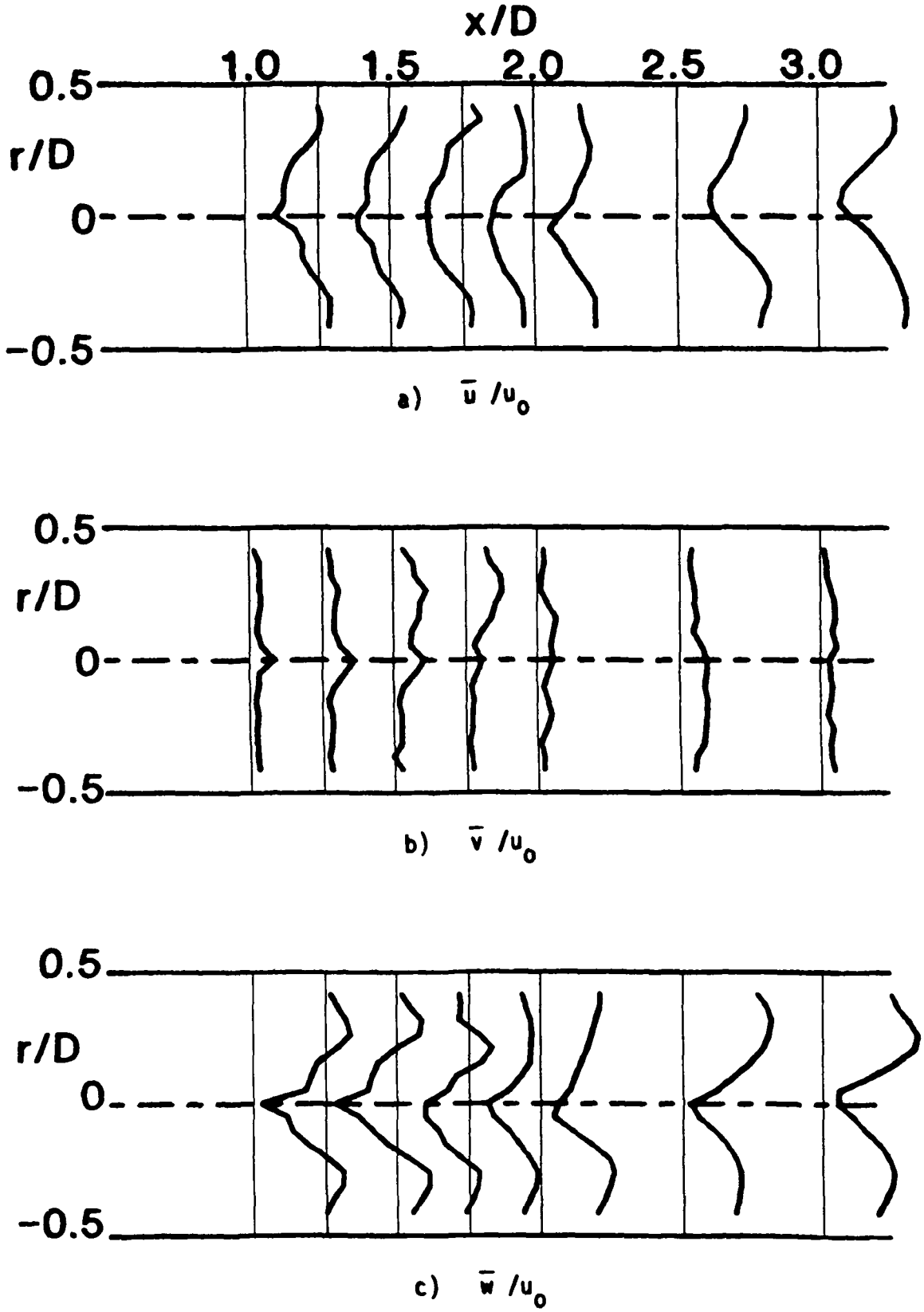

Figure 9. Time-Mean and Turbulent Flowfield (Hot-Wire Data) R = 4, ϕ = 45 Degrees, Traverse Angle θ = 60 Degrees

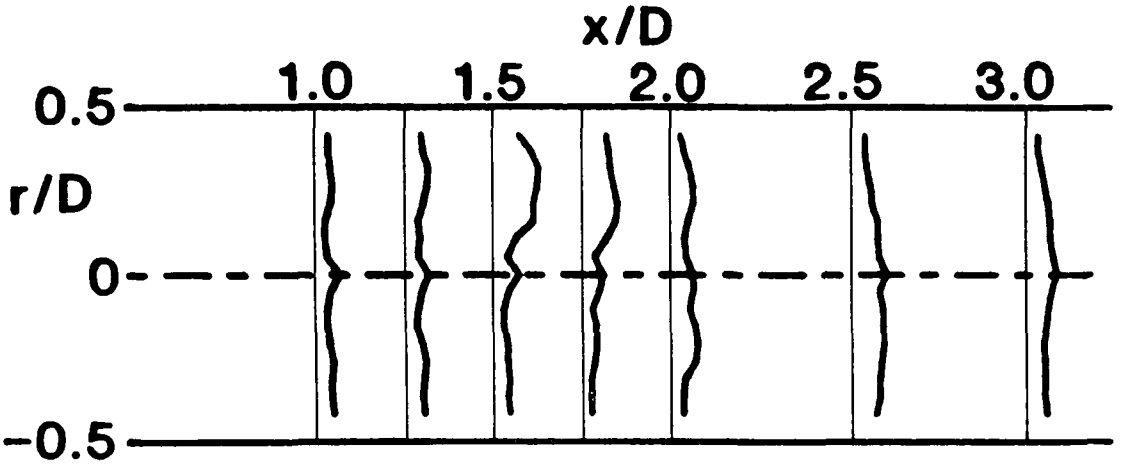

d) u'_{rms}/u_o x 2

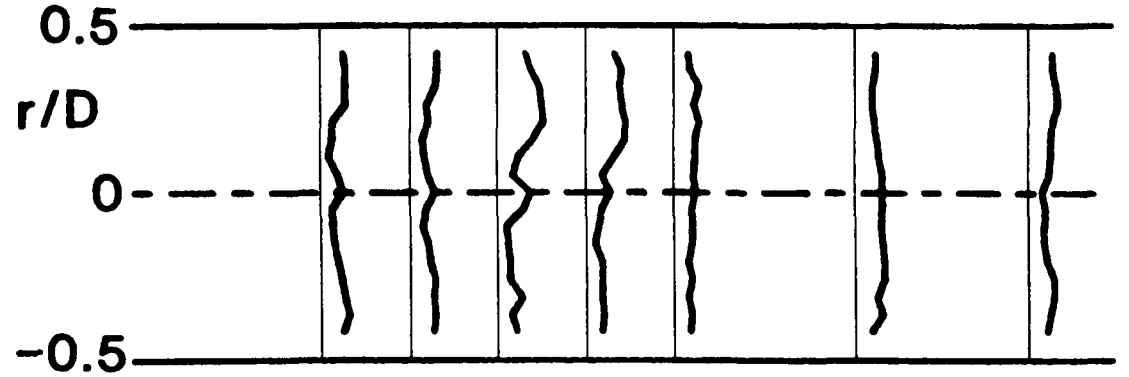

e) v'_{rms}/u_o x 2

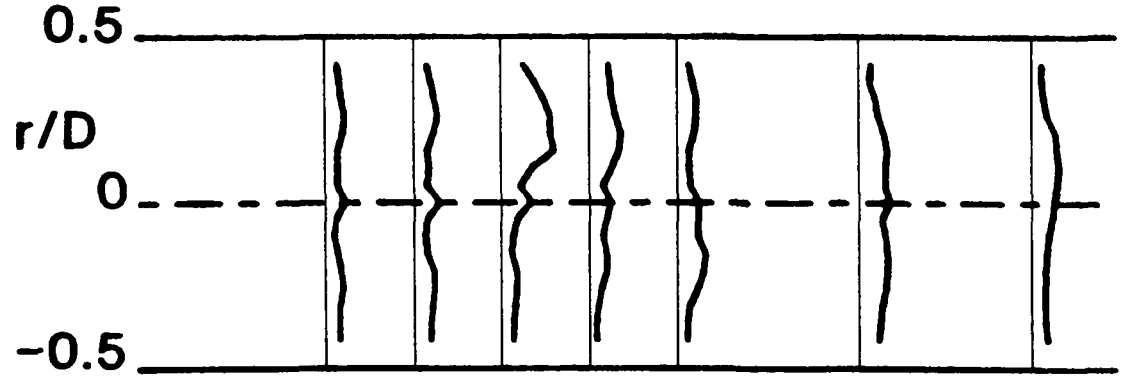

f) w'_{rms}/u_o x 2

Figure 9. (Continued)

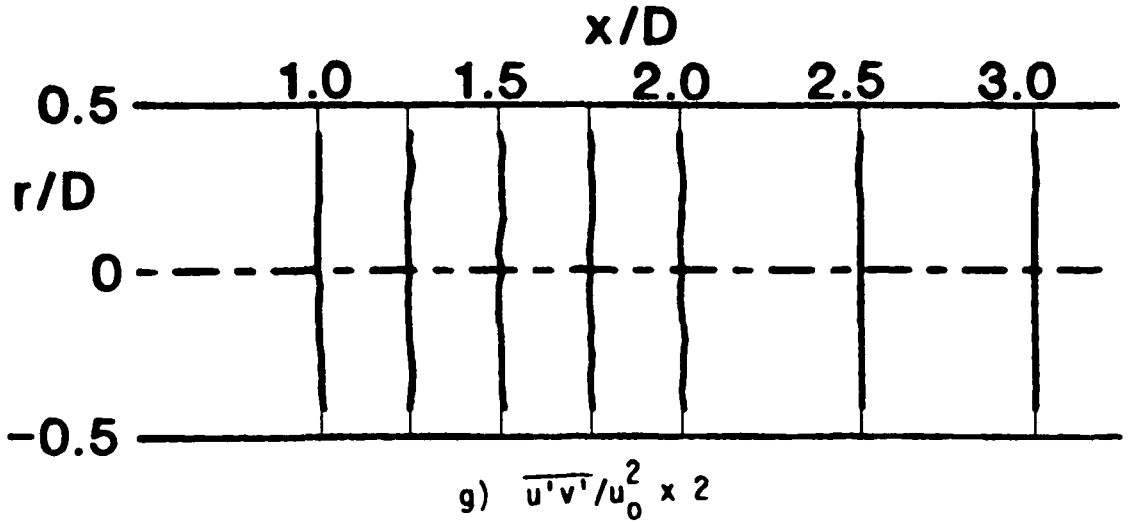

g) $\overline{u'v'}/u_o^2 \times 2$

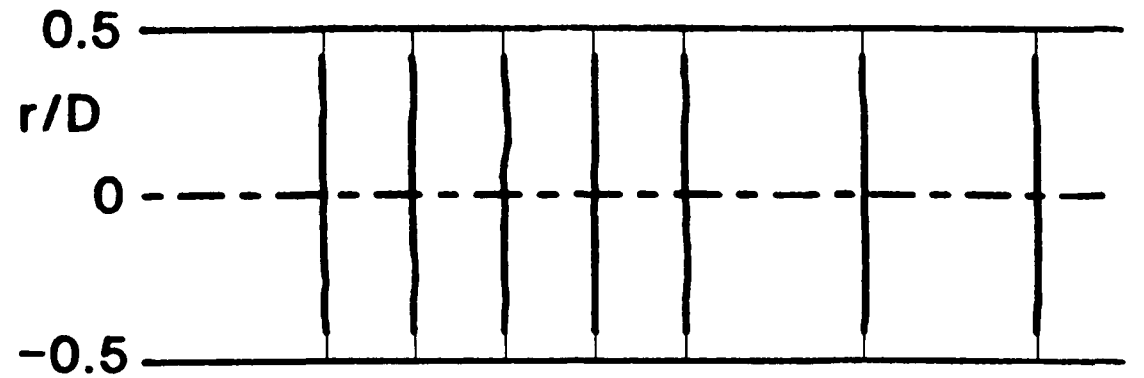

h) $\overline{u'w'}/u_o^2 \times 2$

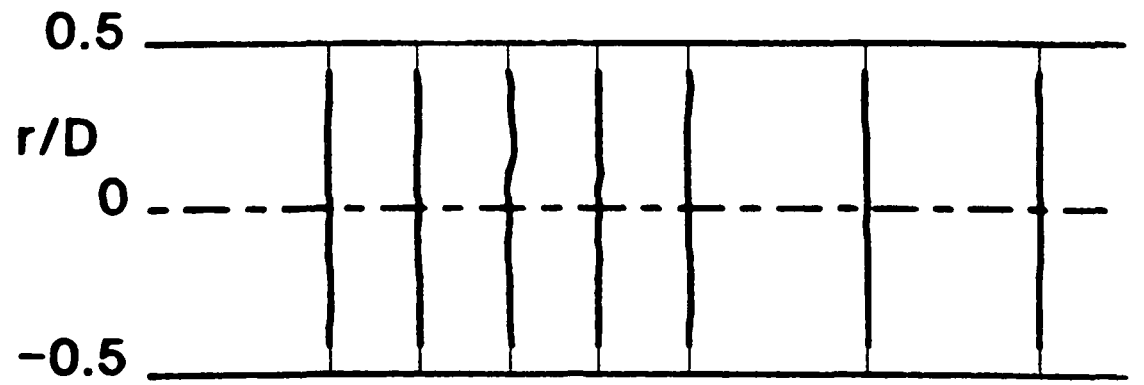

i) $\overline{v'w'}/u_o^2 \times 2$

Figure 9. (Continued)

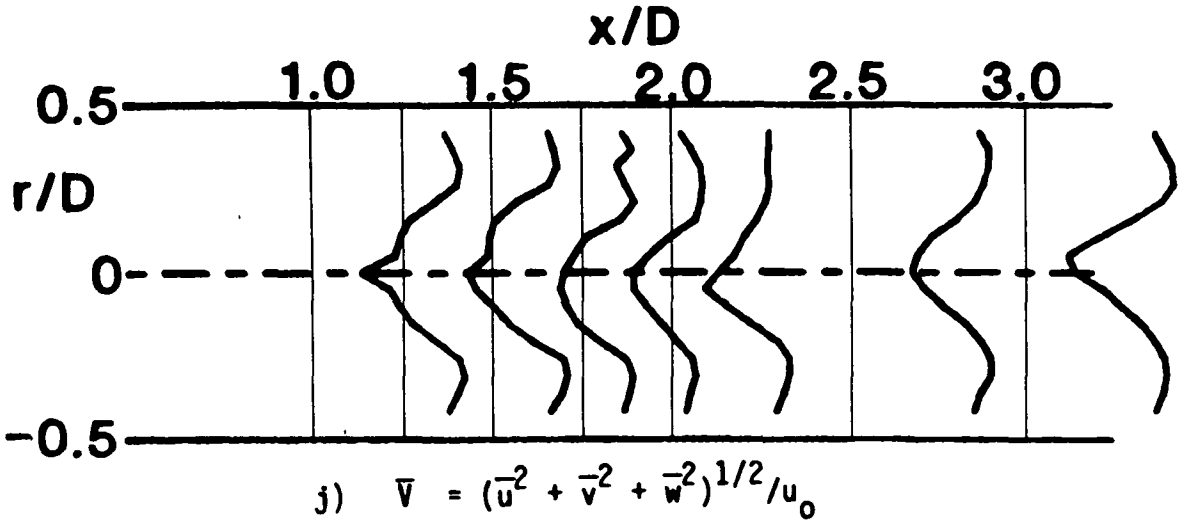

j) $\bar{V} = (\bar{u}^2 + \bar{v}^2 + \bar{w}^2)^{1/2}/u_o$

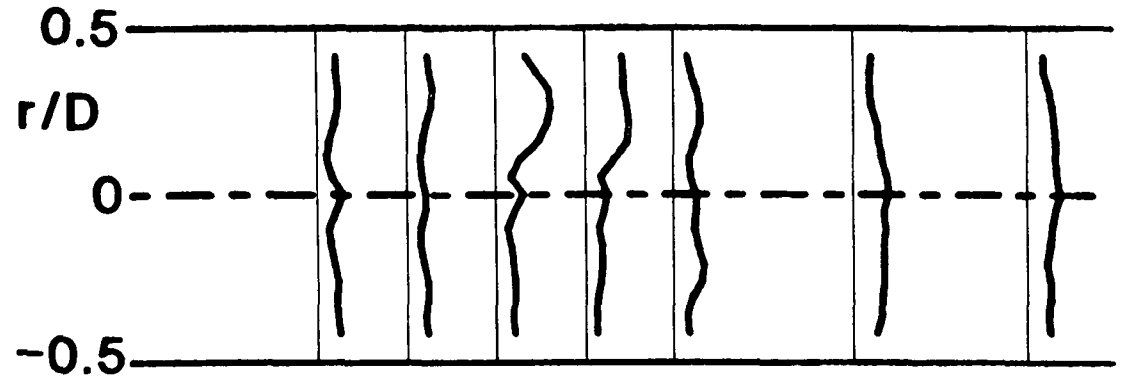

k) $u'_{rms}/\bar{u} \times 2$

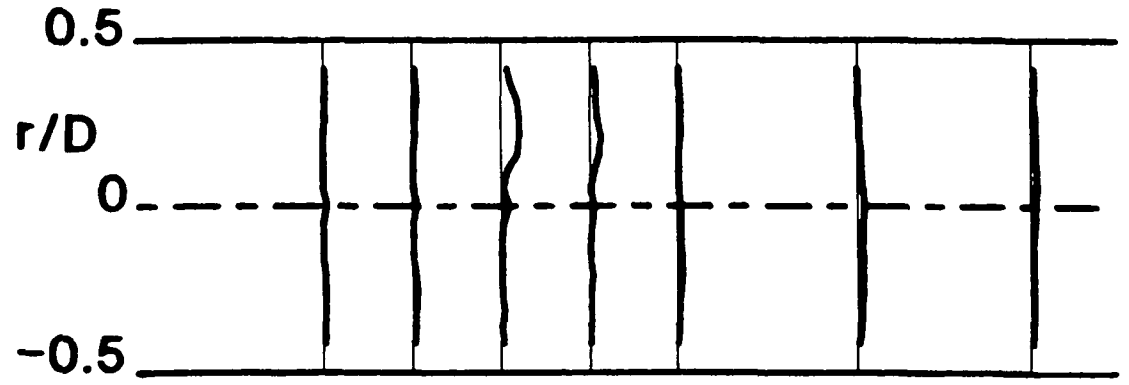

l) $\frac{1}{2}(u'^2_{rms} + v'^2_{rms} + w'^2_{rms})/u_o^2 \times 2$

Figure 9. (Continued)

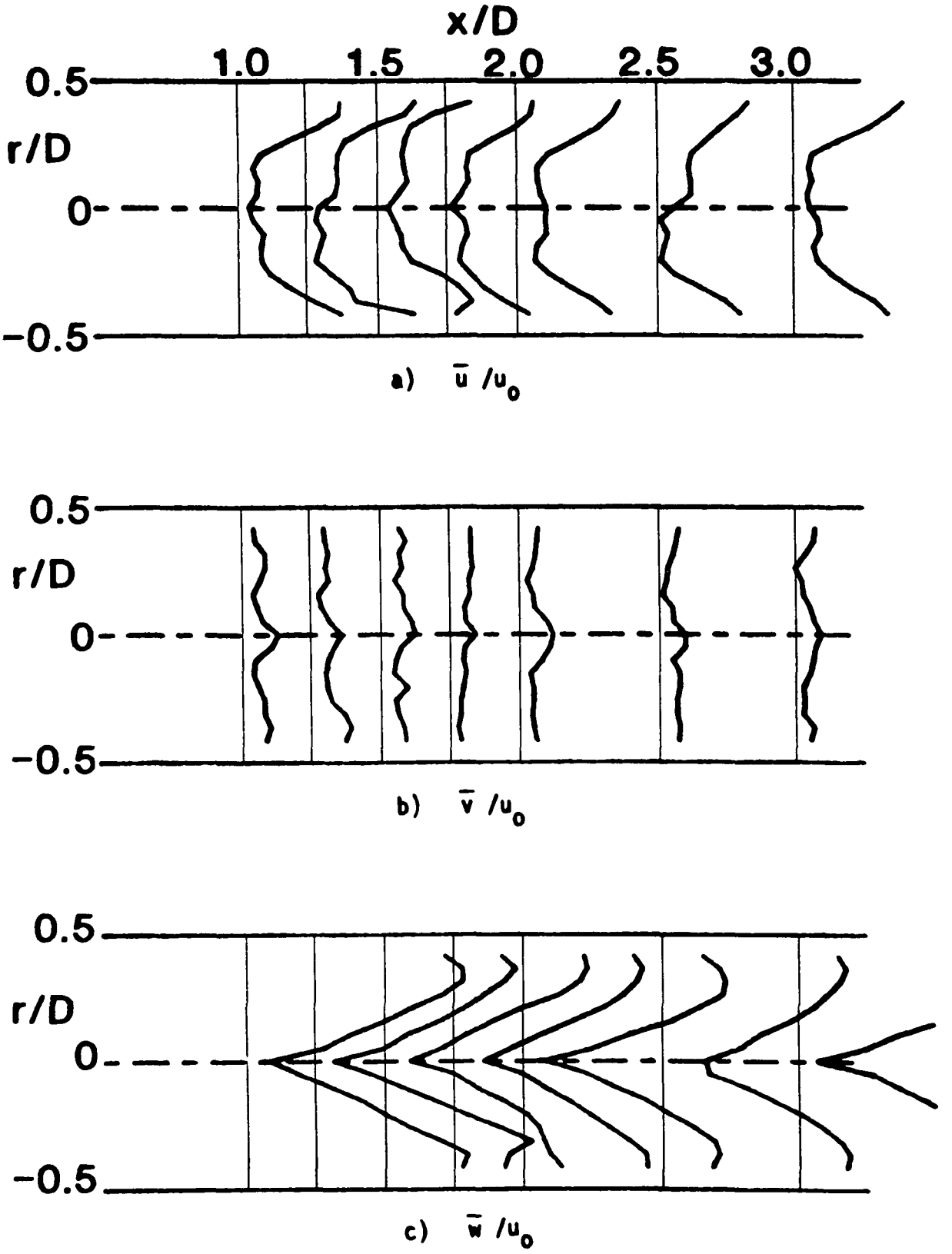

Figure 10. Time-Mean and Turbulent Flowfield (Hot-Wire Data) R = 4, ϕ = 70 Degrees, Traverse Angle θ = 270 Degrees

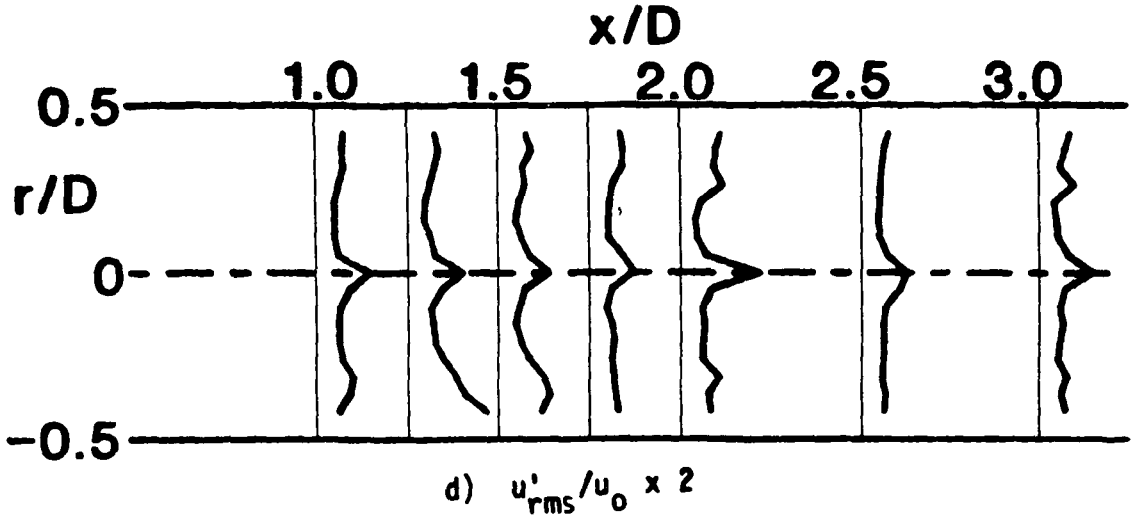

d) $u'_{rms}/u_o \times 2$

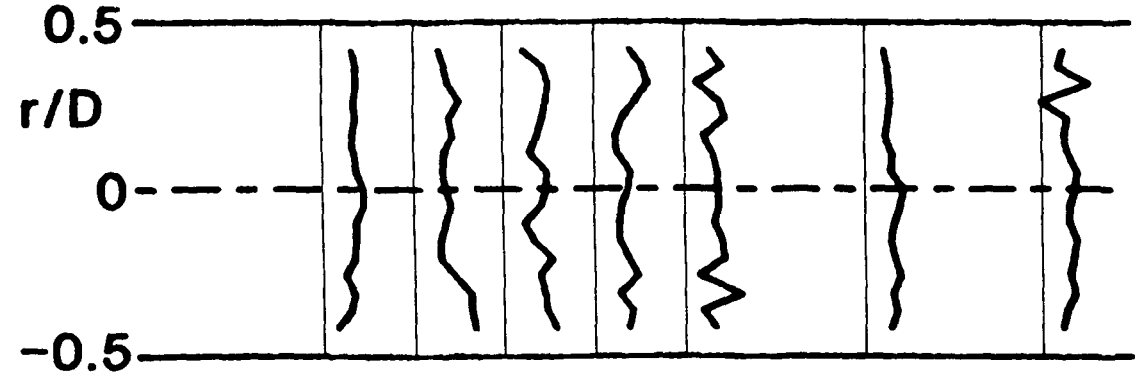

e) $v'_{rms}/u_o \times 2$

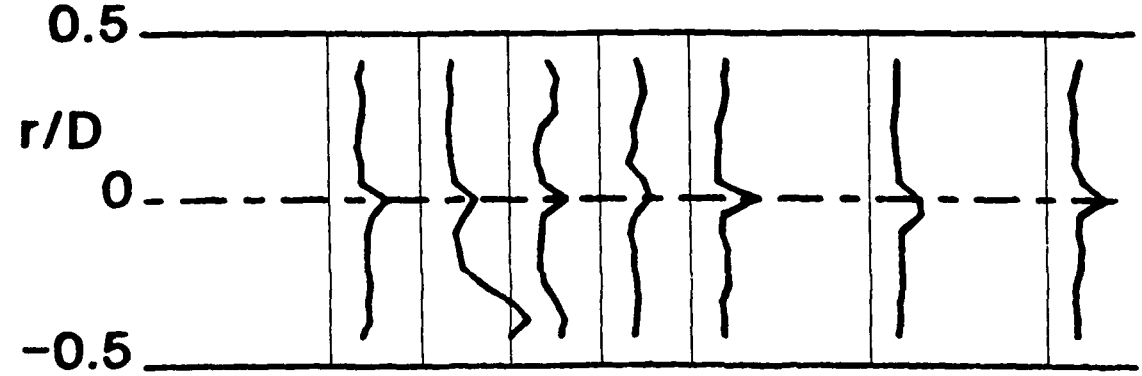

f) $w'_{rms}/u_o \times 2$

Figure 10. (Continued)

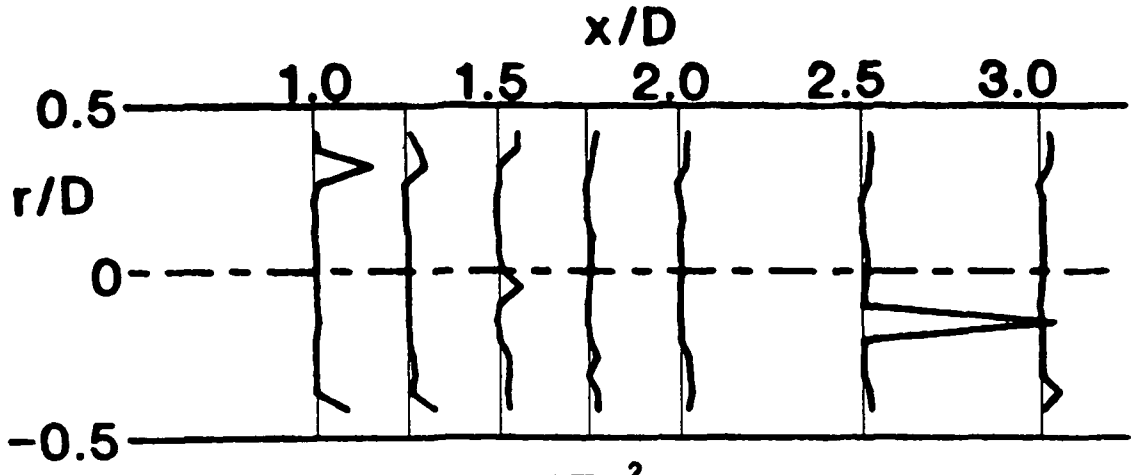

g) $\overline{u'v'}/u_o^2 \times 2$

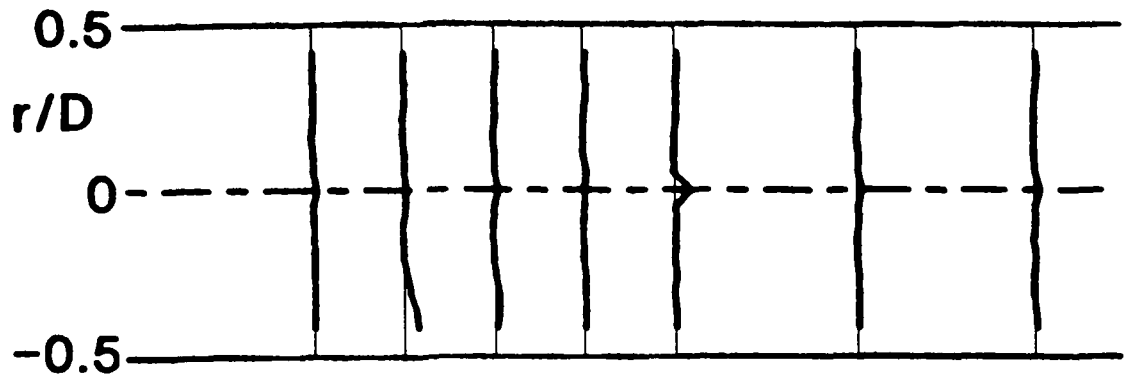

h) $\overline{u'w'}/u_o^2 \times 2$

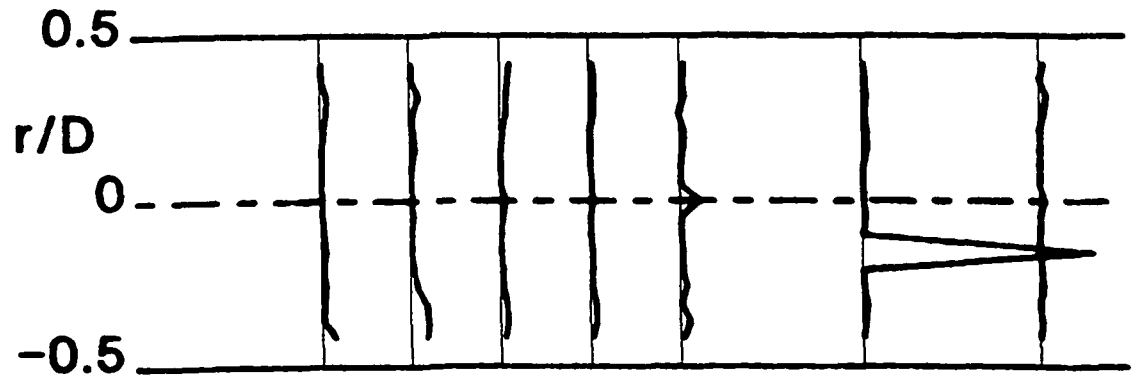

i) $\overline{v'w'}/u_o^2 \times 2$

Figure 10. (Continued)

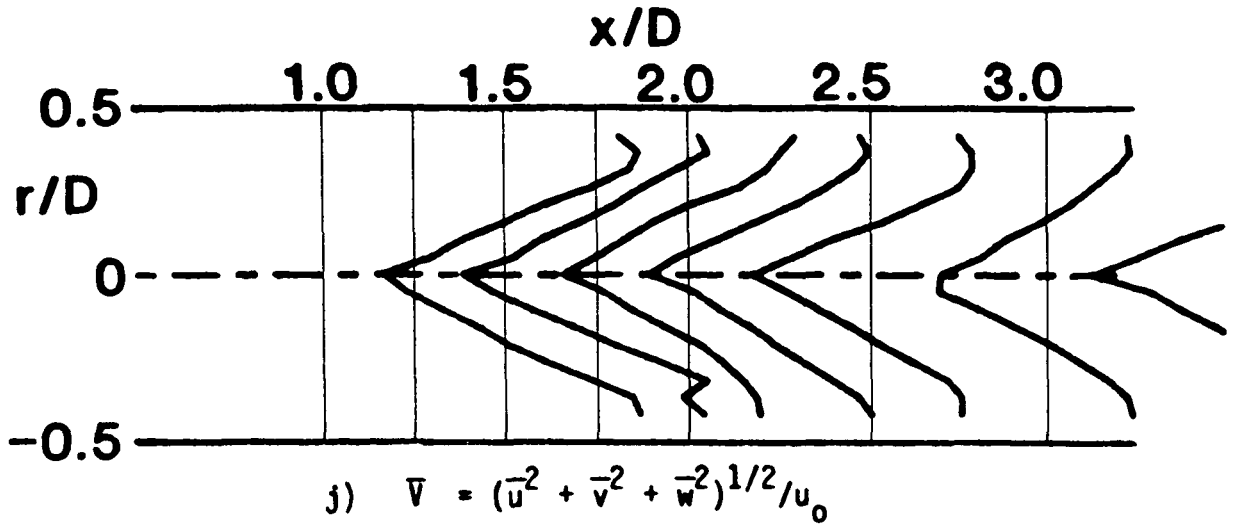

j) $\bar{V} = (\bar{u}^2 + \bar{v}^2 + \bar{w}^2)^{1/2}/u_o$

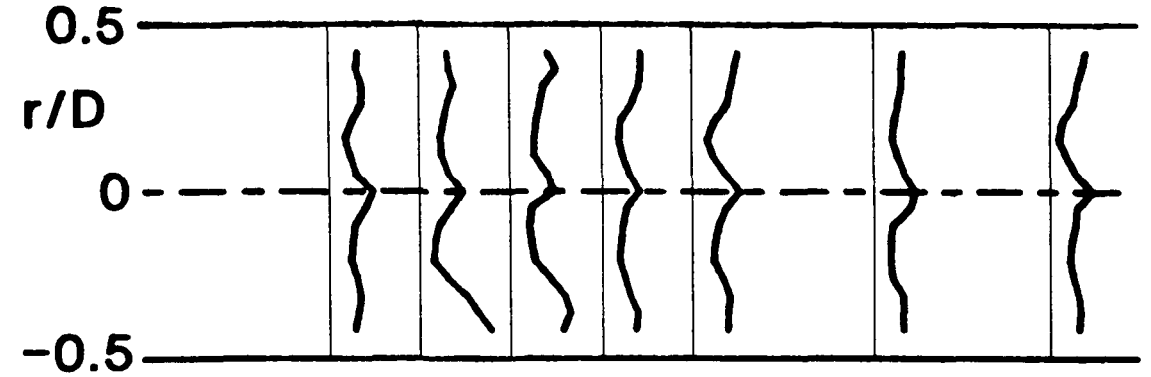

k) $u'_{rms}/\bar{u} \times 2$

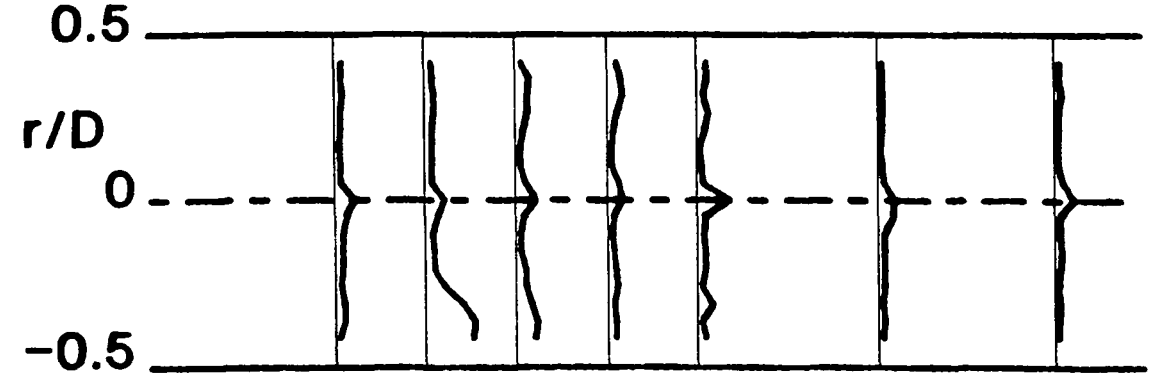

l) $\frac{1}{2}(u'^2_{rms} + v'^2_{rms} + w'^2_{rms})/u_o^2 \times 2$

Figure 10. (Continued)

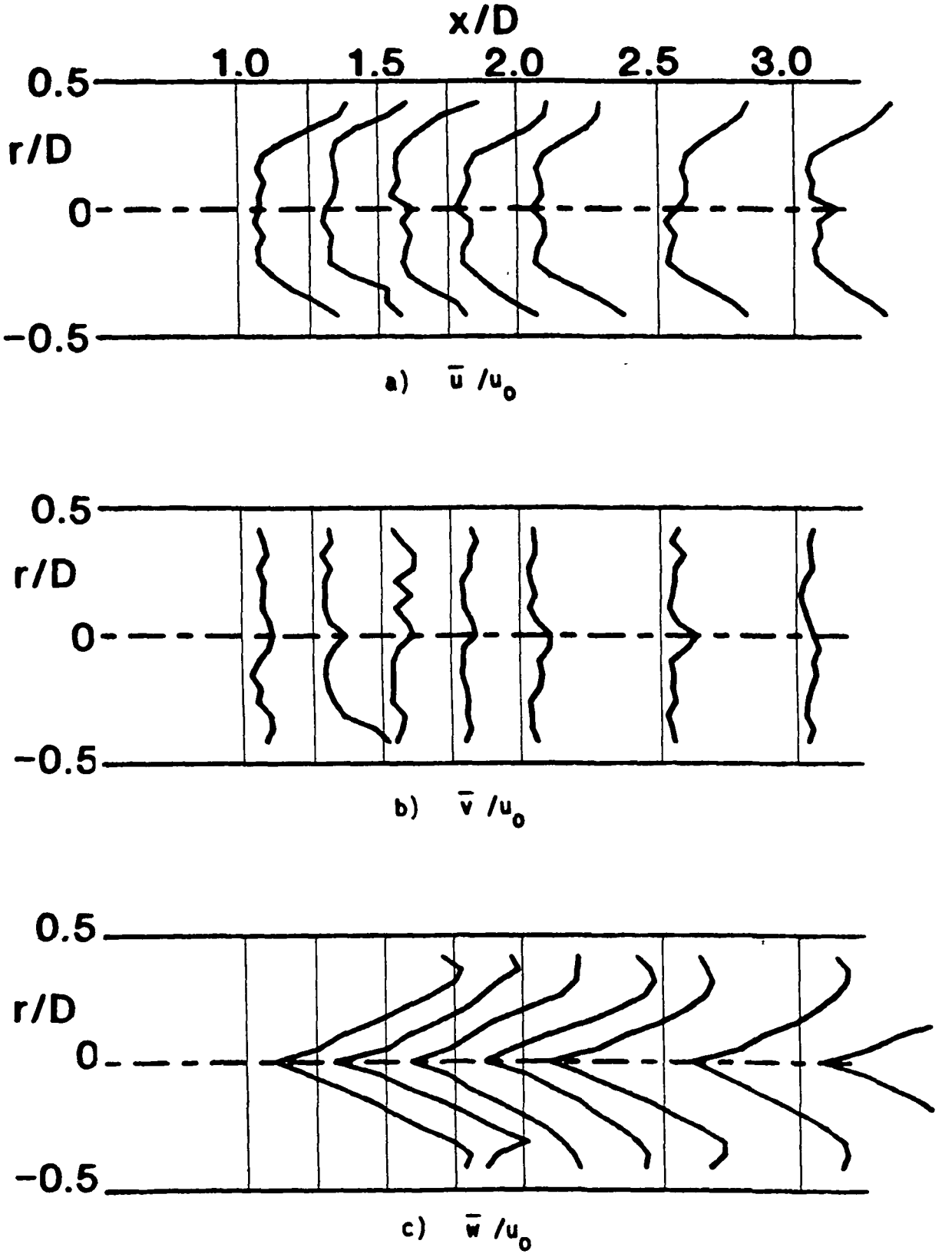

Figure 11. Time-Mean and Turbulent Flowfield (Hot-Wire Data) R = 4, ϕ = 70 Degrees, Traverse Angle θ = 300 Degrees

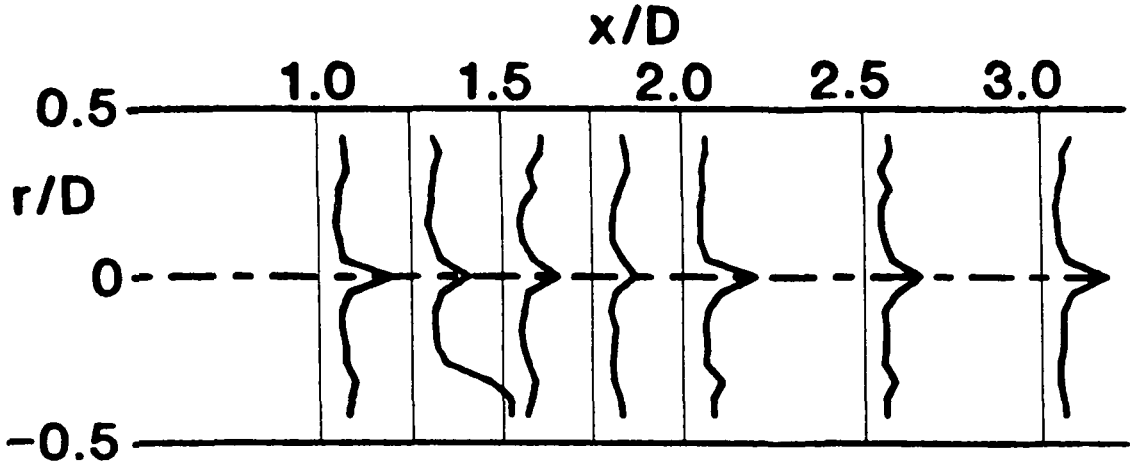

d) u'_{rms}/u_o x 2

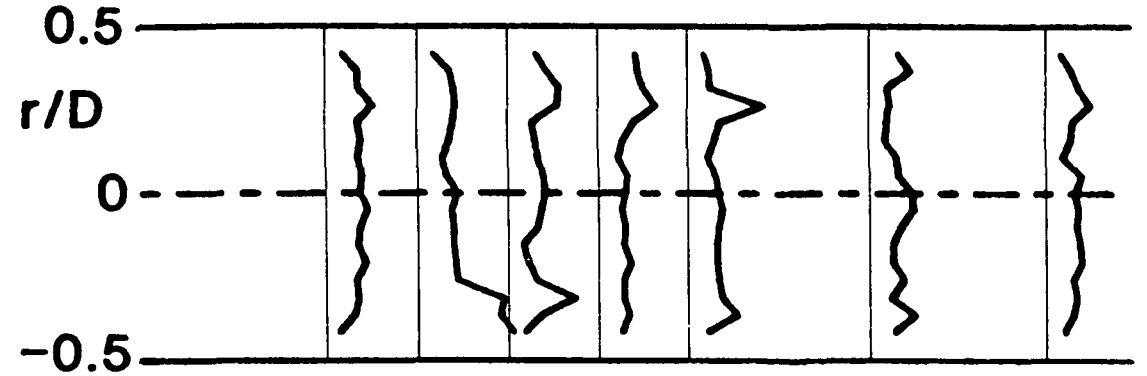

e) v'_{rms}/u_o x 2

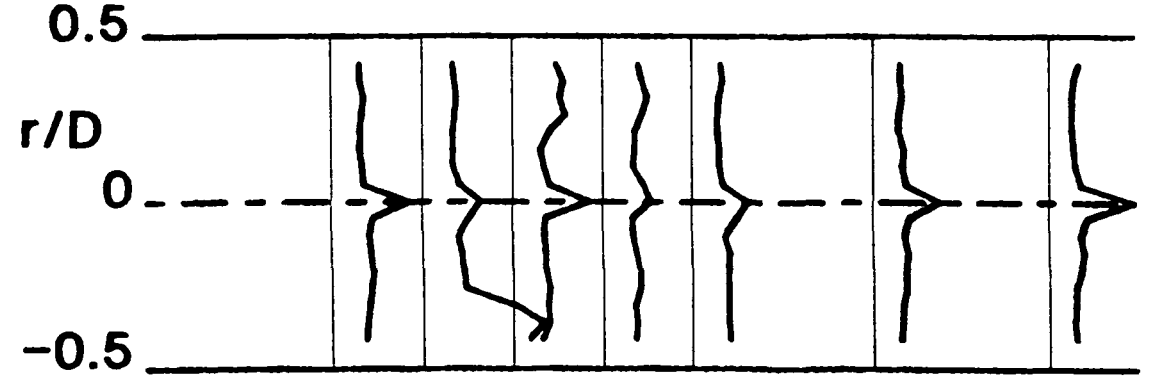

f) w'_{rms}/u_o x 2

Figure 11. (Continued)

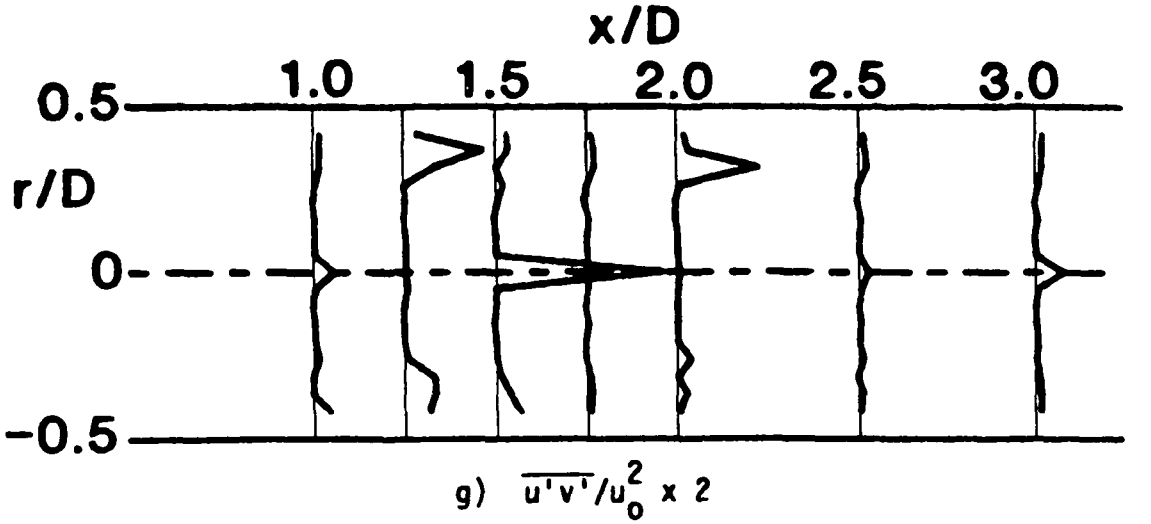

g) $\overline{u'v'}/u_o^2 \times 2$

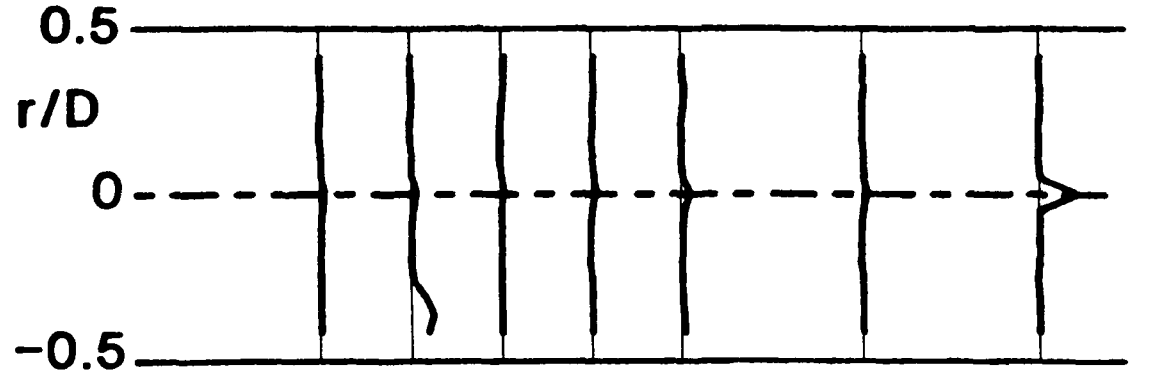

h) $\overline{u'w'}/u_o^2 \times 2$

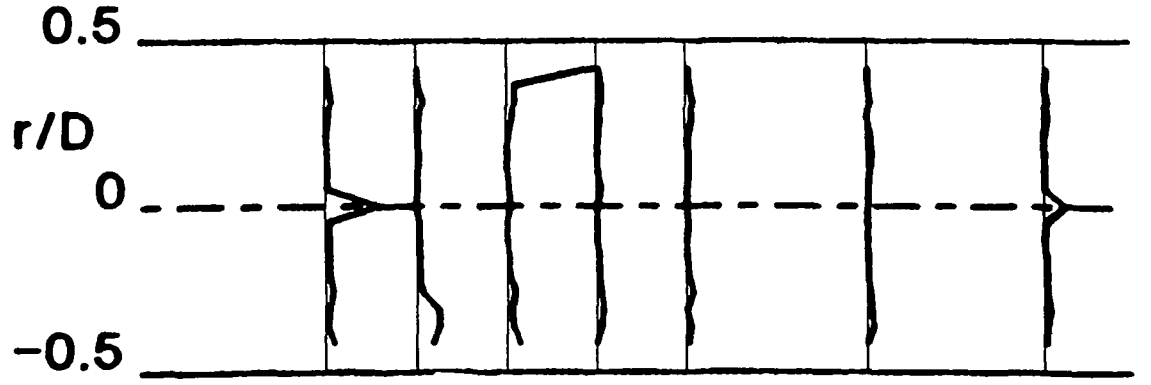

i) $\overline{v'w'}/u_o^2 \times 2$

Figure 11. (Continued)

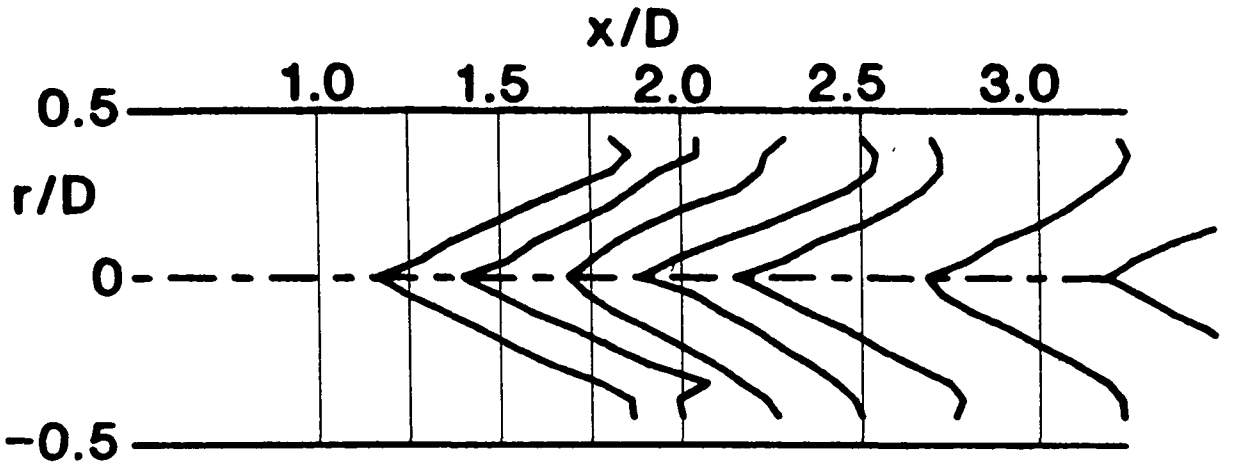

j) $\bar{V} = (\bar{u}^2 + \bar{v}^2 + \bar{w}^2)^{1/2}/u_o$

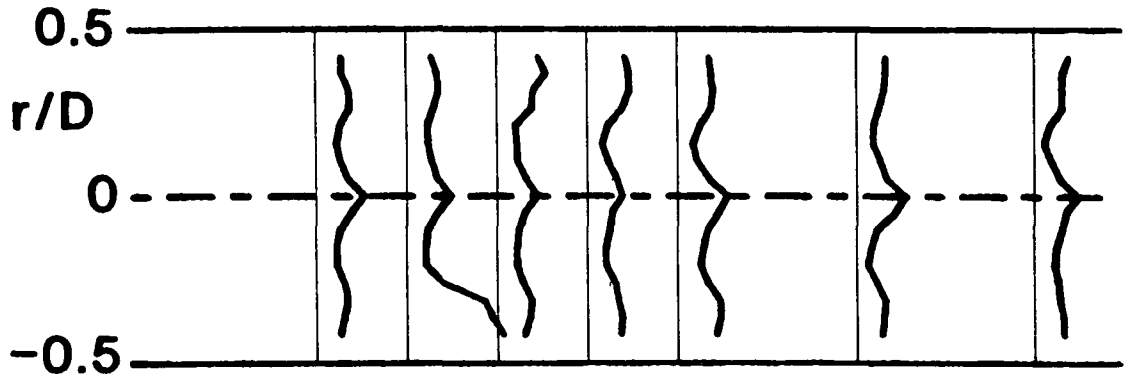

k) $u'_{rms}/\bar{u} \times 2$

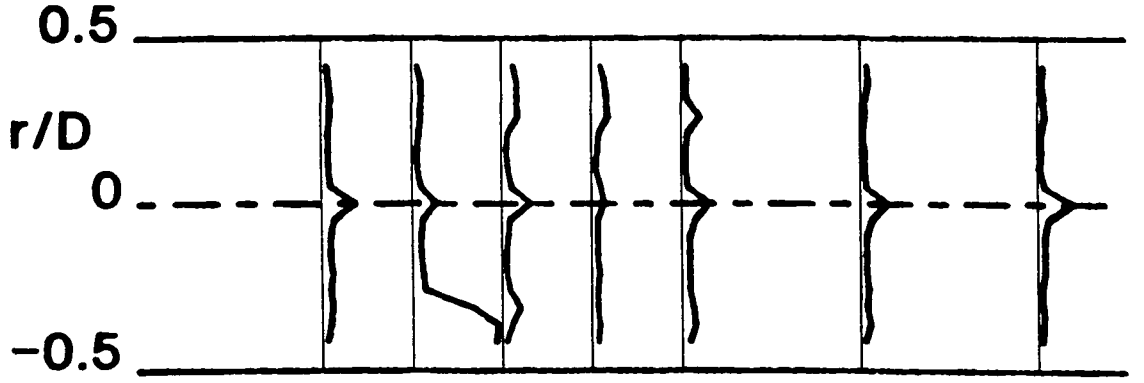

l) $\frac{1}{2}(u'^2_{rms} + v'^2_{rms} + w'^2_{rms})/u_o^2 \times 2$

Figure 11. (Continued)

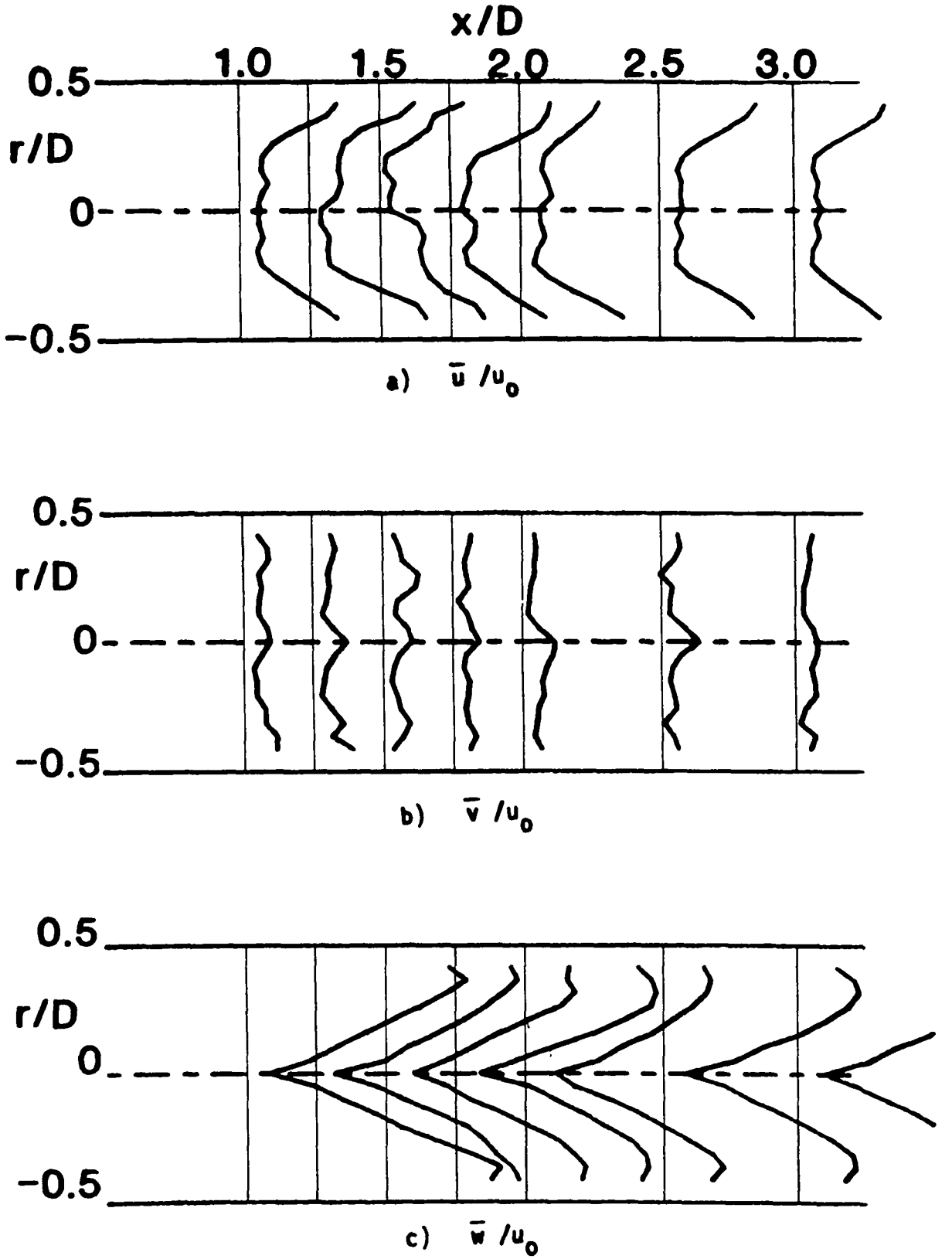

Figure 12. Time-Mean and Turbulent Flowfield (Hot-Wire Data) R = 4, ϕ = 70 Degrees, Traverse Angle θ = 330 Degrees

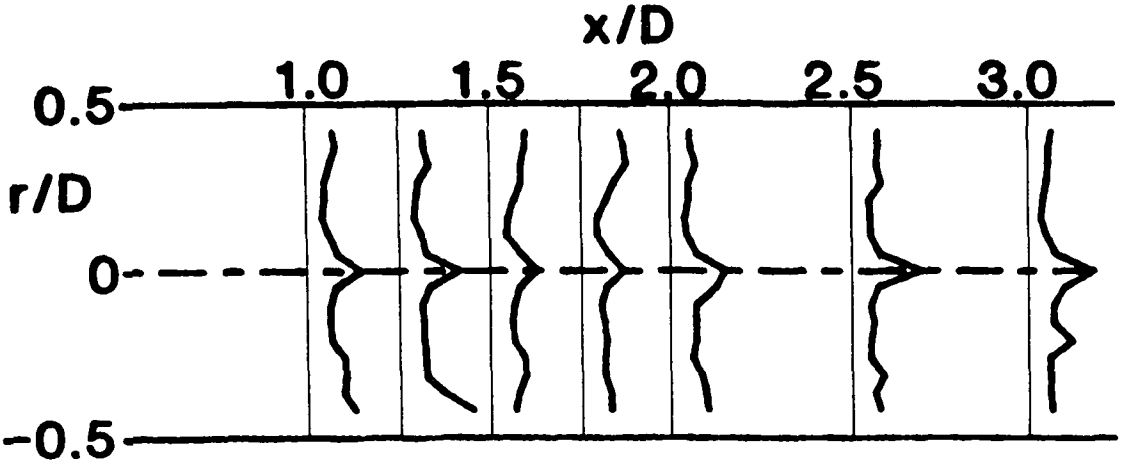

d) u'_{rms}/u_o x 2

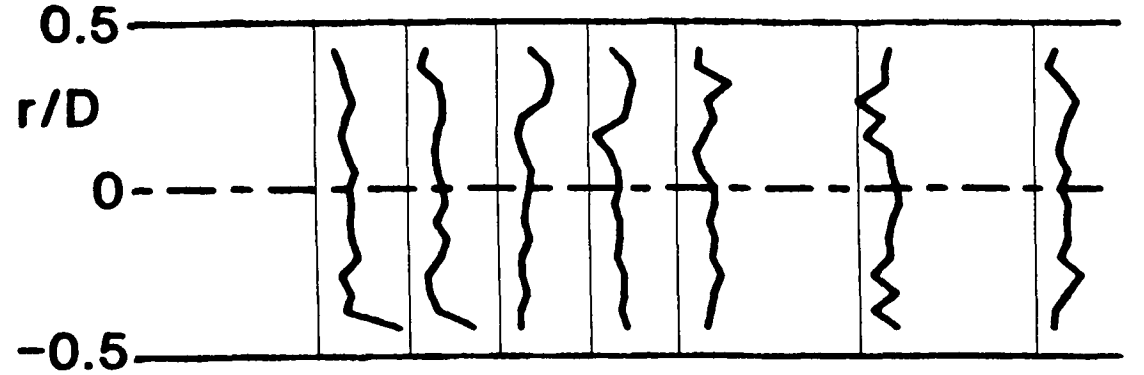

e) v'_{rms}/u_o x 2

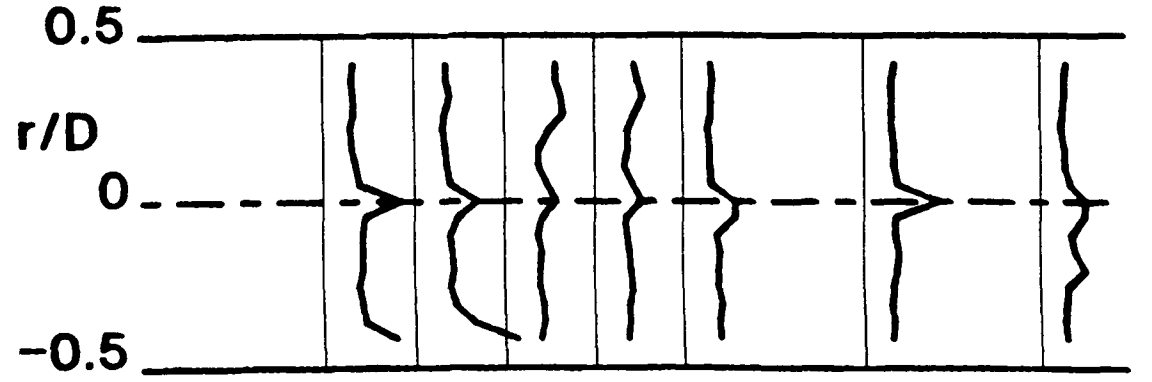

f) w'_{rms}/u_o x 2

Figure 12. (Continued)

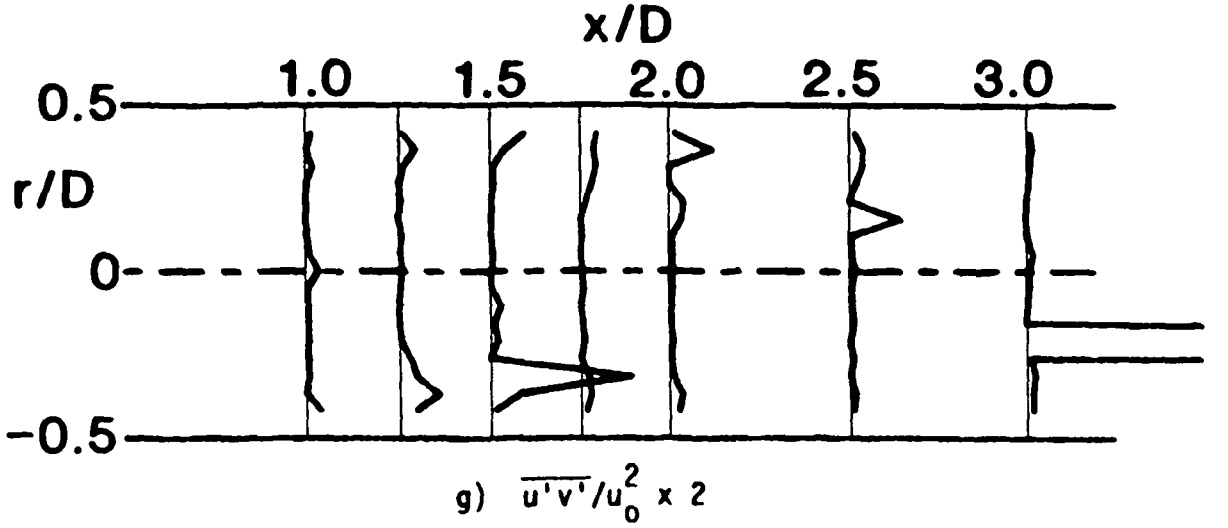

g) $\overline{u'v'}/u_0^2 \times 2$

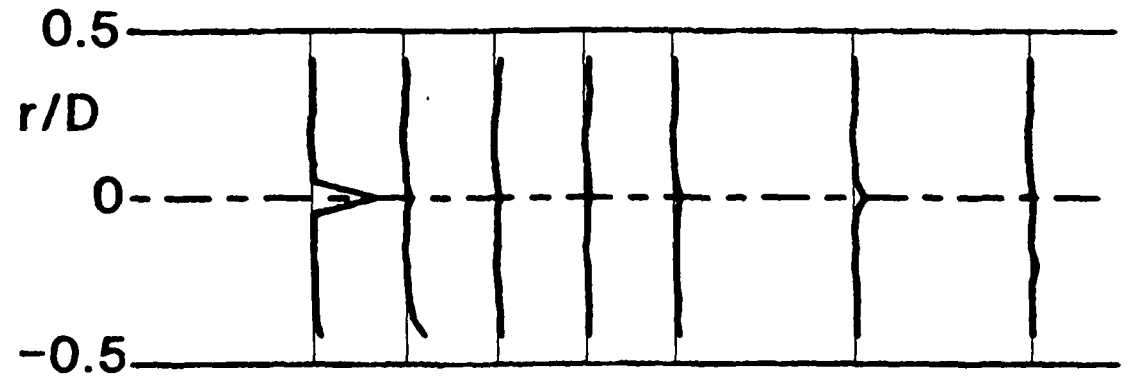

h) $\overline{u'w'}/u_0^2 \times 2$

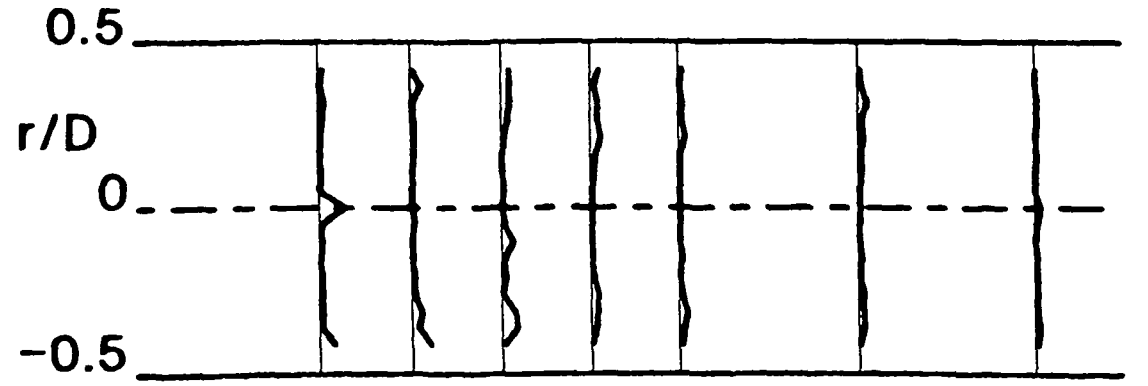

i) $\overline{v'w'}/u_0^2 \times 2$

Figure 12. (Continued)

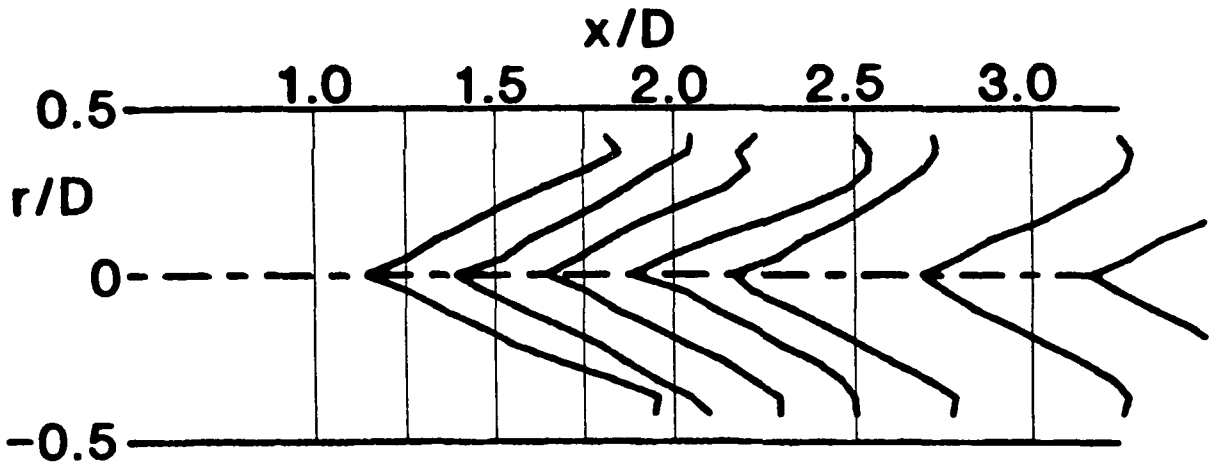

j) $\bar{V} = (\bar{u}^2 + \bar{v}^2 + \bar{w}^2)^{1/2}/u_o$

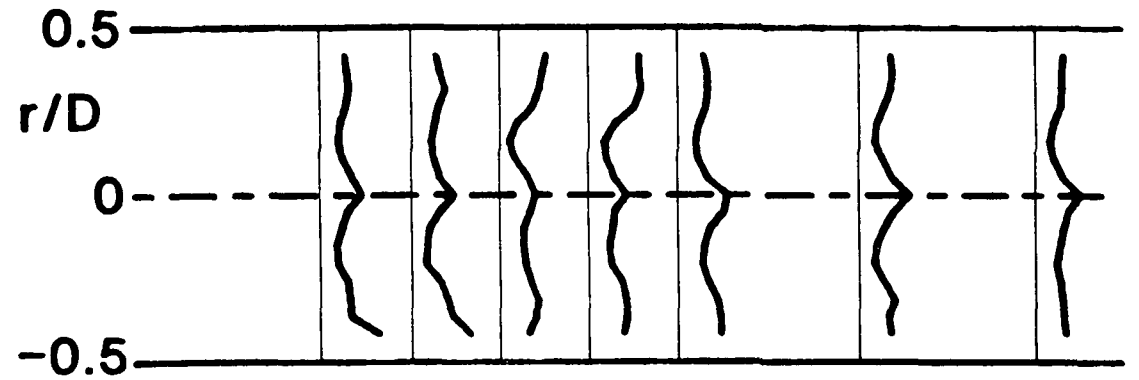

k) $u'_{rms}/\bar{u} \times 2$

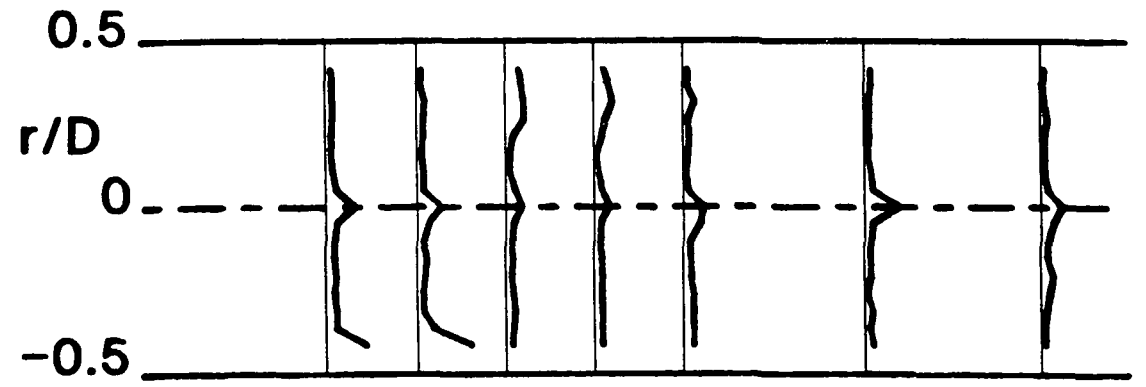

l) $\frac{1}{2}(u'^2_{rms} + v'^2_{rms} + w'^2_{rms})/u_o^2 \times 2$

Figure 12. (Continued)

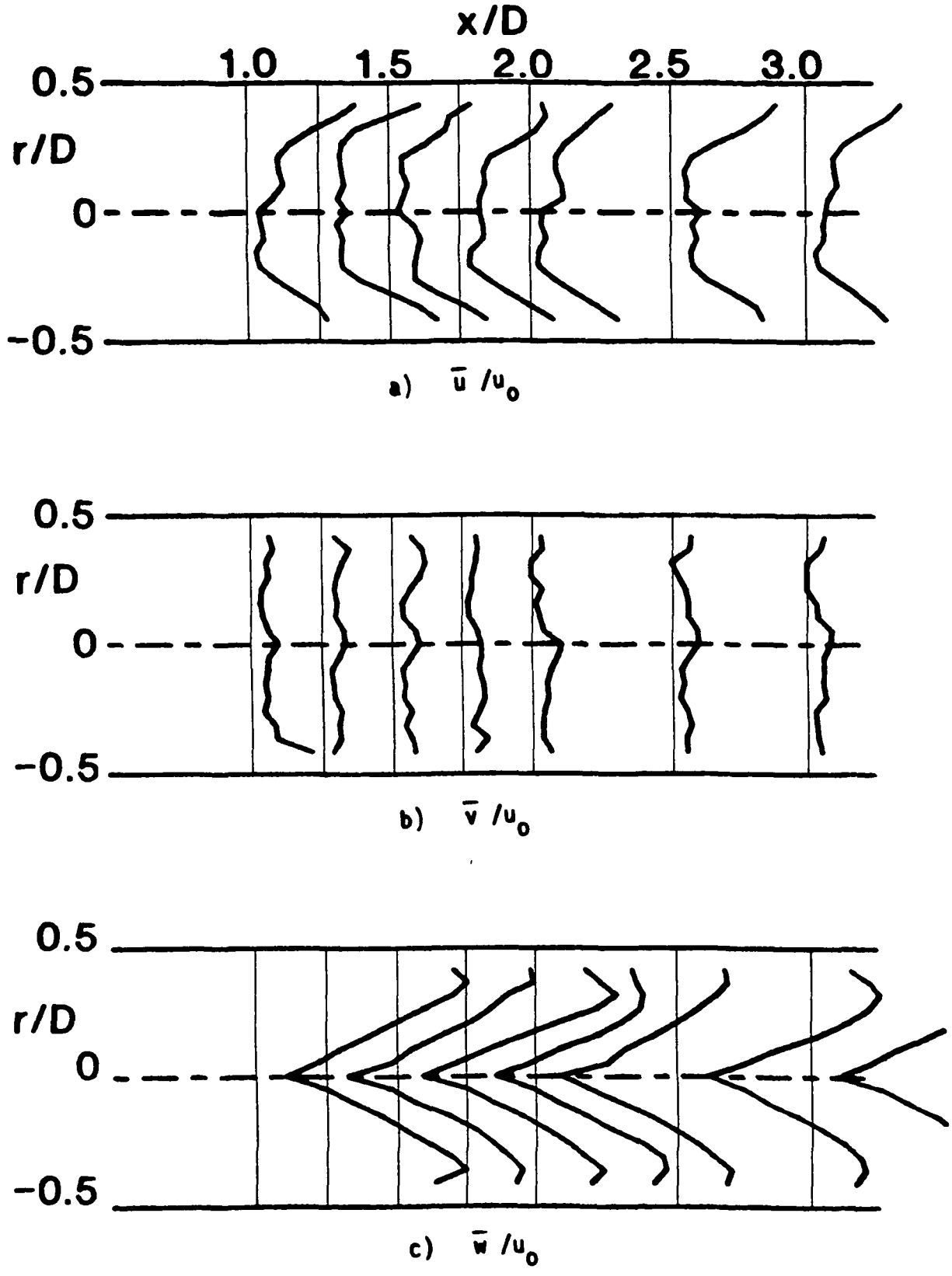

Figure 13. Time-Mean and Turbulent Flowfield (Hot-Wire Data) R = 4, ϕ = 70 Degrees, Traverse Angle θ = 0 Degrees

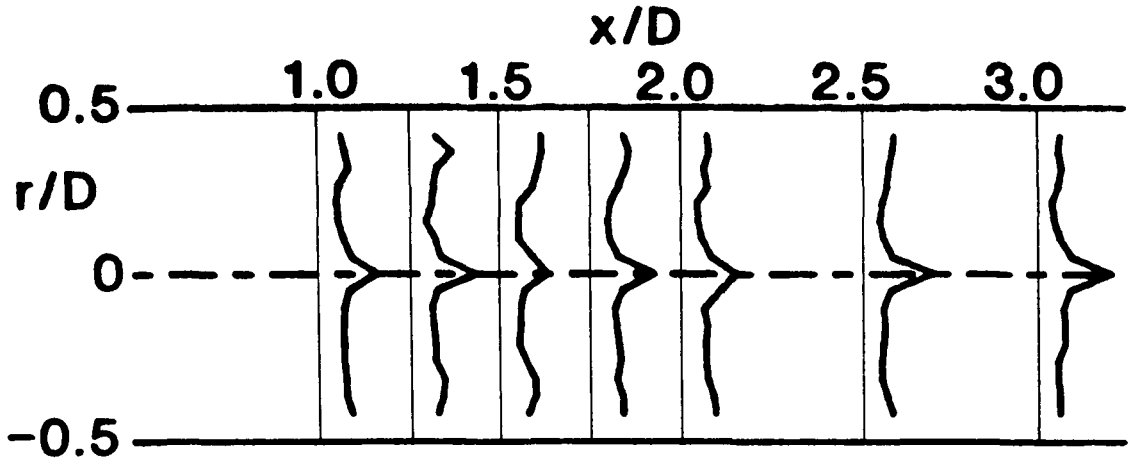

d) $u'_{rms}/u_o \times 2$

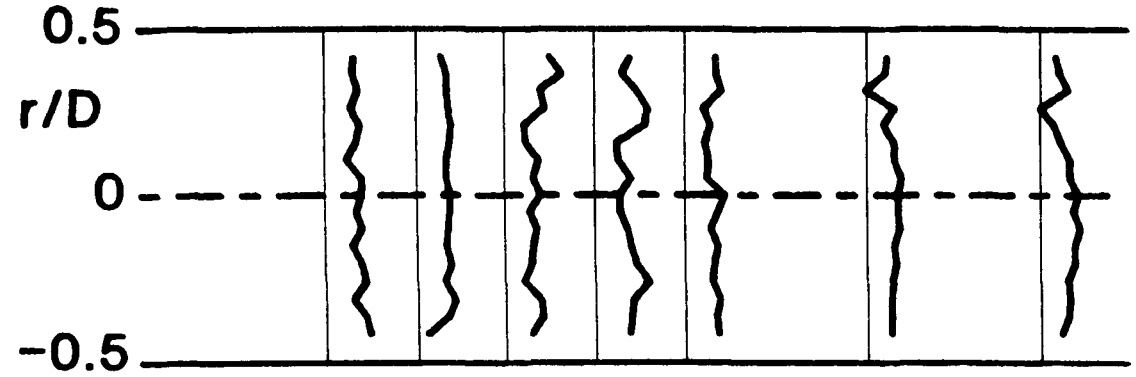

e) $v'_{rms}/u_o \times 2$

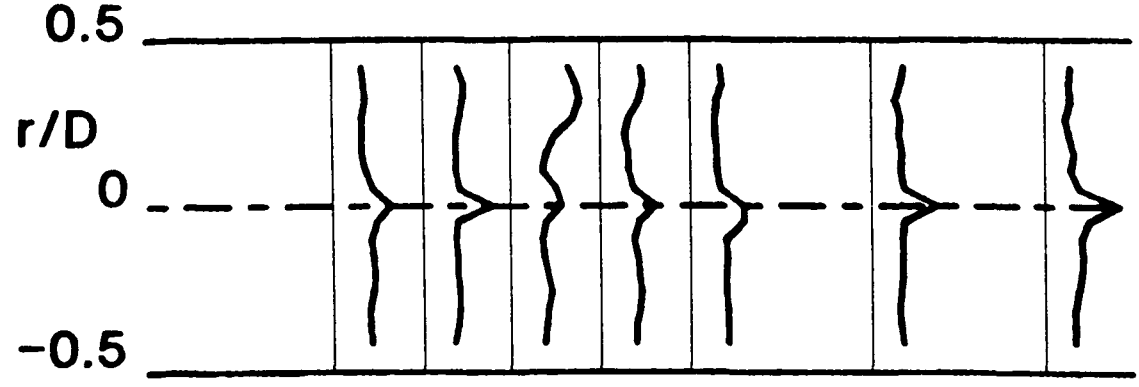

f) $w'_{rms}/u_o \times 2$

Figure 13. (Continued)

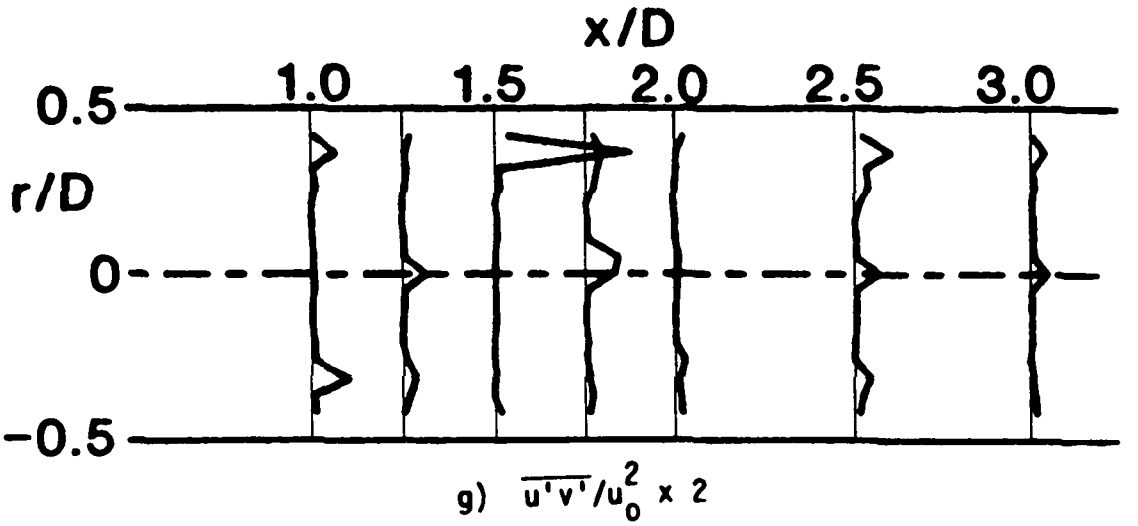

g) $\overline{u'v'}/u_0^2 \times 2$

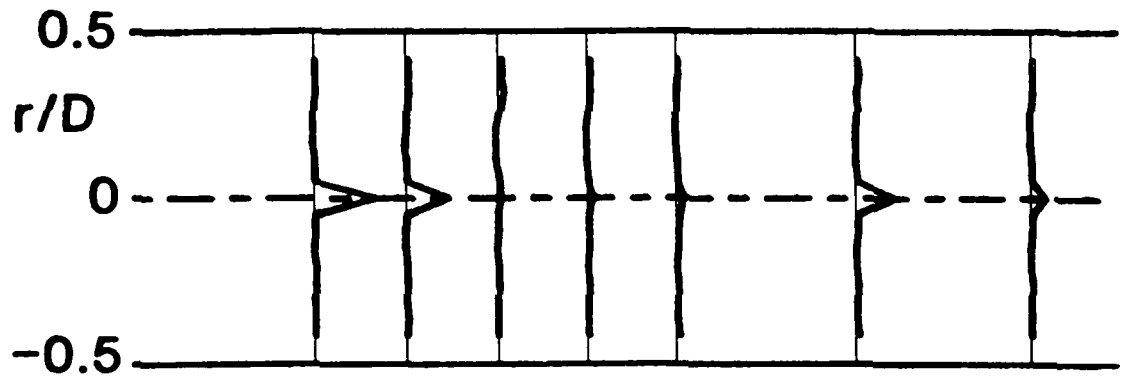

h) $\overline{u'w'}/u_0^2 \times 2$

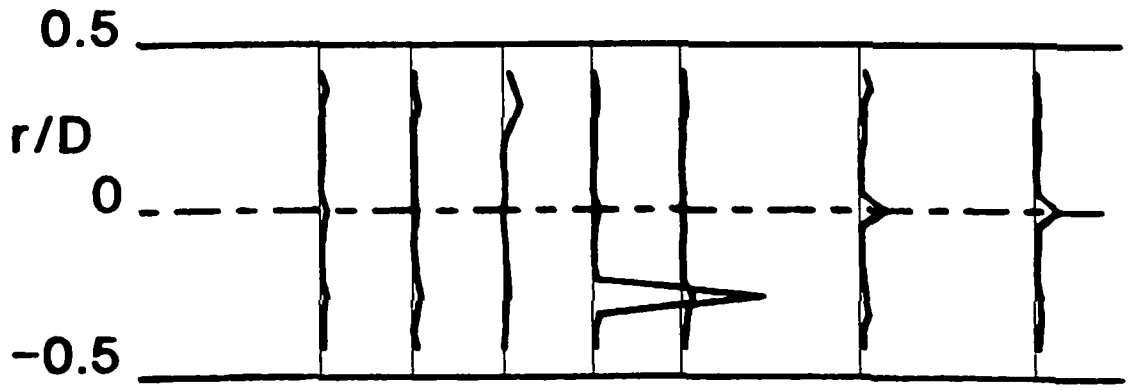

i) $\overline{v'w'}/u_0^2 \times 2$

Figure 13. (Continued)

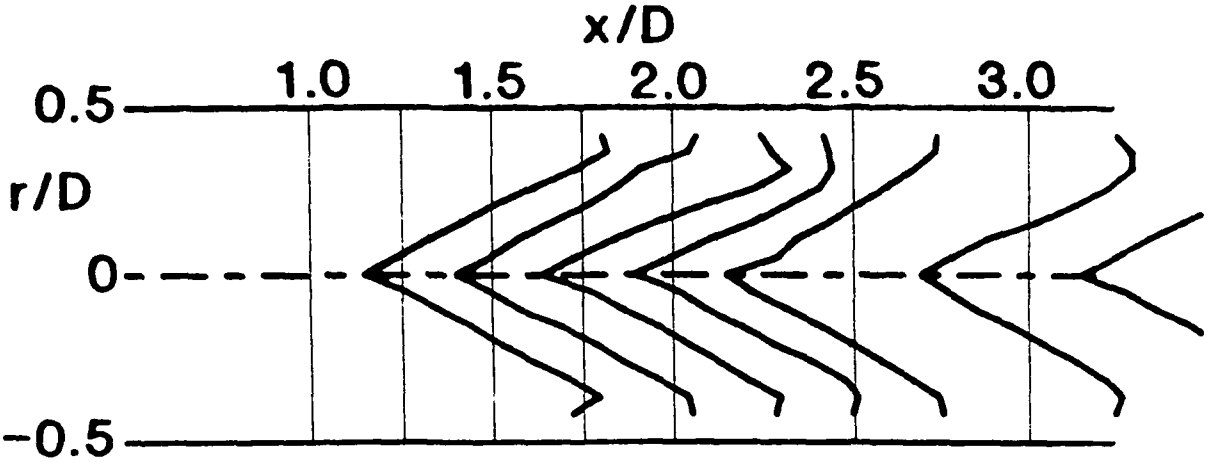

j) $\bar{V} = (\bar{u}^2 + \bar{v}^2 + \bar{w}^2)^{1/2}/u_o$

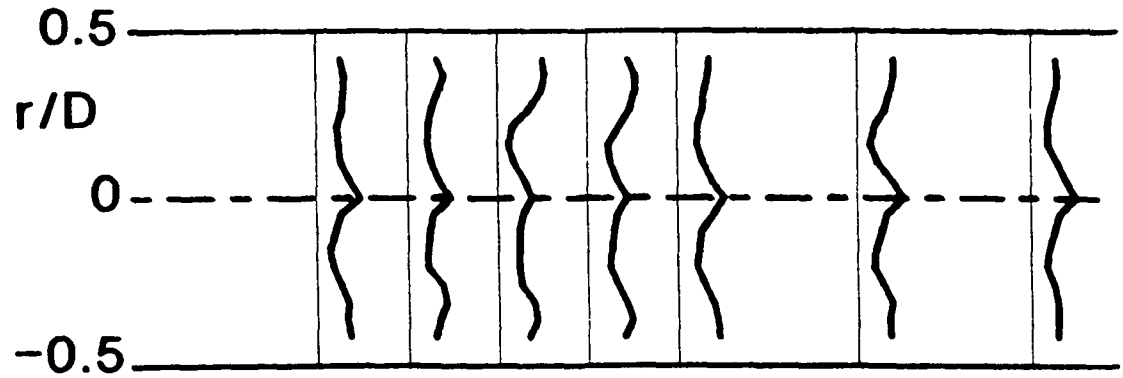

k) $u'_{rms}/\bar{u} \times 2$

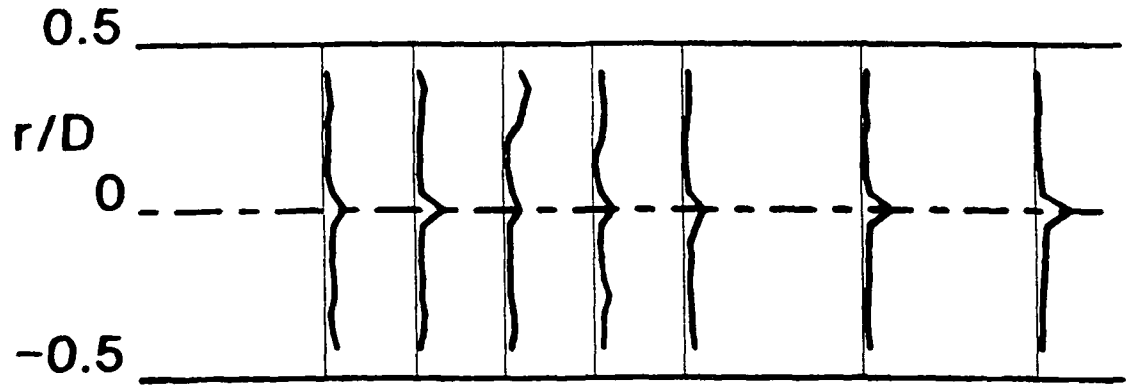

l) $\frac{1}{2}(u'^2_{rms} + v'^2_{rms} + w'^2_{rms})/u_o^2 \times 2$

Figure 13. (Continued)

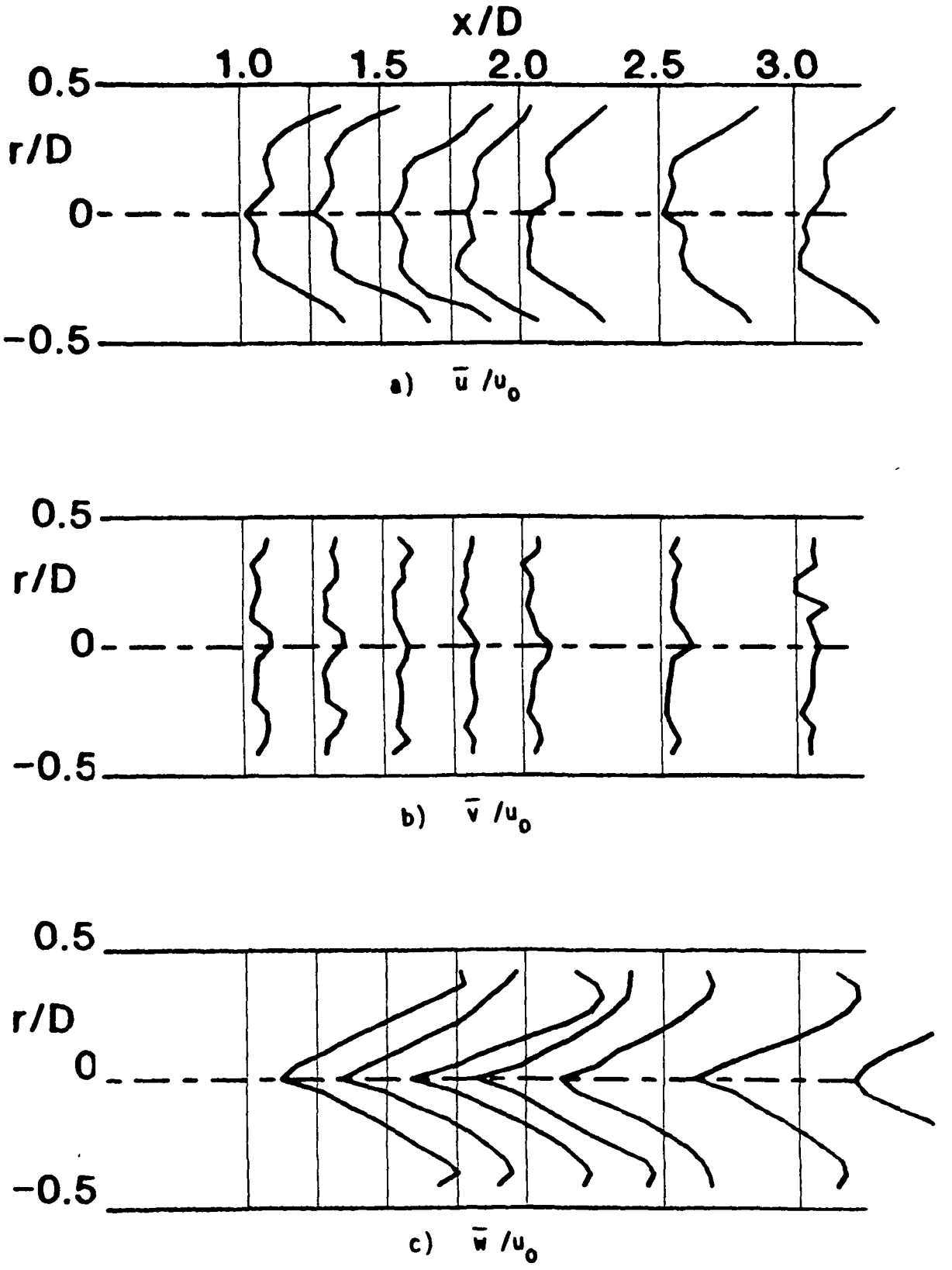

Figure 14. Time-Mean and Turbulent Flowfield (Hot-Wire Data) R = 4, ϕ = 70 Degrees, Traverse Angle θ = 30 Degrees

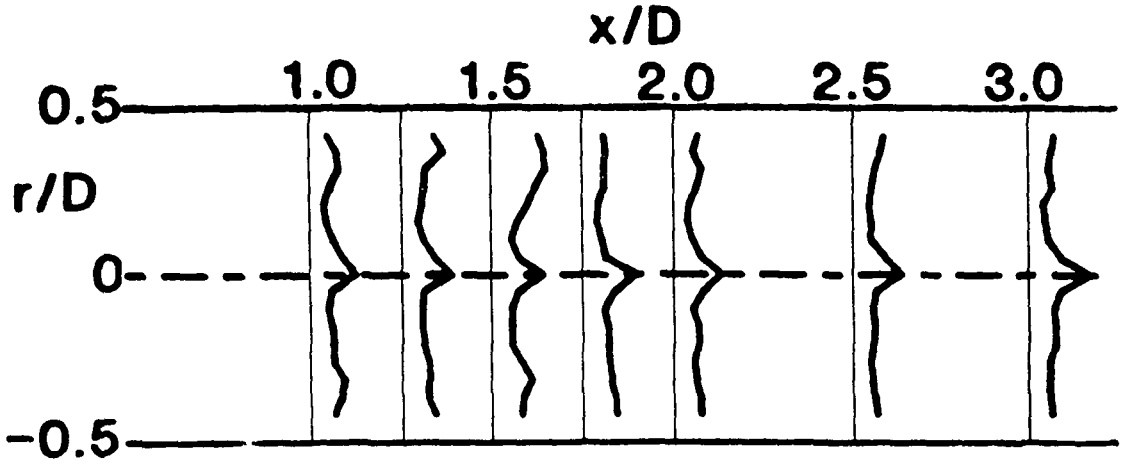

d) $u'_{rms}/u_o \times 2$

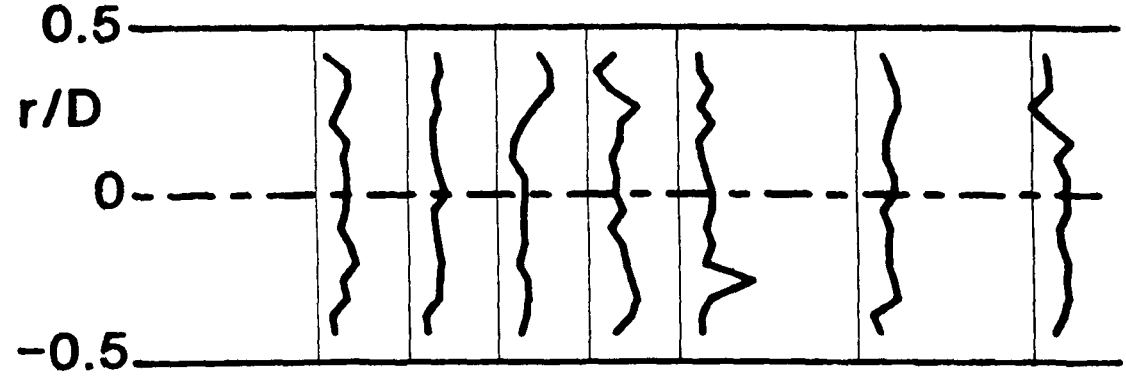

e) $v'_{rms}/u_o \times 2$

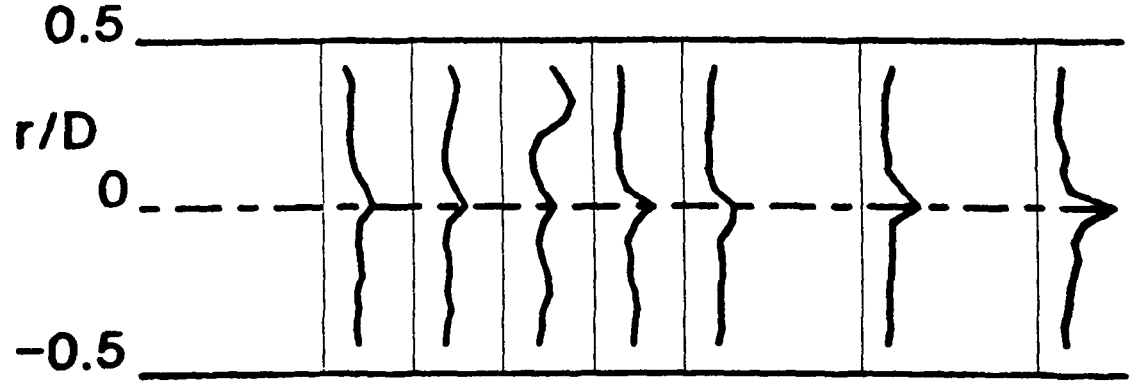

f) $w'_{rms}/u_o \times 2$

Figure 14. (Continued)

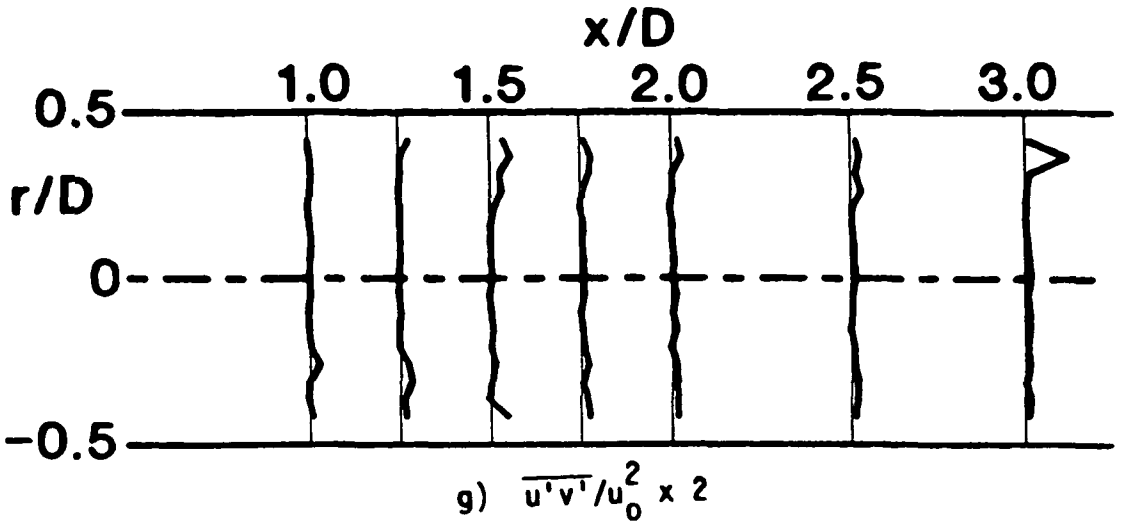

g) $\overline{u'v'}/u_0^2 \times 2$

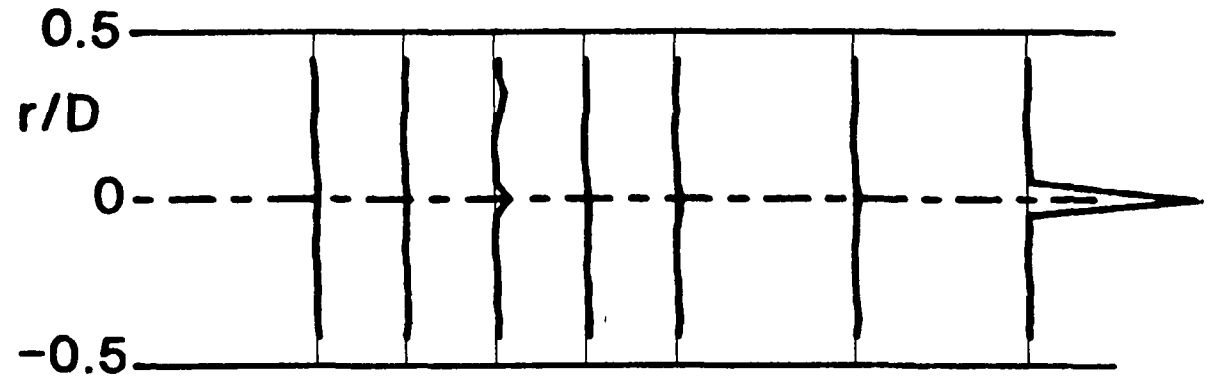

h) $\overline{u'w'}/u_0^2 \times 2$

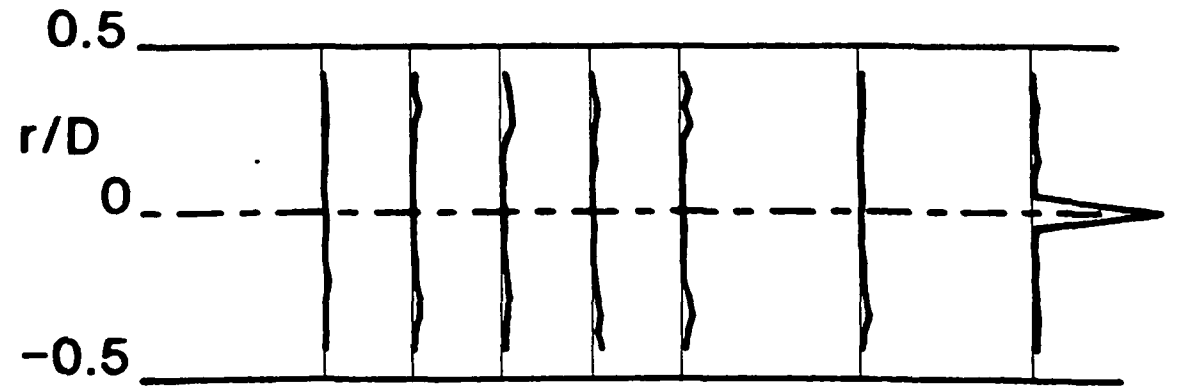

i) $\overline{v'w'}/u_0^2 \times 2$

Figure 14. (Continued)

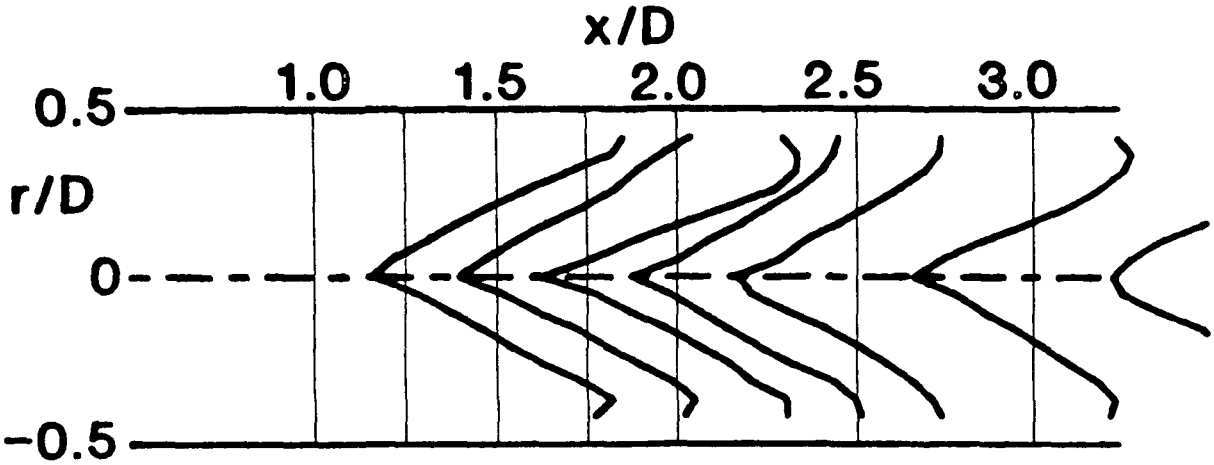

j) $\bar{V} = (\bar{u}^2 + \bar{v}^2 + \bar{w}^2)^{1/2}/u_o$

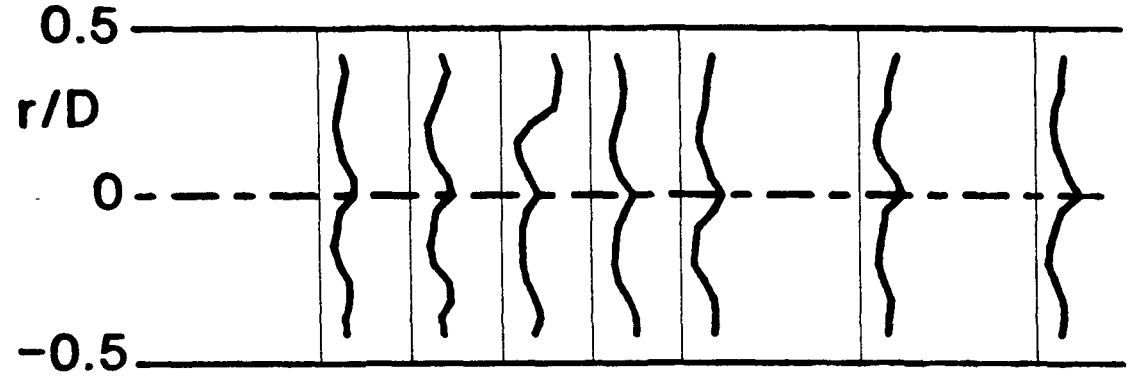

k) $u'_{rms}/\bar{u} \times 2$

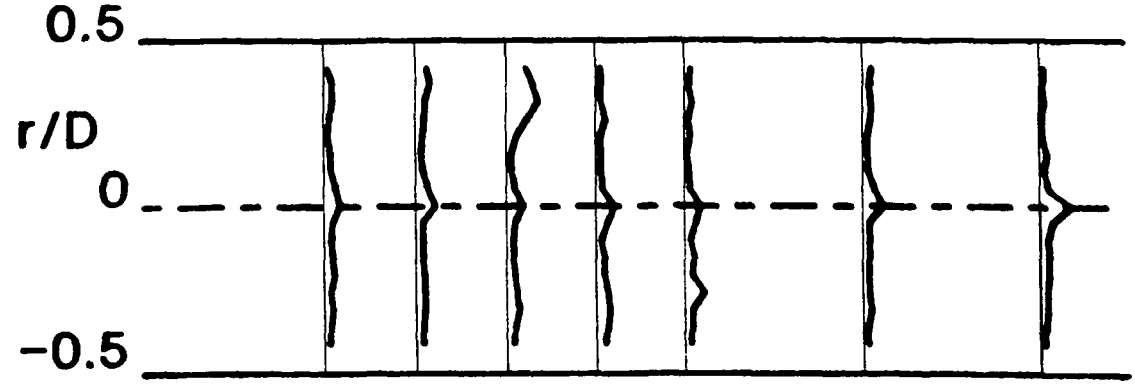

l) $\frac{1}{2}(u'^2_{rms} + v'^2_{rms} + w'^2_{rms})/u_o^2 \times 2$

Figure 14. (Continued)

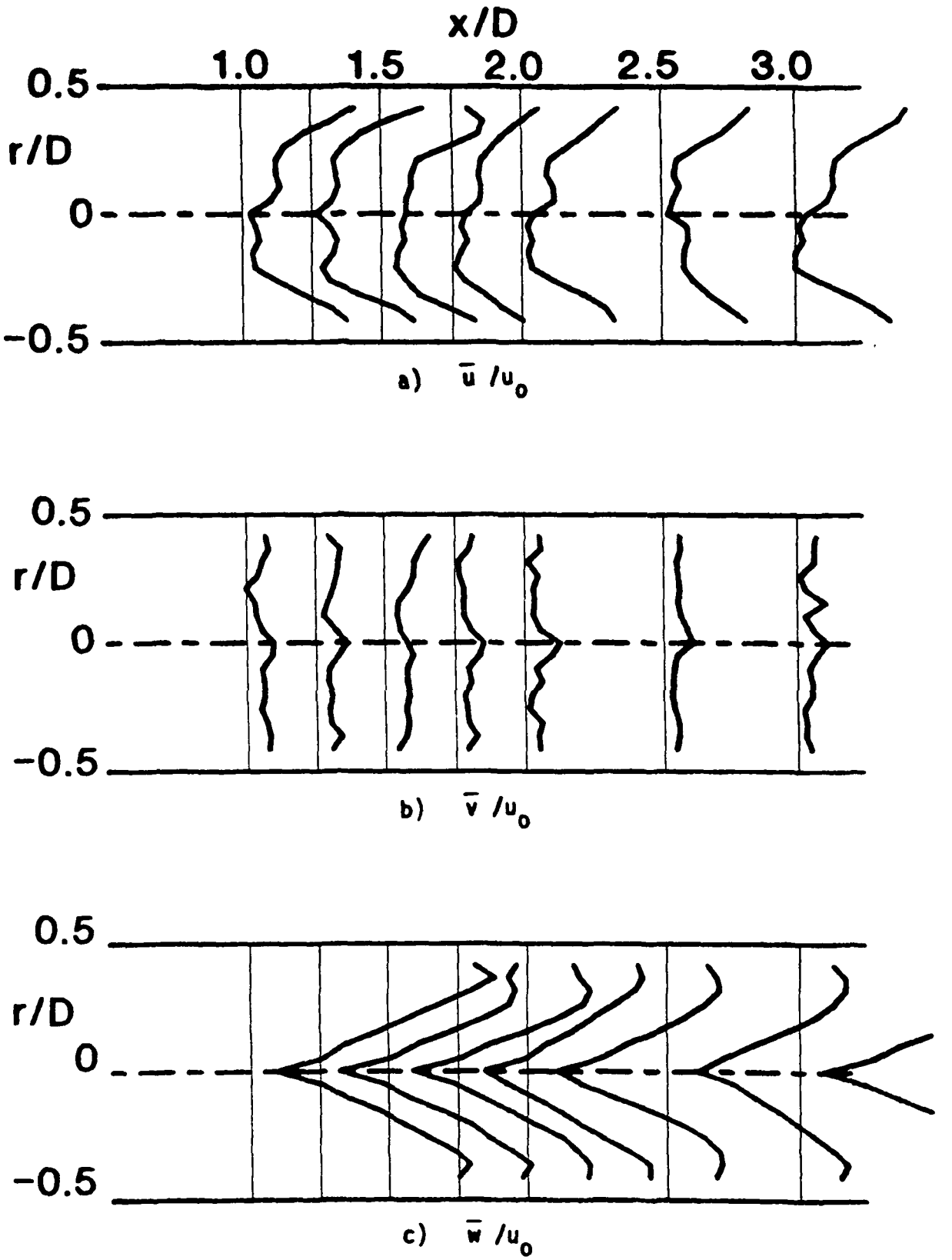

Figure 15. Time-Mean and Turbulent Flowfield (Hot-Wire Data) R = 4, ϕ = 70 Degrees, Traverse Angle θ = 60 Degrees

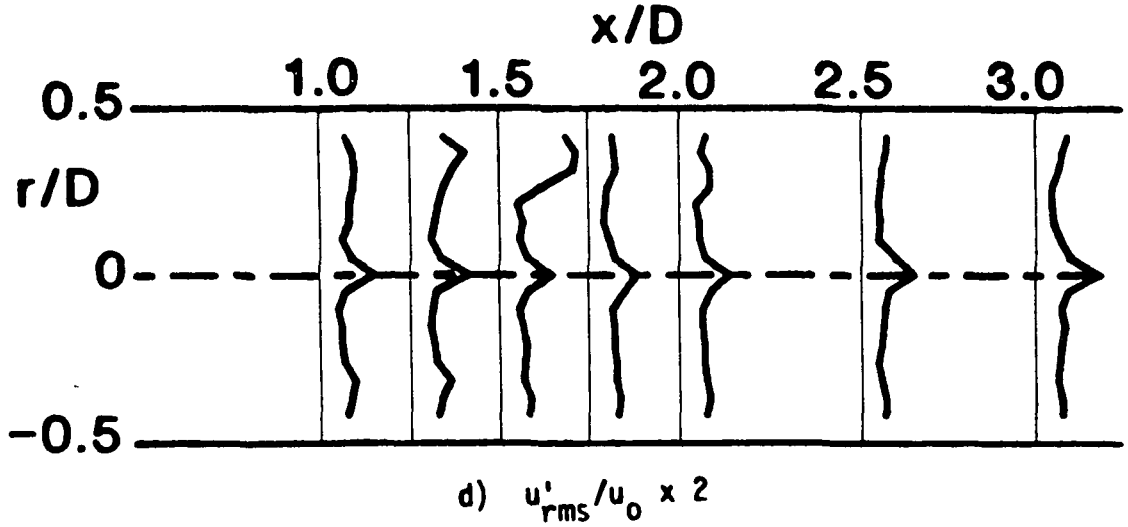

d) $u'_{rms}/u_o \times 2$

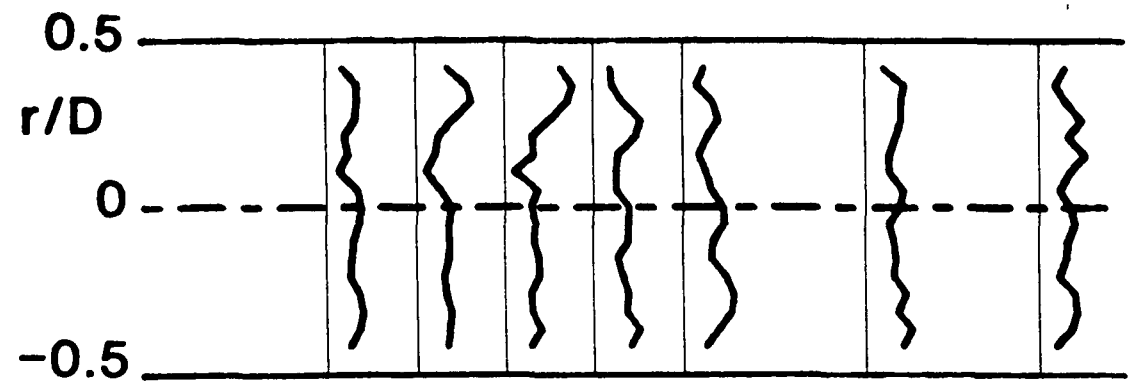

e) $v'_{rms}/u_o \times 2$

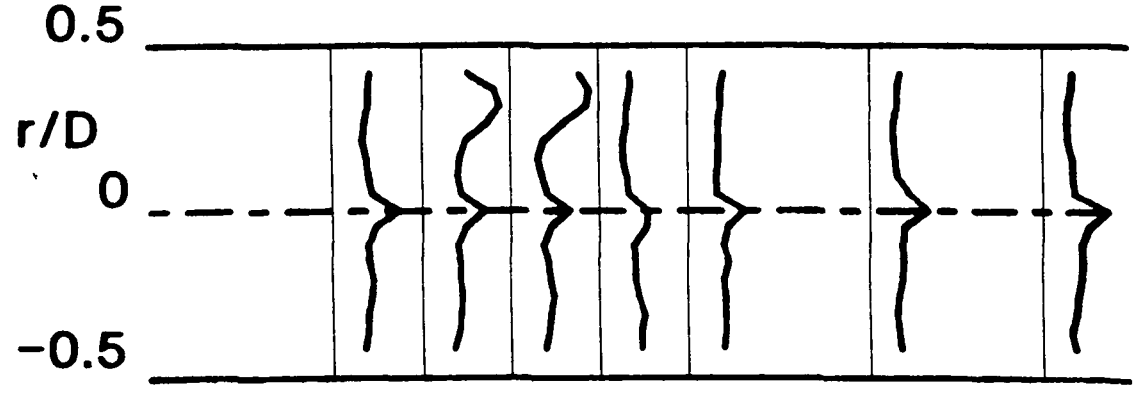

f) $w'_{rms}/u_o \times 2$

Figure 15. (Continued)

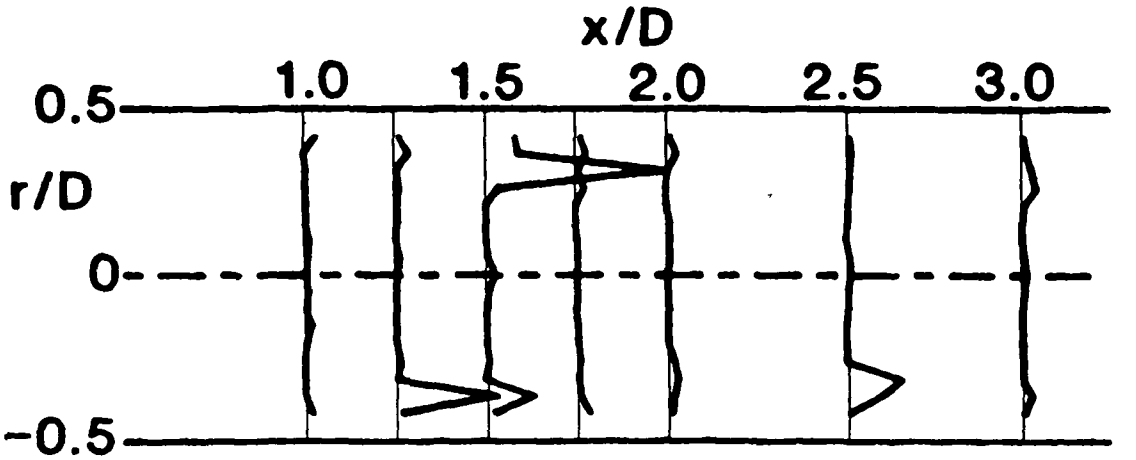

g) $\overline{u'v'}/u_o^2 \times 2$

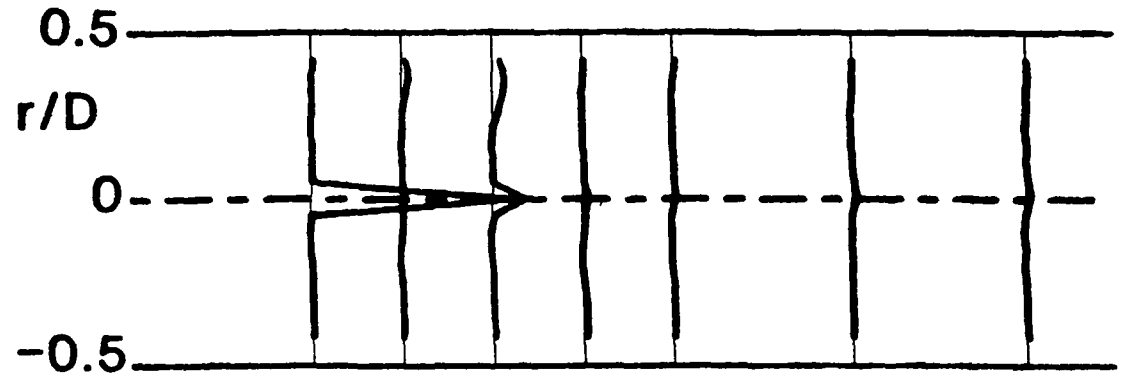

h) $\overline{u'w'}/u_o^2 \times 2$

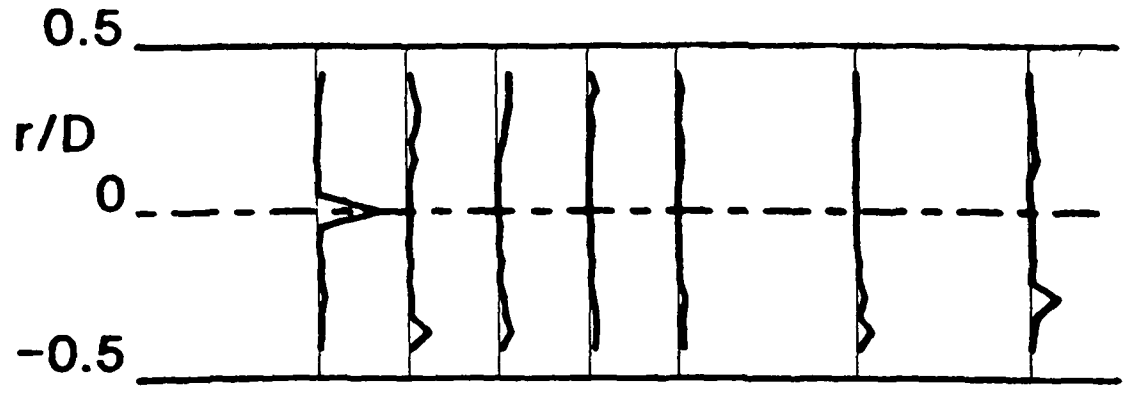

i) $\overline{v'w'}/u_o^2 \times 2$

Figure 15. (Continued)

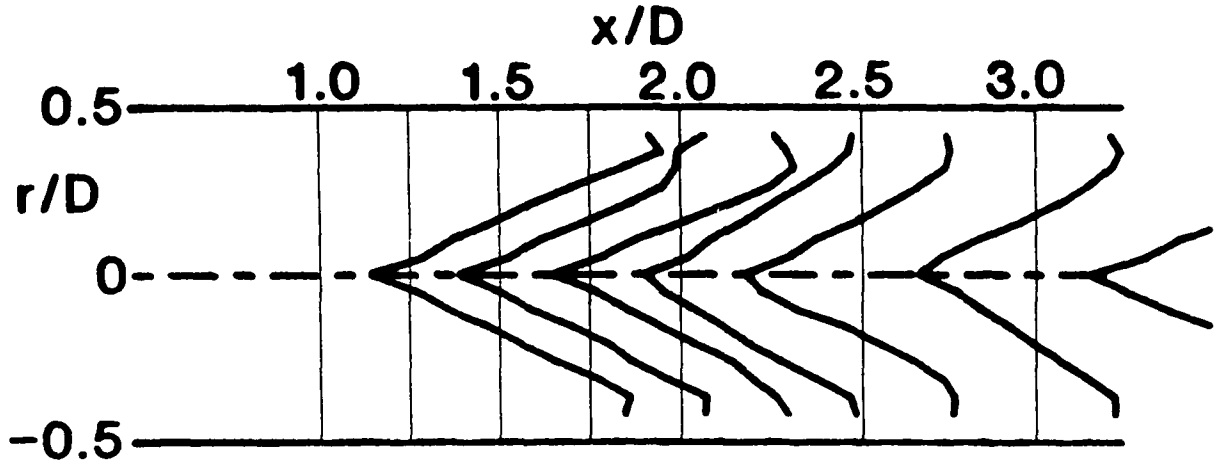

j) $\bar{V} = (\bar{u}^2 + \bar{v}^2 + \bar{w}^2)^{1/2}/u_o$

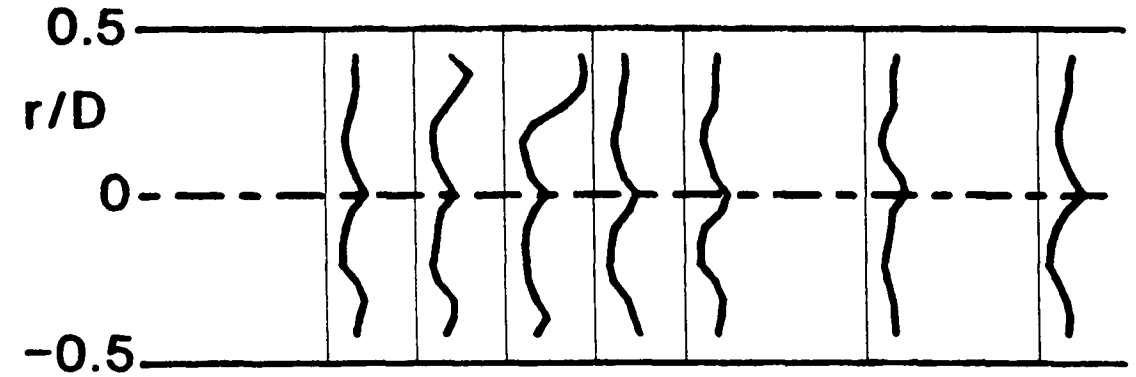

k) $u'_{rms}/\bar{u} \times 2$

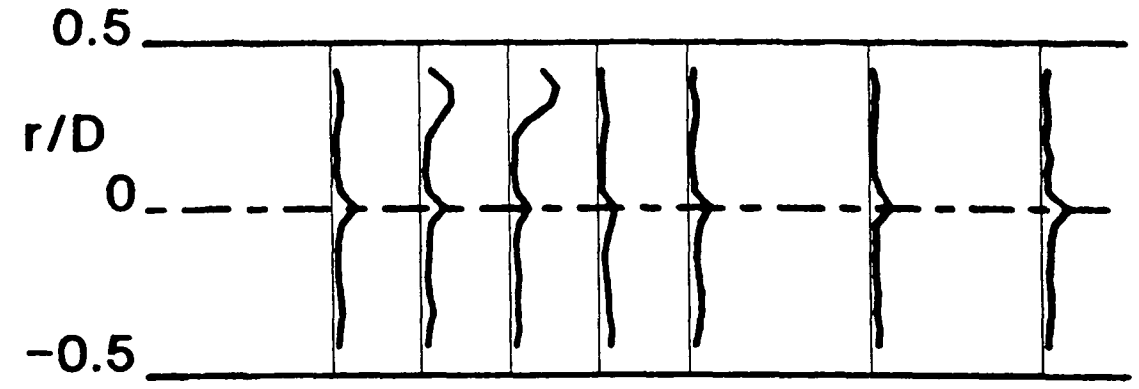

l) $\frac{1}{2}\,(u'^2_{rms} + v'^2_{rms} + w'^2_{rms})/u_o^2 \times 2$

Figure 15. (Continued)

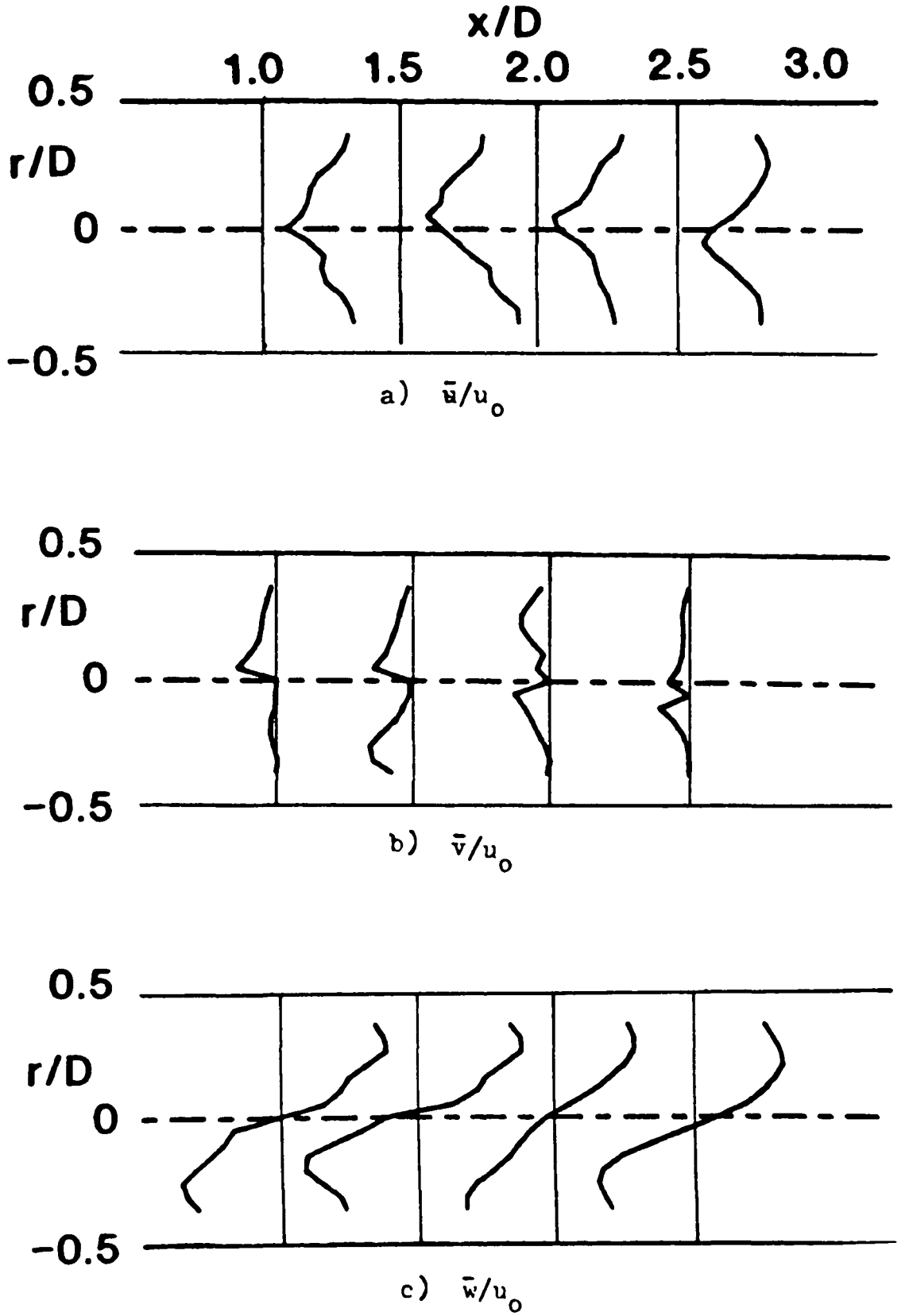

Figure 16. Time-Mean Flowfield (Five-Hole Pitot Probe Data) R = 4, ϕ = 45 Degrees, Traverse Angle θ = 270 Degrees

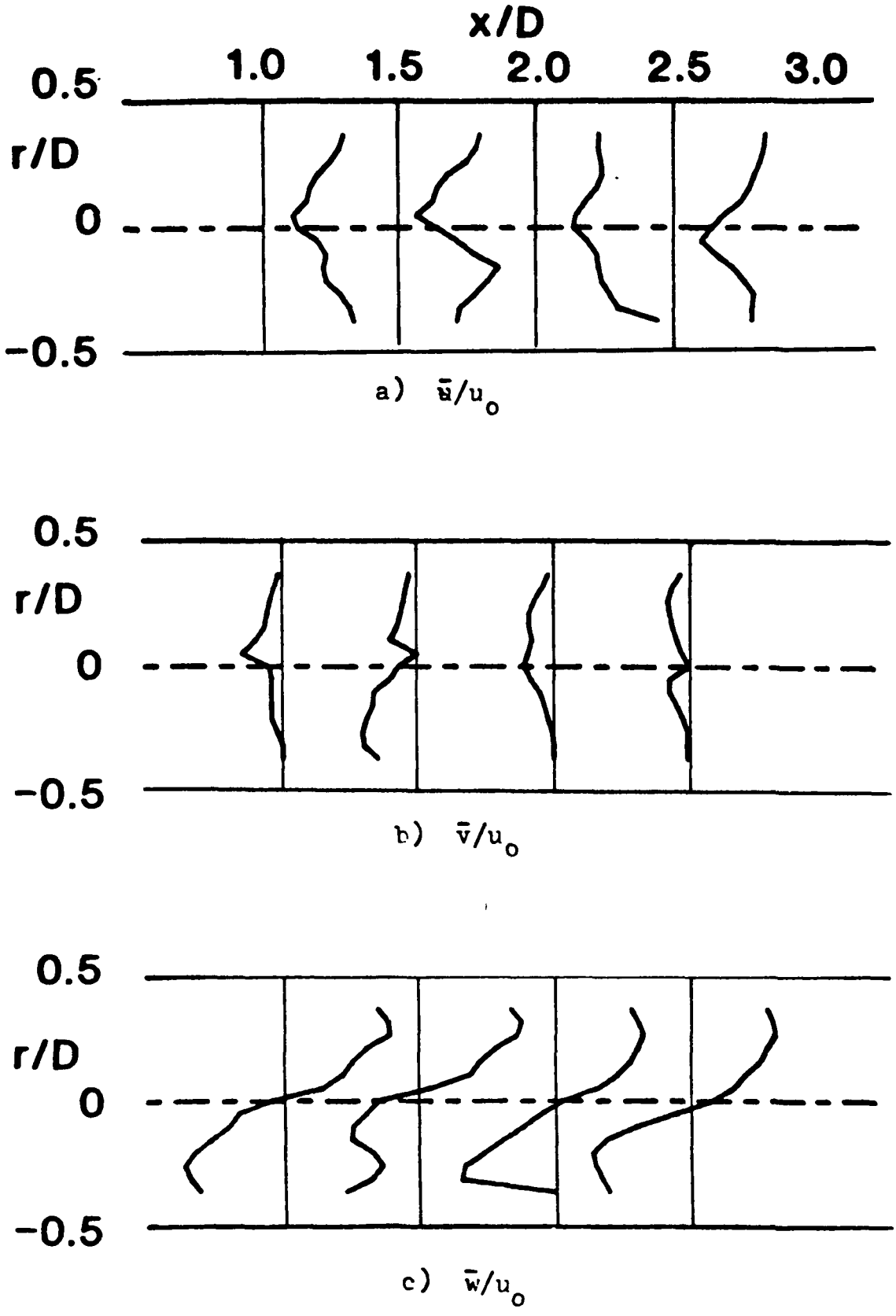

Figure 17. Time-Mean Flowfield (Five-Hole Pitot Probe Data) R = 4, ϕ = 45 Degrees, Traverse Angle θ = 300 Degrees

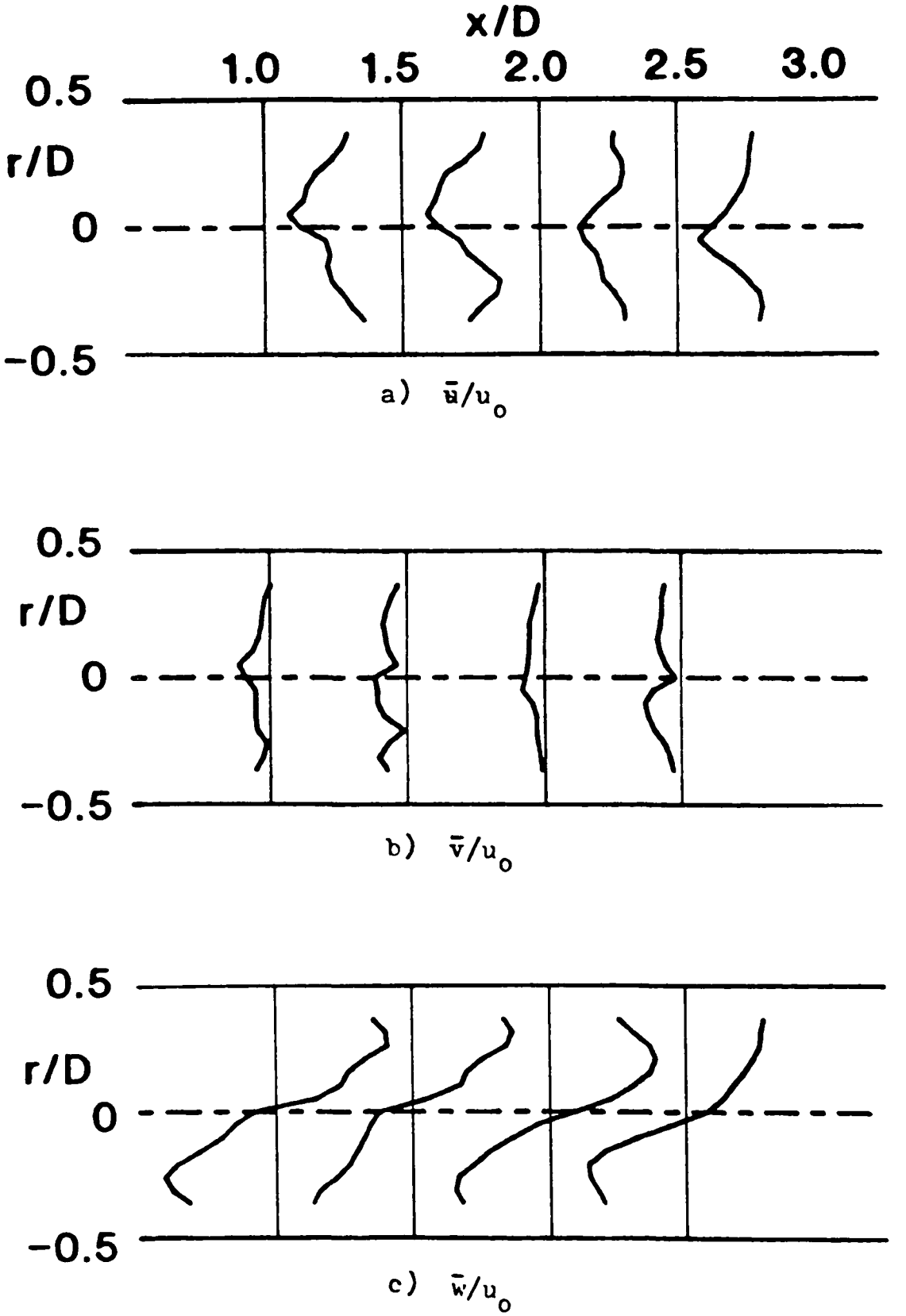

Figure 18. Time-Mean Flowfield (Five-Hole Pitot Probe Data) R = 4, ϕ = 45 Degrees, Traverse Angle θ = 330 Degrees

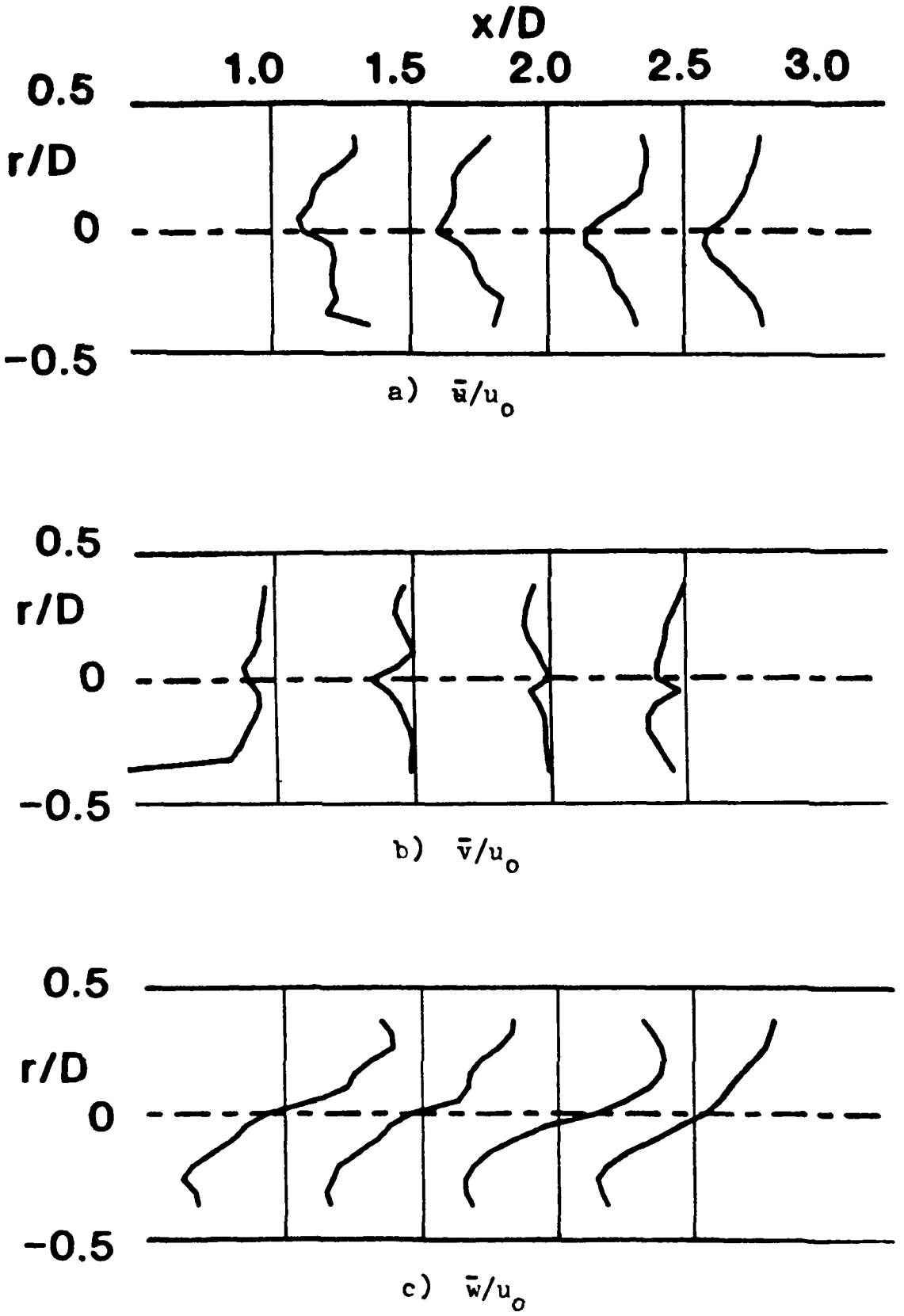

Figure 19. Time-Mean Flowfield (Five-Hole Pitot Probe Data) R = 4, ϕ = 45 Degrees, Traverse Angle θ = 0 Degrees

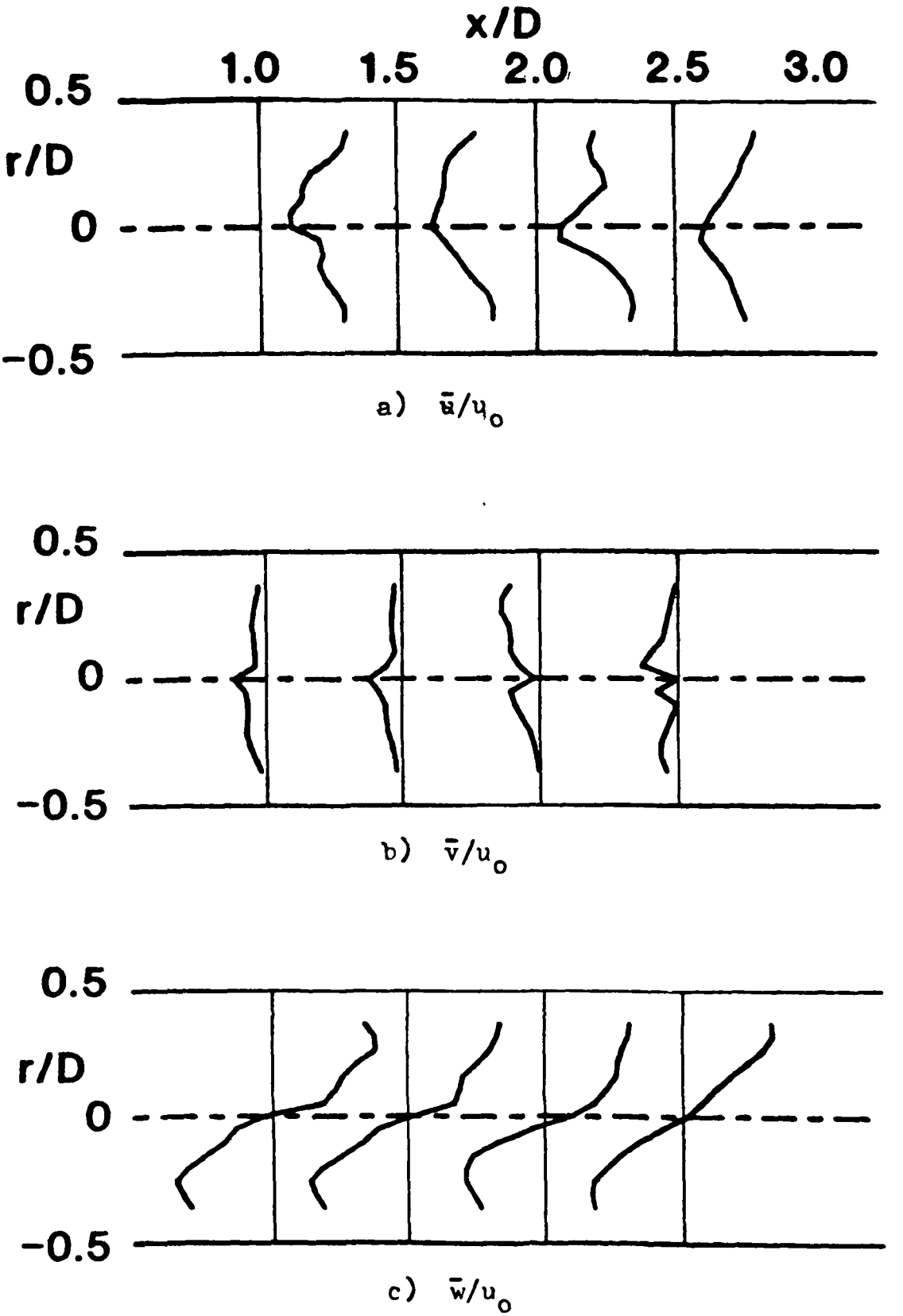

Figure 20. Time-Mean Flowfield (Five-Hole Pitot Probe Data) R = 4, ϕ = 45 Degrees, Traverse Angle θ = 30 Degrees

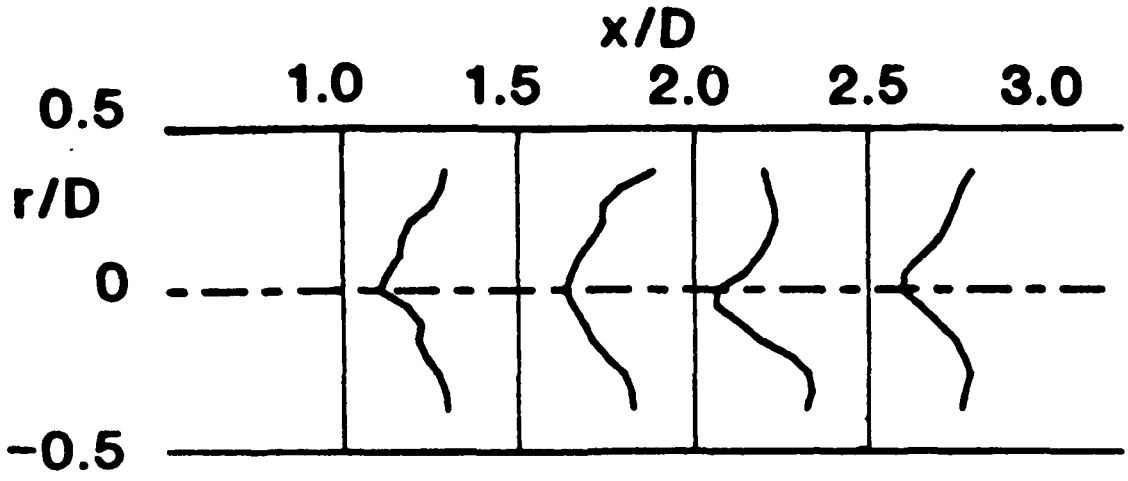

a) $\bar{u}/u_o$

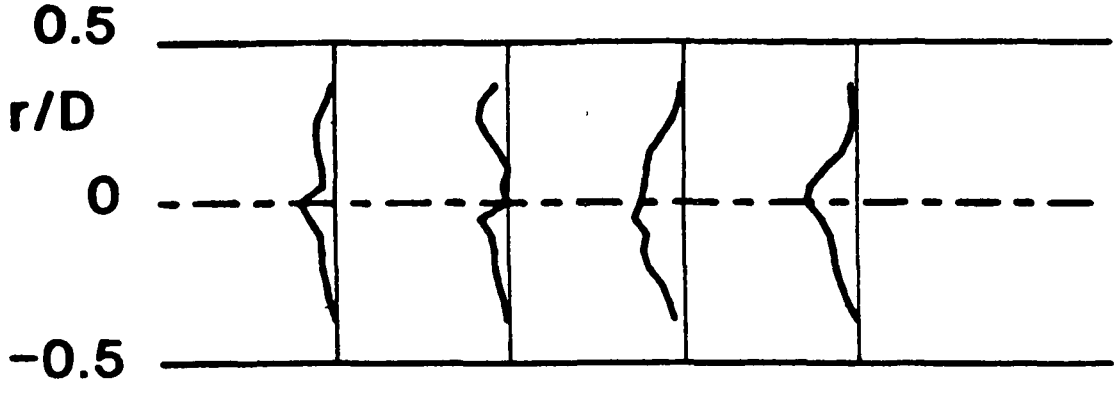

b) $\bar{v}/u_o$

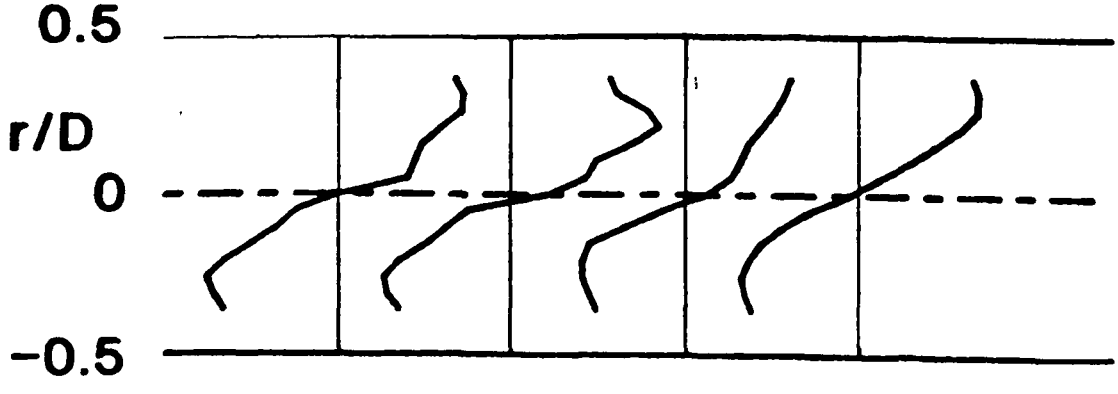

c) $\bar{w}/u_o$

Figure 21. Time-Mean Flowfield (Five-Hole Pitot Probe Data) R = 4, ϕ = 45 Degrees, Traverse Angle θ = 60 Degrees

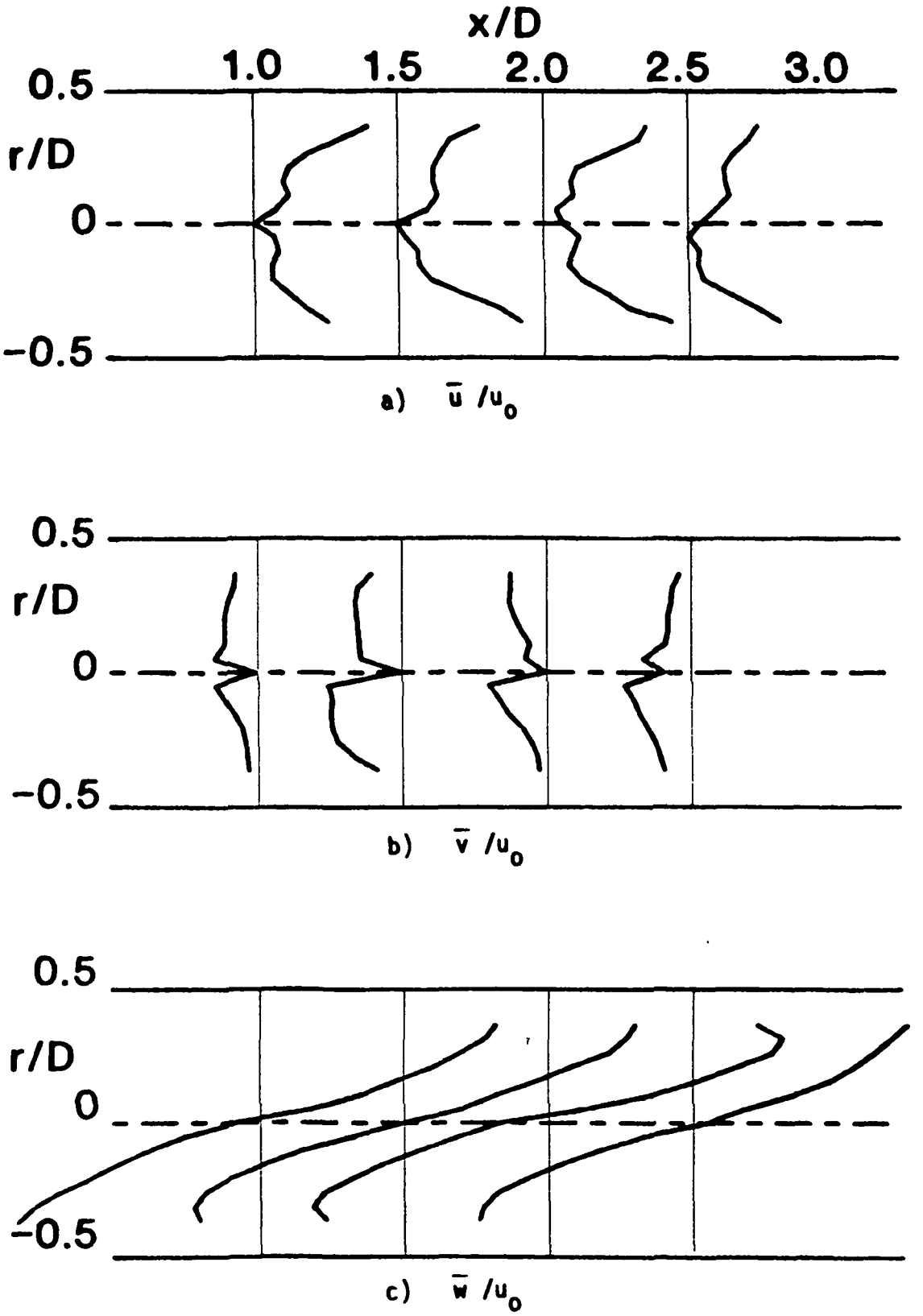

Figure 22. Time-Mean Flowfield (Five-Hole Pitot Probe Data) R = 4, ϕ = 70 Degrees, Traverse Angle θ = 270 Degrees

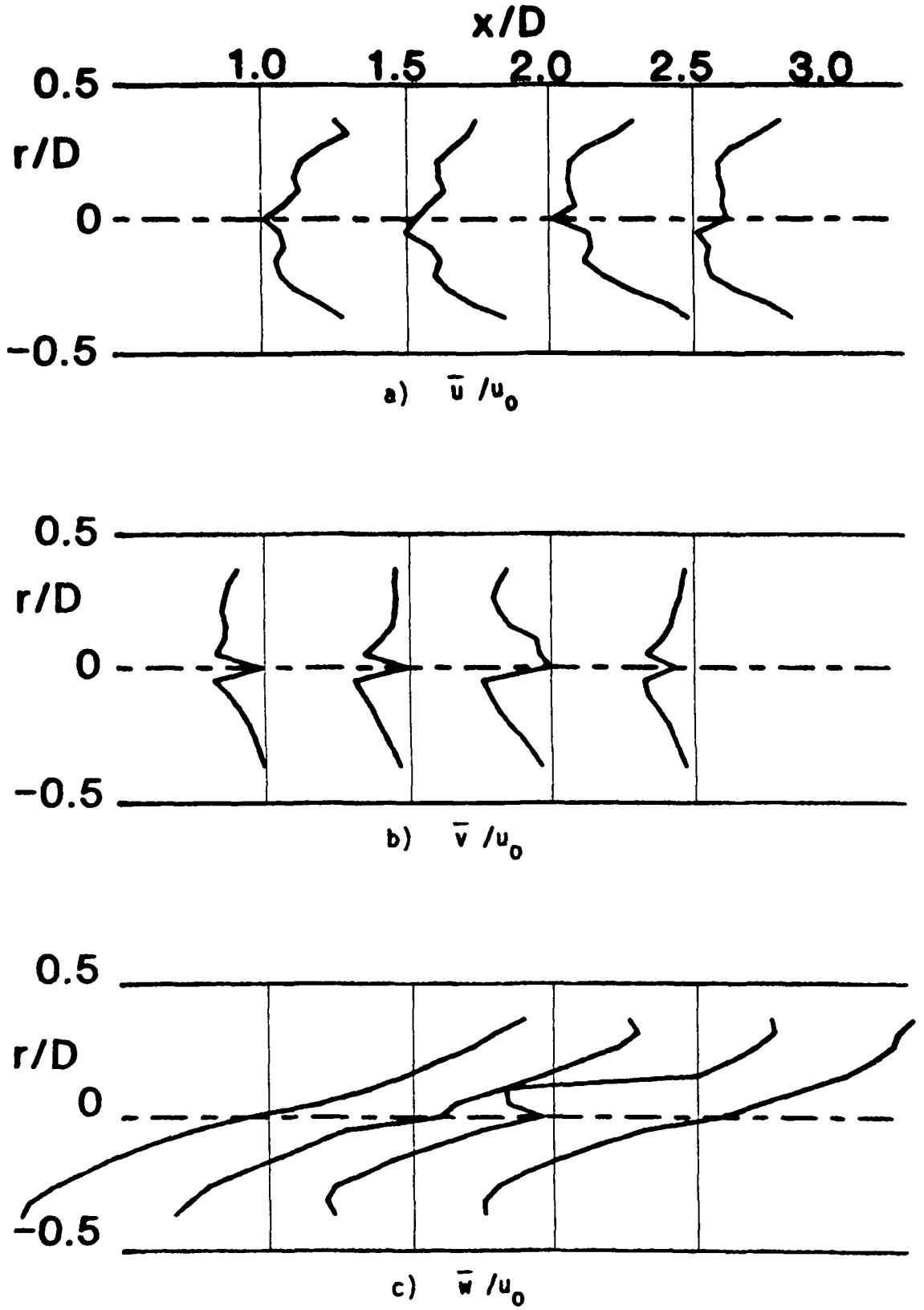

Figure 23. Time-Mean Flowfield (Five-Hole Pitot Probe Data) R = 4, ϕ = 70 Degrees, Traverse Angle θ = 300 Degrees

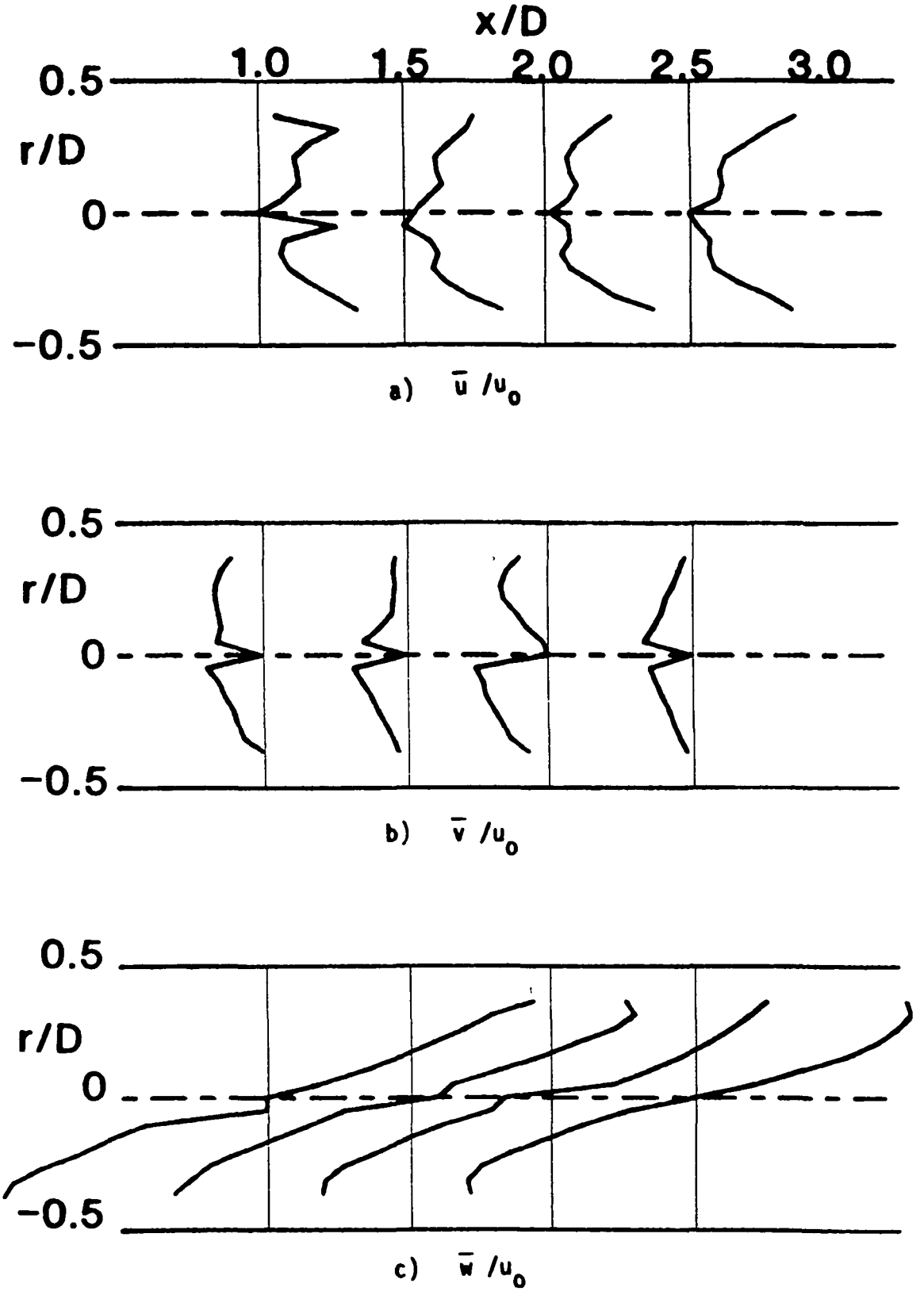

Figure 24. Time-Mean Flowfield (Five-Hole Pitot Probe Data) R = 4, ϕ = 70 Degrees, Traverse Angle θ = 330 Degrees

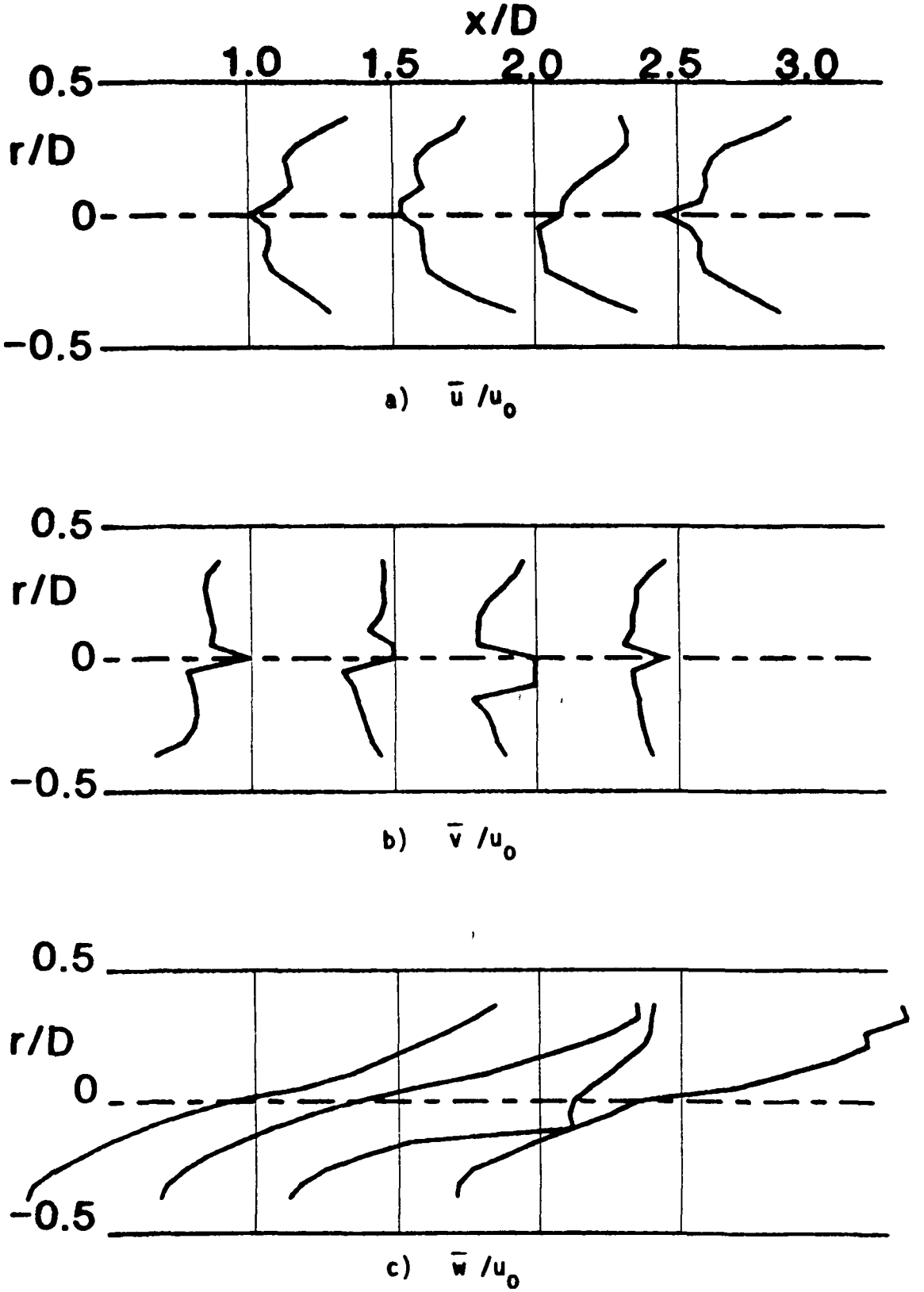

Figure 25. Time-Mean Flowfield (Five-Hole Pitot Probe Data) R = 4, ϕ = 70 Degrees, Traverse Angle θ = 0 Degrees

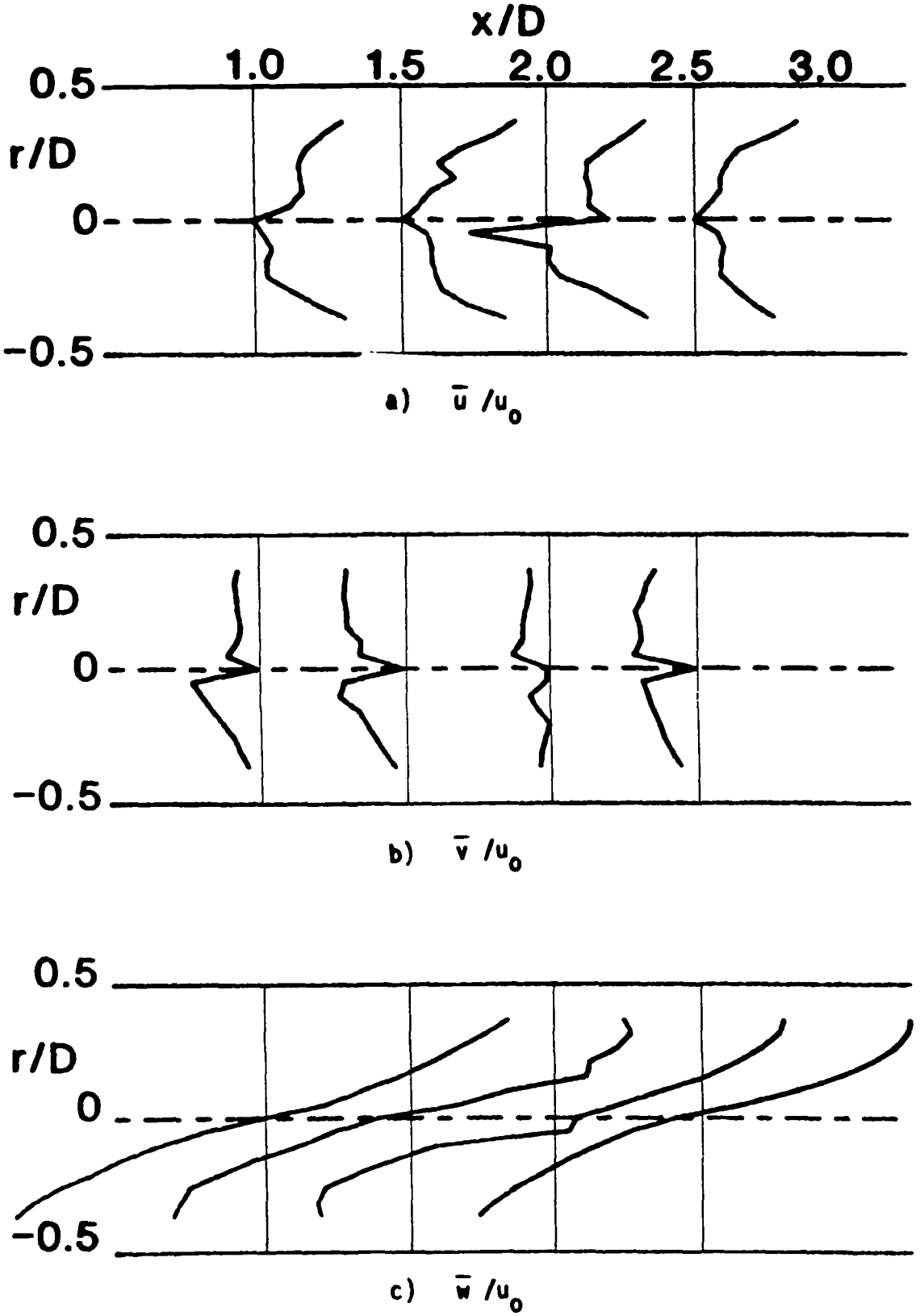

Figure 27. Time-Mean Flowfield (Five-Hole Pitot Probe Data) R = 4, ϕ = 70 Degrees, Traverse Angle θ = 60 Degrees

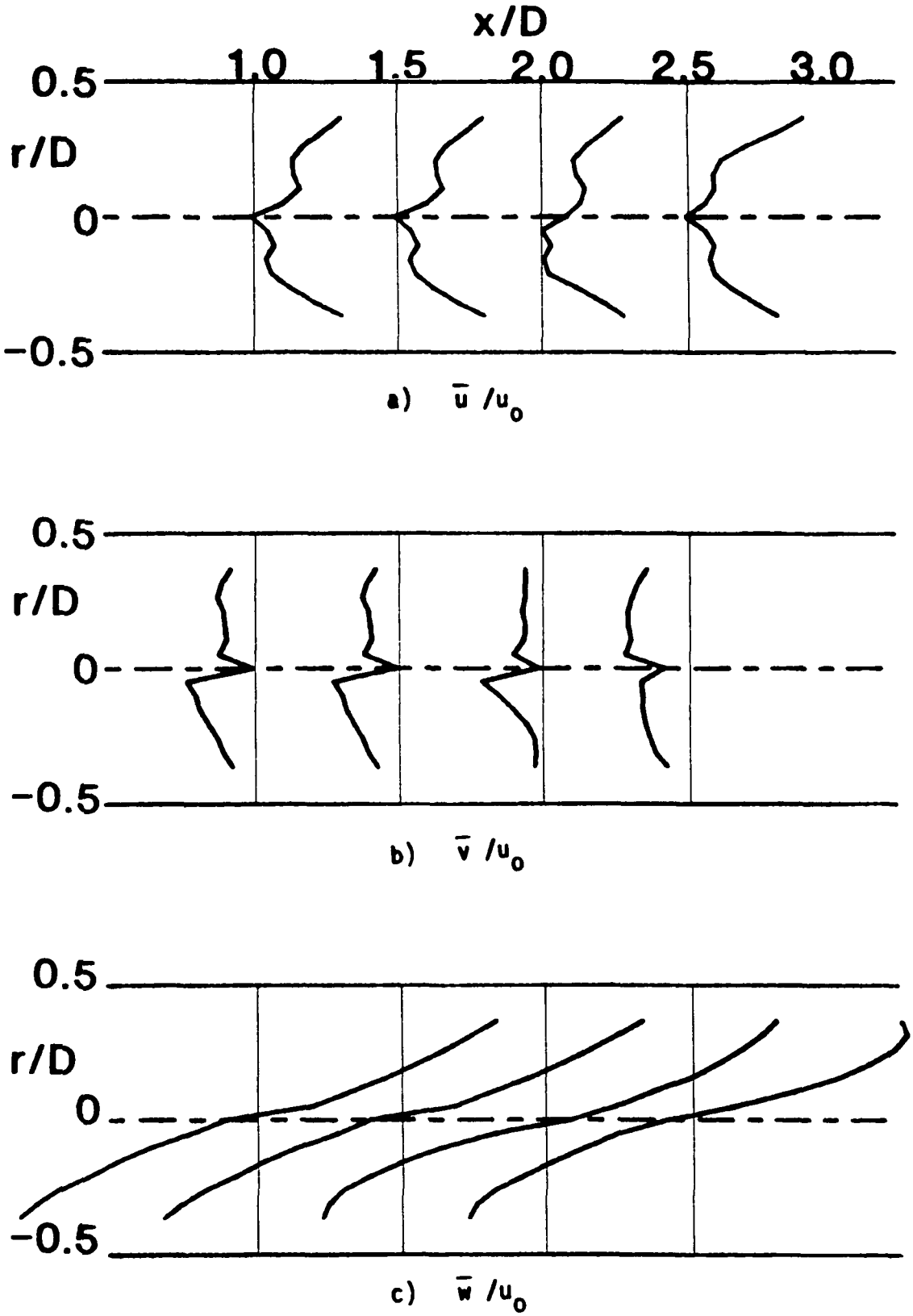

Figure 26. Time-Mean Flowfield (Five-Hole Pitot Probe Data) R = 4, ϕ = 70 Degrees, Traverse Angle θ = 30 Degrees

1 Report No	2 Government Accession No	3 Recipient's Catalog No
NASA CR-175040		

4 Title and Subtitle	5 Report Date
Measurements of a Single Lateral Jet Injected into Swirling Crossflow	January 1986
	6 Performing Organization Code
7 Author(s)	8 Performing Organization Report No
L.H. Ong and D.G. Lilley	None
	10 Work Unit No
9 Performing Organization Name and Address	11 Contract or Grant No
Oklahoma State University School of Mechanical and Aerospace Engineering Stillwater, Oklahoma 74078	NAG 3-549
	13 Type of Report and Period Covered
12 Sponsoring Agency Name and Address	Contractor Report
National Aeronautics and Space Administration Washington, D.C. 20546	14 Sponsoring Agency Code
	533-04-1A

15 Supplementary Notes

Final Report. Project Manager, James D. Holdeman, Internal Fluid Mechanics Division, NASA Lewis Research Center, Cleveland, Ohio 44135. This report was a dissertation submitted by L.H. Ong to the faculty of the Graduate College of Oklahoma State University in partial fulfillment of the requirements for the degree Master of Science in December 1985.

16 Abstract

Experiments have been conducted to document the time-mean and turbulent flowfield of a deflected turbulent jet in a confined swirling crossflow. The jet-to-crossflow velocity ratio of 4 was investigated with swirler vane angles of 45 and 70 degrees. A six-orientation single hot-wire technique was used to measure the velocities and turbulence properties of the flow. In addition, a five-hole pitot probe technique was used to measure the time-mean velocities for verification purposes. The results are presented in the form of r-x plots to aid visualization of the fully three-dimensional flowfield. The swirl in the crossflow intensified the local velocity at the location of the injected jet, which effectively reduced the jet-to-crossflow velocity ratio. This caused the trajectory of the injected jet to follow the path of the local flow direction of the crossflow, and reduce its penetration into the crossflow. The time-mean velocity measurements using the hot-wire corresponded to pitot-probe data obtained in identical flow conditions. Turbulence stress data show the same trends as previous swirl flow data without lateral injection. The lateral jet was found to deflect the axis of the precessing vortex core.

17 Key Words (Suggested by Author(s))	18 Distribution Statement
Turbulent jets; Jets in crossflow; Confined flows; Turbulent mixing; Deflected jets; Axisymmetric combustor	Unclassified - unlimited STAR Category 07

19 Security Classif (of this report)	20 Security Classif (of this page)	21 No of pages	22 Price*
Unclassified	Unclassified	91	A05

*For sale by the National Technical Information Service, Springfield, Virginia 22161